Study and Interpretation of the Millimeter-wave Spectrum of Venus

By

Antoine K. Fahd

Paul G. Steffes, Principal Investigator

School of Electrical Engineering

Georgia Institute of Technology

Atlanta, GA. 30332-0250

(404) 894-3128

June, 1992

Technical Report No. 1992-1

Prepared under NASA grant NAGW-533

Study and Interpretation of the Millimeter-wave Spectrum of Venus

APPROVED

Professor Paul G. Steffes, Chairperson

Professor A.J. Gasiewski

Professor W. Scott

Date Approved by Chairperson 5/13/92

ACKNOWLEDGMENTS

I am grateful to my advisor, Dr. P.G. Steffes for his guidance, support and patience. I thank the following faculty members for their time and careful examination of this document: Dr. A.J. Gasiewski (reader), Dr. W. Scott (reader), Dr. R. Callen (chairman of the qualifying and proposal committees) and Dr. C. G. Justus.

I thank the following individuals for their contributions to this work: Dr. D.P. Campbell, Mr. J.J. Gallagher (deceased), Dr. R. Moore, and Mr. S. Halpbern of the Georgia Tech Research Institute (GTRI); Dr. T.E. Brewer and Dr. A. Gasiewski (Georgia Tech-School of E.E.), for their generous assistance with the laboratory equipment and for providing illuminating discussion. I also thank Dr. I. dePater (Berkeley), and Dr. T.R. Spilker (JPL) for their comments and helpful suggestions.

I would also like to thank my family and friends who gave me support and encouragement through my tenure as a graduate student: Kozhaya (deceased), Antoinette, Michael and Joumana Fahd, Milia and Fady Garabet, Mary Rashid and the rest of the Fahd and Khairallah families. I also thank Robert Troxler, Joanna Joiner, and Jon Jenkins.

This work was supported by the Planetary Atmospheres Program of the National Aeronautics and Space Administration under grant NAGW-533.

TABLE OF CONTENTS

LIST OF FIGURES

LIST OF TABLES

SUMMARY

The effects of the Venus atmospheric constituents on its millimeter wavelength emission are investigated. Specifically, this research describes the methodology and the results of laboratory measurements which are used to calculate the opacity of some of the major absorbers in the Venus atmosphere. The pressure-broadened absorption of gaseous SO_2/CO_2 and gaseous H_2SO_4/CO_2 has been measured at millimeter-wavelengths. We have also developed new formalisms for computing the absorptivities of these gases based on our laboratory work. The complex dielectric constant of liquid sulfuric acid has been measured and the expected opacity from the liquid sulfuric acid cloud layer found in the atmosphere of Venus has been evaluated. The partial pressure of gaseous H_2SO_4 has been measured which resulted in a more accurate estimate of the dissociation factor of H_2SO_4. A radiative transfer model has been developed in order to understand how each atmospheric constituent affects the millimeter-wave emission from Venus. Our results from the radiative transfer model are compared with recent observations of the microwave and millimeter-wave emissions from Venus. Our main conclusion from this work is that gaseous H_2SO_4 is the most likely cause of the variation in the observed emission from Venus at 112 GHz.

CHAPTER 1

INTRODUCTION

1.1 Background and Motivation

Over the past two decades, much information regarding the atmosphere of Venus has been derived from radio occultation measurements, radio emission measurements, and laboratory measurement of the microwave properties of simulated Venus atmospheres. Much of the reported laboratory work was performed at microwave frequencies in order to interpret the radio observations that were carried out at wavelengths longer than 1 cm. As a result, a better understanding of the composition of the atmosphere of Venus was achieved.

Recently, radio observations of Venus at millimeter-wavelengths have shown significant spatial and temporal variations in its measured emission. A complete explanation of this measured variation requires accurate modelling of the effects of the atmospheric constituents of Venus which in turn

requires accurate data concerning their opacities. Although much laboratory work has been performed to measure the opacity of these constituents at microwave frequencies, the determination of the absorption coefficients at millimeter-wavelengths from the results at lower frequencies is not straightforward. Hence, a direct measurement of the absorption coefficients of the major absorbers in the atmosphere of Venus at wavelengths shorter than 1 cm has become necessary.

Within the atmosphere of Venus, gaseous CO_2 is considered the dominant absorber and its abundance constitutes 96 % of the atmosphere of Venus (Oyama et al., 1979) while gaseous N_2 constitutes about 3 %. Besides CO_2 and N_2, gaseous SO_2, H_2SO_4, and H_2O vapor are also present and they constitute about 0.02 % of the atmosphere of Venus. In addition, a cloud layer consisting of liquid sulfuric acid droplets (Knollenberg and Hunten, 1980) is also present. Hence, accurate modelling of the emission of Venus at millimeter-wavelengths requires the knowledge of the opacity of each of these constituents. This need has prompted this research, which can be divided into three main categories:

* Laboratory measurements of the opacity of sulfur-bearing atmospheric constituents of Venus at millimeter-wavelengths.
* Incorporation of the laboratory results into a radiative transfer model to determine the expected emission from the atmosphere of Venus and comparison with observations.

* Determination of new abundance profiles for the atmospheric constituents of Venus based on our results and the measured emission of Venus at millimeter-wavelengths.

The first step in this research was the direct measurement of the partial pressure of gaseous sulfuric acid, which is needed for accurate determination of the saturation abundance of gaseous H_2SO_4 in laboratory experiments and in the Venus atmosphere. This work is used to develop a more accurate expression of the microwave opacity of gaseous sulfuric acid in a CO_2 atmosphere. The second major step is the measurement of the microwave and millimeter-wave opacity of gaseous SO_2. Third, the opacity of liquid sulfuric acid has been measured under Venus-like conditions at millimeter-wavelengths. And most significantly, a measurement of the opacity of gaseous H_2SO_4 has been performed at 94 GHz under Venus-like conditions. New formalisms have been developed to account for the opacity of H_2SO_4/CO_2 and SO_2/CO_2 gaseous mixtures based on our laboratory results.

Finally, the resulting opacities of these constituents are incorporated into a radiative transfer model to study their effects on the emission of Venus. Using our radiative transfer model and the reported emissions from Venus, we developed a new upper limit on the abundance of gaseous SO_2 and H_2SO_4 in the atmosphere of Venus. This new updated profile can then be used to better understand the physical and

chemical properties of the atmosphere of Venus. In addition, our results are used to account for the measured spatial variation in the observed millimeter-wave emission of Venus.

1.2 Organization

The organization of this thesis is as follows:

Chapter 2 describes the measurement of the microwave and millimeter-wave opacity of gaseous SO_2 under Venus-like conditions. A new formalism based on the Van Vleck-Weisskopf theory is employed to accurately model the expected opacity of SO_2/CO_2 gaseous mixture.

The determination of the complex dielectric constant of liquid sulfuric acid is described in Chapter 3. In addition, a theoretical characterization of the dielectric constant of H_2SO_4 at millimeter-wavelengths is also described.

Chapter 4 and appendix A describe in detail the determination of the partial pressure of gaseous H_2SO_4 and consequently the dissociation factor of gaseous sulfuric acid. The application of our results to the atmosphere of Venus is also described in section 4.2.

Chapter 5 describes the approach and results for the measurement of the opacity of gaseous H_2SO_4 at 94 GHz. A theoretical characterization of the opacity of H_2SO_4 is also provided.

The theory and application of a microwave and millimeter-wave radiative transfer model are described in Chapter 6. The model utilizes the results of the laboratory measurements reported in previous chapters. The effect of each constituent on the millimeter-wave emission from Venus is also discussed. New abundance profiles for the atmospheric constituents of Venus are reported in Chapter 6.

A summary of the major conclusions and contributions of this work is provided in Chapter 7. In addition, suggestions for future research are discussed.

CHAPTER 2

MICROWAVE AND MILLIMETER-WAVE OPACITY OF GASEOUS SULFUR DIOXIDE (SO_2) UNDER VENUS-LIKE CONDITIONS

2.1 Motivation for Experiment

Laboratory measurement of the microwave and millimeter-wavelength opacity of gaseous sulfur dioxide (SO_2) under simulated Venus conditions is of great importance in understanding the effects of SO_2 on the emission from Venus. Although some laboratory measurements of the microwave absorption properties of gaseous SO_2 under Venus-like conditions have been made at 13 and 3.6 cm (Steffes and Eshleman, 1981), no laboratory measurements of the opacity of SO_2 have been made at shorter wavelengths. The microwave measurements of the opacity of SO_2 reported by Steffes and Eshleman (1981) showed that the absorption coefficient of gaseous SO_2 in a CO_2 atmosphere was consistent with an f^2 (f=frequency) dependence at pressures between 1 and 6

atmospheres and at frequencies below 8.5 GHz. Similarly, Janssen and Poynter (1981) developed a theoretical expression for the absorption coefficient of gaseous SO_2 based on a best-fit expression of contributions from SO_2 absorption lines below 3000 GHz which also concluded that the absorption coefficient of gaseous SO_2 in a CO_2 atmosphere with pressure greater than 1 bar has an f^2 dependence throughout the microwave and millimeter-wavelength regions. Although this assumption may be valid for frequencies at which the measurements were made, the simple extrapolation of SO_2 absorptivity to higher frequencies by using such expressions may not be valid. Thus, a direct measurement of the opacity of gaseous sulfur dioxide (SO_2) at higher frequencies has been greatly needed for proper modeling of the effects of SO_2 on the emission from Venus.

This chapter describes the methodology and the results of laboratory measurements of the absorptivity of gaseous SO_2 in a predominantly CO_2 atmosphere at wavelengths of 0.32, 1.3 and 13.3 cm. The motivation for the absorptivity measurement at 1.3 cm is the availability of highly accurate microwave emission data for Venus. (See, for example, Steffes et al., 1990). In addition, this chapter describes an innovative technique for measuring the absorption coefficient of weakly absorbing gases which takes into account the effects of dielectric loading in the resonator used in the experiments.

A comparison between our measured results and the absorption computed using a Van Vleck-Weisskopf formalism is also presented.

2.2 Experimental Approach

Two measurement configurations were used to measure the absorptivity of gaseous SO_2 in a CO_2 atmosphere: The Microwave configuration and the Millimeter-wave configuration.

2.2.1 Microwave Configuration

The experimental configuration used to measure the opacity of gaseous SO_2 at 2.24 and 21.7 GHz is similar to that previously used by Steffes (1986) for characterizing the absorption of gaseous sulfuric acid (H_2SO_4) in a CO_2 environment. The experimental setup consists of a spectrometer which contains two subsystems: A microwave subsystem and a planetary atmospheric simulator subsystem as shown in Figure 2.1.

The microwave subsystem consists of two microwave sweep oscillators. One oscillator is used to cover the 2 to 12 GHz frequency band while the second oscillator is used to cover the 18-26 GHz frequency band. The two microwave sweep oscillators are adjusted appropriately for each resonance so that they sweep through the entire frequency band affected by the resonance. The output of each oscillator is then fed

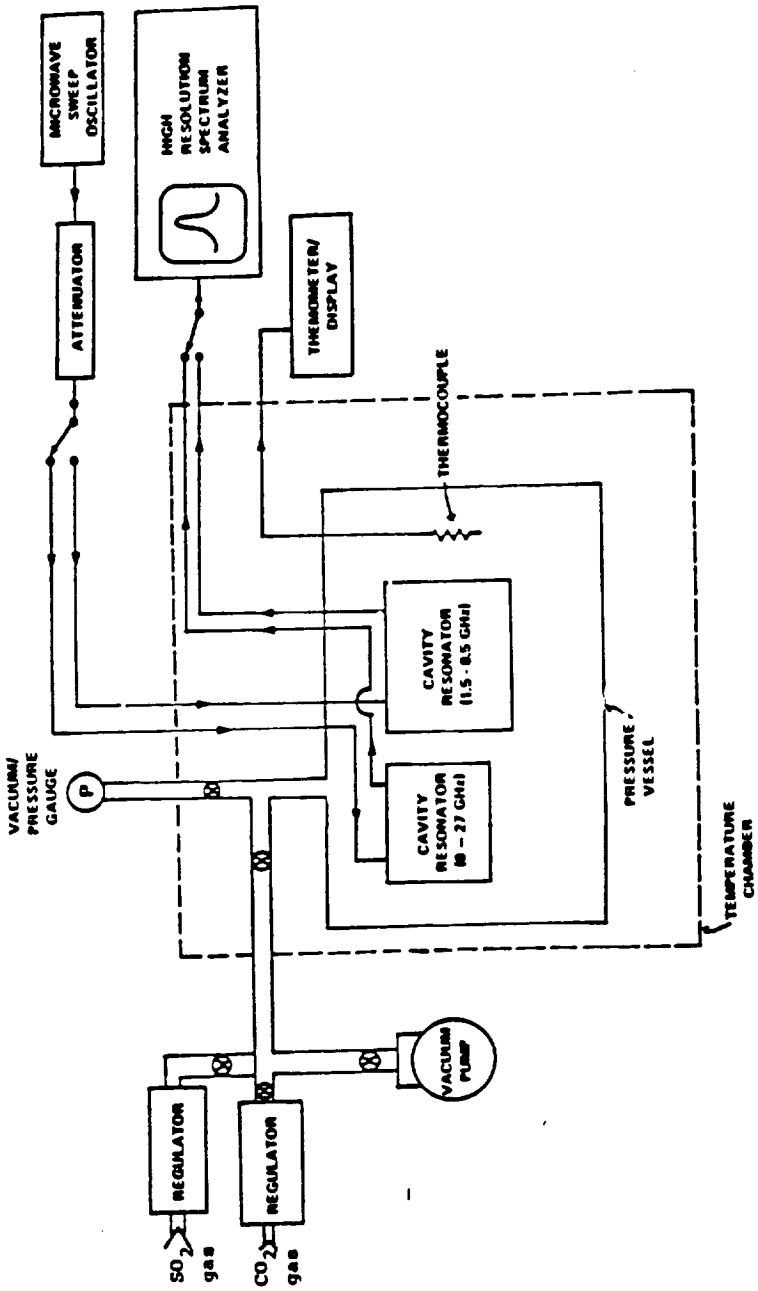

Figure 2.1 Block diagram of Georgia Tech Spectrometer, as configured for measurements of microwave refraction and absorption of gases under simulated Venus conditions.

through a separate attenuator which is used to minimize any reflections from the resonators employed in this configuration. Two distinct circular cylindrical cavity resonators are employed in this subsystem. One resonator is used at 2.24 GHz while the second resonator operates at 21.7 GHz. The output of the attenuator is connected to the appropriate resonator via a semi-rigid coaxial cable (for 21.7 GHz resonator) and a flexible coaxial cable (for 2.24 GHz). The outputs of the two resonators are then fed to a high resolution spectrum analyzer (HP 8562B) which is adjusted to display each resonance accordingly.

The planetary atmospheric simulator subsystem consists of a stainless steel pressure vessel (the pressure vessel can withstand pressures up to 8 atmospheres) in which the two resonators are placed. CO_2 and SO_2 gas cylinders are incorporated in this configuration to provide the appropriate gas mixture needed for the measurements. An oil diffusion pump is used to evacuate the pressure vessel prior to the introduction of the gas mixture. The vacuum status of the pressure vessel is monitored via a thermocouple vacuum gauge that is able to measure pressures between 0 and 800 Torr with 1 Torr display resolution and an accuracy of 1% of full scale. In addition, a positive pressure gauge (0-80 psig) with a display resolution of 1 psig and an accuracy of ±3 psig is

used to measure the internal pressure of the vessel resulting from the introduction of the SO_2/CO_2 mixture into the system. The temperature of the spectrometer is monitored via a Fisher brand thermometer able to measure temperatures between -20 and 110 C with 1 C resolution and an accuracy of ±2 C. A network of 3/8" stainless-steel tubing and valves connect the components of the pressure subsystem so that each component may be isolated from the system as necessary. During the measurement process, precautions are taken to allow proper ventilation of sulfur dioxide so that the experiment could take place indoors.

Regarding the purity of the gases used in the measurements, research grade gases are employed in our measurement process. The two gases used in our experiment (SO_2 and CO_2) have listed purities of 99.98 % (this figure was supplied by the gas vendor). To minimize impurities in the pressure vessel, we first filled the vessel with 6 atm of pure gaseous CO_2. Next, the pressure vessel is evacuated until a pressure of approximately 1 Torr is reached. This process is repeated several times before each measurement in order to flush out any impurities before the introduction of the gaseous mixture which is actually measured.

2.2.2 Millimeter-Wave Configuration

In addition to the measurement of the microwave opacity of gaseous sulfur dioxide, we have completed measurements of the opacity of SO_2 in a CO_2 atmosphere at millimeter wavelengths. The schematic diagram of this experiment is shown in Figure 2.2. As shown in the figure, the system is composed of a Fabry-Perot resonator, a backward wave oscillator (BWO), a microwave oscillator, a harmonic mixer, and a high resolution spectrum analyzer. The output of the BWO (94.1 GHz) is fed into the resonator via a network of WR-10 rigid waveguides. The output of the resonator is then mixed with the tenth harmonic of the phase-locked microwave oscillator. As a result, an intermediate frequency of about 500 MHz is produced which is viewed on a high resolution spectrum analyzer.

A sketch of the W-band Fabry-Perot resonator is shown in Figure 2.3. The resonator consists of two gold plated mirrors (one planar with radius of 5 cm and one concave with a radius of 11.5 cm) separated by a distance of 15 cm. This type of Fabry-Perot resonator contains a superior focusing system which can yield a quality factor on the order of 30,000. The two mirrors are positioned on a movable mount in order to facilitate any changes in the mirrors' separation without disturbing the alignments of the two mirrors. Electromagnetic energy is coupled both to and from the resonator through twin irises located on the flat mirror. The two irises are sealed

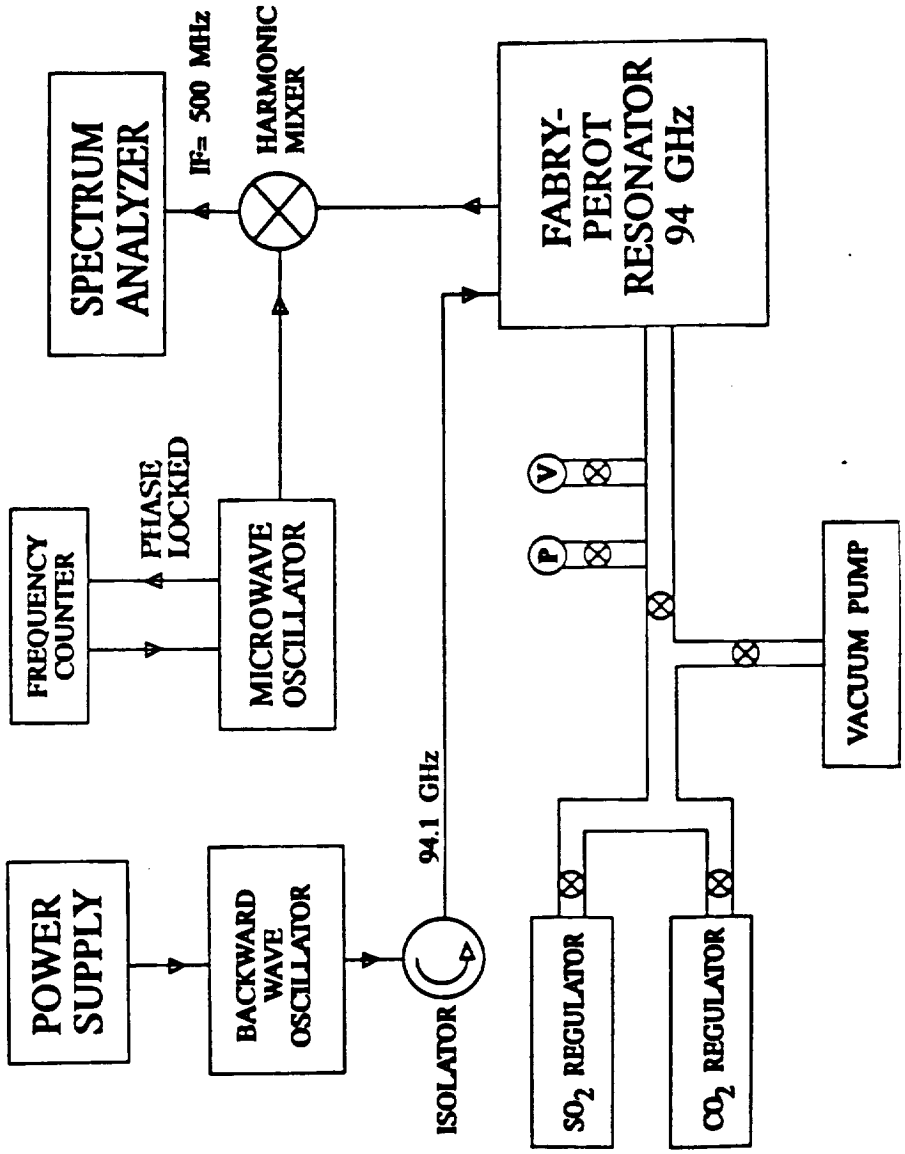

Figure 2.2 Block diagram of the millimeter-wave setup for measuring the absorption coefficient of gaseous sulfur dioxide (SO_2) under Venus-like conditions.

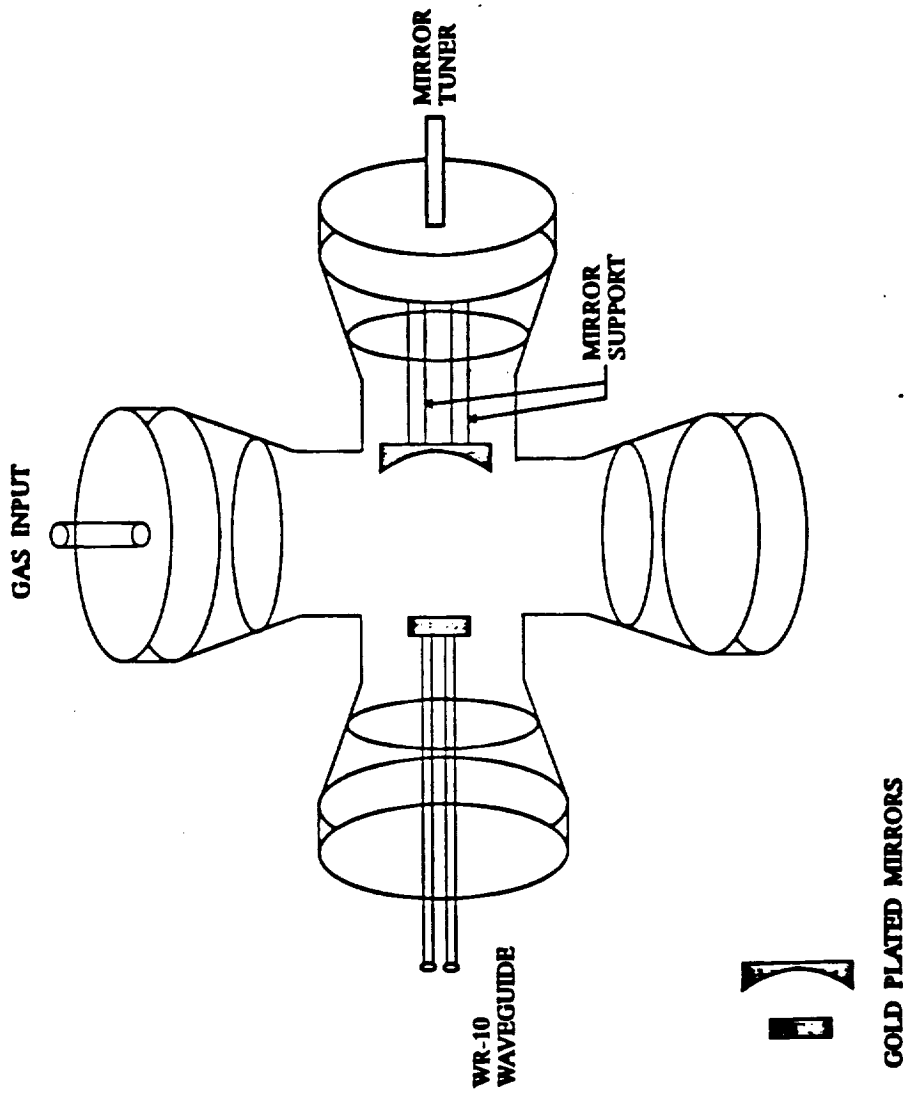

Figure 2.3 Sketch of the Fabry-Perot resonator used in the measurements of the absorption coefficient of SO_2/CO_2 at 94.1 GHz.

with rectangular pieces of mica held in place by a mixture of rosin and beeswax.

The gaseous pressure subsystem used in the millimeter-wavelength setup is similar to that employed in the microwave setup with the exception that the Fabry-Perot resonator is housed in a sealed cross-shaped glass vessel instead of the stainless steel vessel.

2.3 Determination of the Absorptivity of SO_2

The absorptivity of a gas mixture can be measured by monitoring the effects of the test gas on the frequency and bandwidth of a particular resonance. The introduction of a gas mixture into a resonant cavity will alter its quality factor, Q, which is defined as the average stored energy divided by the energy lost per radian change in phase. In a laboratory measurement process, the quality factor can be determined by measuring the resonant frequency (f_o) and the half-power bandwidth (δf) of the cavity under test so that,

$$Q = \frac{f_o}{\delta f} \quad . \tag{2.1}$$

Any additional losses due to the introduction of the test gas mixture (within the cavity) will decrease the overall Q and will cause the frequency response of the resonator to be broader than that of the same empty resonator. For a

relatively low-loss gas mixture, the relation between the absorptivity of the gas mixture and the quality factor of the cavity can be written as per Steffes and Eshleman (1981),

$$\alpha = \frac{\pi}{\lambda}\left(\frac{1}{Q_{ug}} - \frac{1}{Q_{ue}}\right) \qquad (2.2)$$

where Q_{ug} is the unloaded quality factor of the cavity with gas present (this is the quality factor that would be observed if we only take into account wall conductivity losses and gas absorptivity losses), while Q_{ue} is the unloaded quality factor of the empty resonator. (The assumption of a low-loss gas implies a gas with a loss tangent $\ll 1$ which is valid for most atmospheric gases. For instance, if tan δ=.01, this yields an absorption coefficient of 10^4-10^5 dB/km at microwave frequencies (3-30 GHz) and 10^5-10^6 dB/km at millimeter-wavelengths (30-300 GHz), which are well above the expected opacities from any atmospheric gas). In general, the transmissivity, t, through a two-port resonator at resonance can be expressed as per Matthaei et al. (1964),

$$t = \left[4\frac{Q_m^2}{Q_e^2}\right] \qquad (2.3)$$

where,

$$Q_m = \frac{1}{\frac{2}{Q_e} + \frac{1}{Q_u}} \qquad (2.4)$$

In the above equation, Q_m is the directly measured quality factor of the resonator while Q_e is the external quality factor which accounts for the coupling loss to one port of the cavity under consideration. Using the above two equations (2.3 & 2.4), one can solve for the unloaded quality factor Q_u which upon substitution in equation (2.2) yields,

$$\alpha = \frac{\pi}{\lambda}\left(Q_{mg}^{-1}\left(1 - t_g^{1/2}\right) - Q_{me}^{-1}\left(1 - t_e^{1/2}\right)\right) \qquad (2.5)$$

where α is the absorptivity of the gas mixture in Nepers/km, and λ is the wavelength in km. (Note: an attenuation constant, or absorption coefficient or absorptivity of 1 Neper/km = 2 optical depths per km (often expressed as km^{-1}) = $20\log_{10}e$ ($\approx$8.686) dB/km, where the first notation is the natural form used in electrical engineering, the second is the prevalent form used in physics and astronomy, and the third is the common (logarithmic) form. The third form is used to avoid a possible factor of two ambiguity in meaning). Q_{mg} is the measured quality factor of the cavity containing the gas mixture, while Q_{me} is the measured quality factor of the evacuated resonator. The transmissivity (t) can be expressed as,

$$t=10^{-S/10} \qquad (2.6)$$

where S is the loss (in dB) through the resonator which can be directly measured. Thus, t_g denotes the transmissivity with the gas mixture present while t_e denotes the measured transmissivity of the empty resonator.

This method of determining the absorptivity of a gas mixture is very valuable since it minimizes the effect that the real part of the dielectric constant (ϵ_r') of the gas has on the measurement of the absorptivity or imaginary part of the gas dielectric constant (ϵ_r''). This effect, known as "dielectric loading" can cause the Q of the resonator to change even in the presence of a lossless gas because of changes to the total coupling of the resonator when the gas is introduced (Ref: Joiner et al., 1989). In addition to coupling variations, the introduction of a gaseous mixture can change the dielectric environment of the resonator thus affecting the observed Q of a given resonance mode. This effect, referred to as "true dielectric loading," is similar to the increase in the energy stored in a capacitor, at RMS potential, as the dielectric constant between its plates is increased. Thus by canceling the effect of the variation in coupling coefficient in the cavity and the effect of true dielectric loading, the measured change in quality factor is solely due to the absorption of the gas mixture.

The first step in the measurement process requires the evacuation of the chamber. Once a good vacuum has been achieved, a direct measurement of the quality factor (Q_{me}) and transmissivity (t_e) is performed. Gaseous SO_2 is then admitted into the pressure vessel until the desired pressure is obtained. Gaseous CO_2 is next introduced into the system so that the total maximum internal pressure is equal to 6 atm (2 atm for the millimeter-wave system). With the gas mixture inside the vessel, the measurements of Q_{mg} and t_g are performed (the gas mixture is allowed to mix for a period of 40-60 minutes before starting the measurement). The total internal pressure is then reduced and the measurement procedure is repeated. Subsequent measurements are likewise made at lower pressures in order to determine the absorptivity of the gas mixture at lower pressure levels (in the determination of the absorptivity, it is assumed that the shift in the center frequency (δf_o) of the resonance under test is small compared to the center frequency (f_o). i.e.: $\delta f_o / f_o \ll 1$) . This approach has the advantage that the same gas mixture is used for the measurement at the various pressures. Thus, even though some uncertainty may exist as to the mixing ratio of the initial mixture, the mixing ratios at subsequent pressures will be the same, and the uncertainty for any pressure dependence will

only be due to the accuracy limits of the absorptivity measurements, and not uncertainty in the mixing ratio.

Throughout the measurement process, careful tracking of the desired resonance is necessary since the introduction of the test gas in the pressure vessel shifts the resonant frequency f_o. This careful tracking insures that the change in the measured quality factor is due to the desired resonance and not to any other resonances that are present in the resonator under test. At the end of the measurement process, the chamber is again evacuated and the quality factor Q_{me} and the transmissivity t_e are measured to ensure the measurement's consistency.

2.4 Experimental Uncertainties

Experimental uncertainties in the measurement of the absorption coefficient (α) of gaseous SO_2/CO_2 mixture can be divided into two major categories: Uncertainties due to noise and instrumental uncertainties. In the case of instrumental uncertainties, most of the uncertainties stem from the accuracy of the equipment used to measure the bandwidth of the resonance (δf). Additional instrumental uncertainties include the measurement accuracy of the resonant frequency (f_o), and the accuracy of measuring the transmissivity (t). For the case of bandwidth, center frequency, and trasmissivity measurement,

accuracies of ± 5% were achieved and are included in the error bars in Figures 2.4,2.5, and 2.6.

Additional instrumental uncertainties result from asymmetry of the resonances, uncertainties in the measured total pressure, temperature uncertainties and uncertainties in mixing ratio. In the case of resonance asymmetry (resonance asymmetry results from the interference of neighboring resonances with the desired resonance), we have found that the absorption coefficients at 2.24 GHz and 94.1 GHz are not greatly affected by the asymmetry effect. In contrast, the asymmetry analysis seem to affect some of the results at 21.7 GHz and the resulting additional uncertainties have been added to the error bars in Figure 2.5. This asymmetry phenomenon can be also described by a quantity referred to as "finesse". The finesse is the ratio of the separation between neighboring peaks to the half power bandwidth of the resonance under consideration. For the case of the 2.24 GHz resonance, a finesse of 175 is obtained, at 21.7 GHz the finesse is equal to 52 while the finesse at 94.1 GHz is 115. Thus, at 21.7 GHz a low finesse number corresponds to a bigger asymmetry effect on the resonance under test.

In the case of pressure measurement, the accuracy was limited by the quality of the pressure gauge used in the experiment which had a ± 0.2 atm accuracy throughout its

usable range. Temperature accuracy was approximately ± 1 C throughout the usable range of the thermometer. However, the uncertainties in the mixing ratio of the gaseous mixture have been determined using an expression developed by Spilker (1990), and the accuracies of the two pressure gauges. (Note that during the mixing process, care was taken as to minimize any fluctuation in the system's temperature.) We have determined the resulting worst case uncertainty for the mixing ratios used in the measurements. For the case of the absorptivity measurements at 2.24 and 21.7 GHz, the mixing ratio was 8.33 % (by number) with 7.89 % and 8.77 % as lower and upper limits respectively. For the measurements at 94.1 GHz, a 6.25 % mixing ratio is used with 5.12 % and 7.38 % as lower and upper limits.

The uncertainties from noise in the system are primarily due to the large insertion loss of the cavities used in the system (required to keep the quality factor high). To account for noise uncertainties, repeated measurements were conducted at each particular pressure. As a result, statistics were developed to account for the variations of Q, t, and δf which were subsequently used to develop 1 sigma error bars for the absorption coefficient of SO_2.

2.5 Experimental Results and Theoretical Characterization of the SO_2 Opacity

Measurements of the absorption coefficient of SO_2/CO_2 gas mixture as function of pressure have been conducted at 2.24, 21.7 and 94.1 GHz. Graphical representations of the measured data are shown in Figures 2.4, 2.5, and 2.6 (note that in Figures 2.5 & 2.6, the abscissae of the points have been offset from the true pressure value to avoid overlap of the symbols and error bars).

In addition, these figures show the computed absorptivity of gaseous SO_2 based on the Van Vleck-Weisskopf formalism where the absorption (α) at frequency f of SO_2 in a CO_2 atmosphere can be expressed for each rotational resonant line as per Townes and Schawlow (1955),

$$\alpha=\alpha_{max} f^2 \nu_o^{-2} \delta\nu^2\left[((\nu_o-f)^2+\delta\nu^2)^{-1}+((\nu_o+f)^2+\delta\nu^2)^{-1}\right] \qquad (2.7)$$

where f is the frequency of interest, α_{max} is the absorption at line center (line center intensities were obtained from the GEISA (Gestion et Etude des Spectroscopiques Atmospherique, Chedin et al., 1982) catalog), ν_o is the resonant line frequency, and $\delta\nu$ is the line width. In our calculation, we used a line width of $\delta\nu_{SO_2/CO_2}$= 7 MHz/Torr (as per Steffes and Eshleman (1981)) for all 1200 resonant lines employed in the model and a line width of $\delta\nu_{SO_2/SO_2}$= 16 MHz/Torr for the self

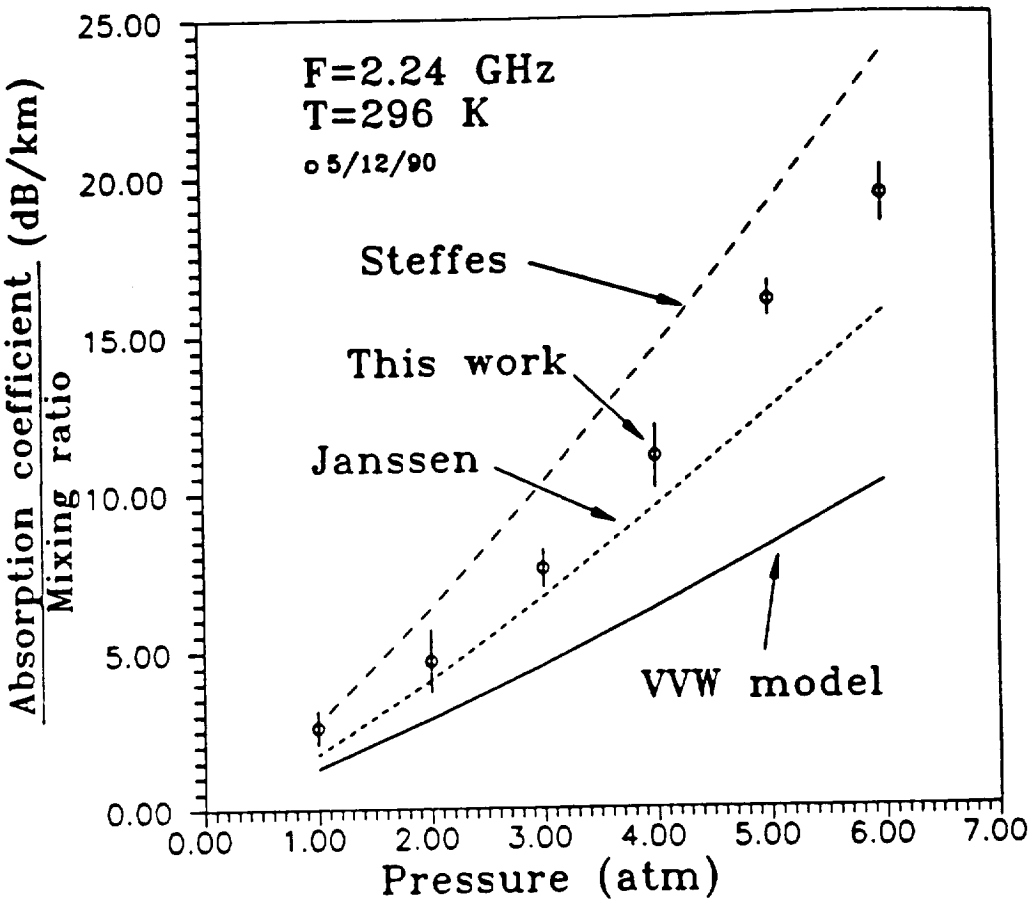

Figure 2.4 Measured absorption coefficient (normalized by mixing ratio) of gaseous SO_2/CO_2 mixture at 2.24 GHz. Measurements were made at 296 K with an SO_2 density of 8.33%.

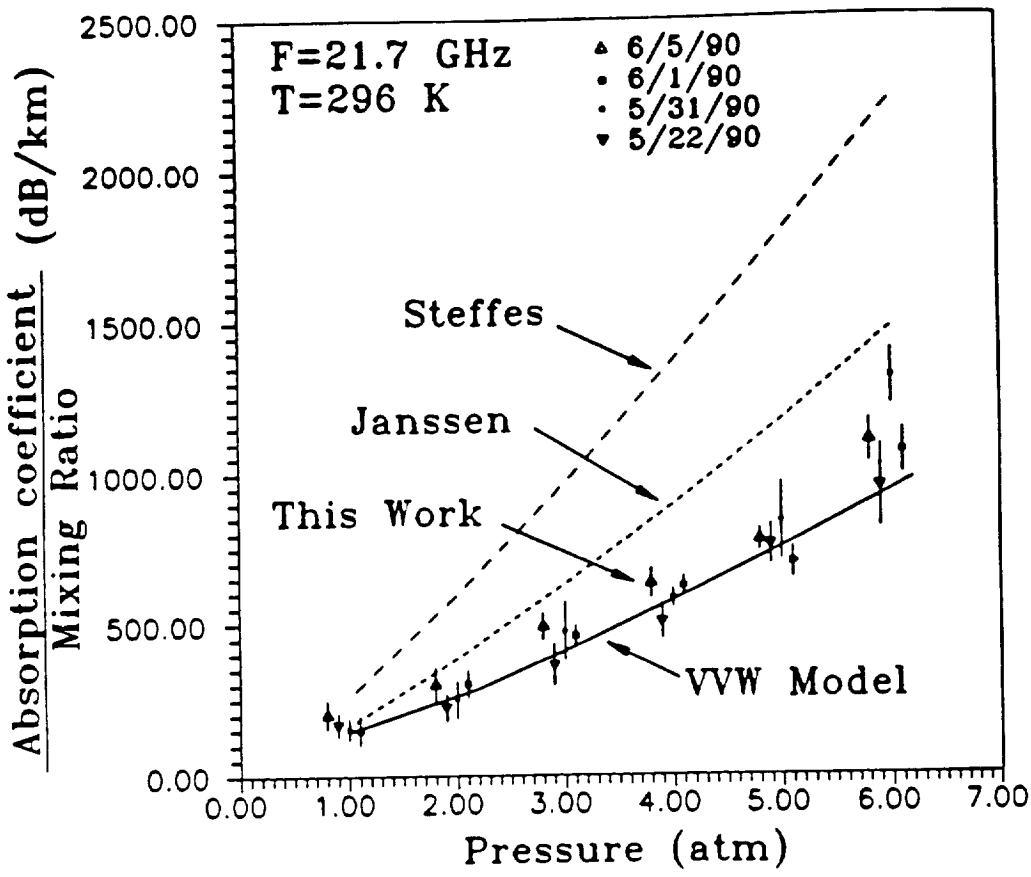

Figure 2.5 Measured absorption coefficient (normalized by mixing ratio) of gaseous SO_2/CO_2 mixture at 21.7 GHz. Measurements were made at 296 K with an SO_2 density of 8.33%.

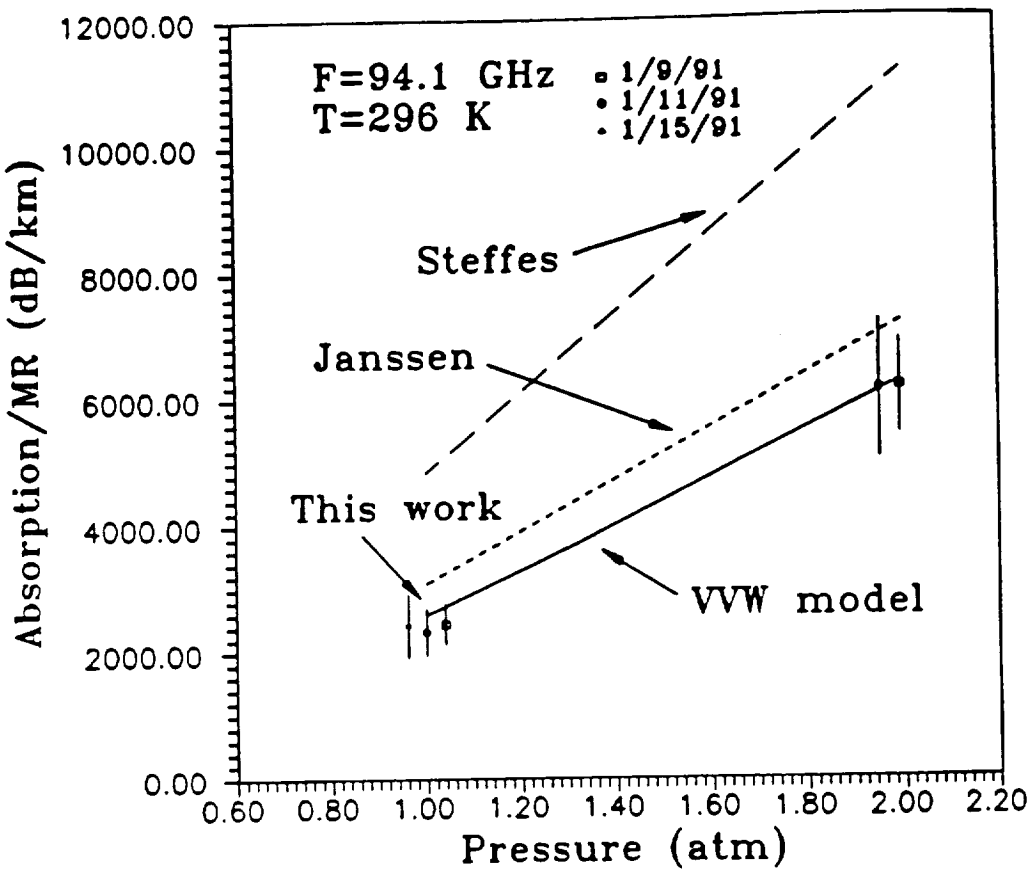

Figure 2.6 Measured absorption coefficient (normalized by mixing ratio) of gaseous SO_2/CO_2 mixture at 94.1 GHz. Measurements were made at 296 K with an SO_2 density of 6.25%.

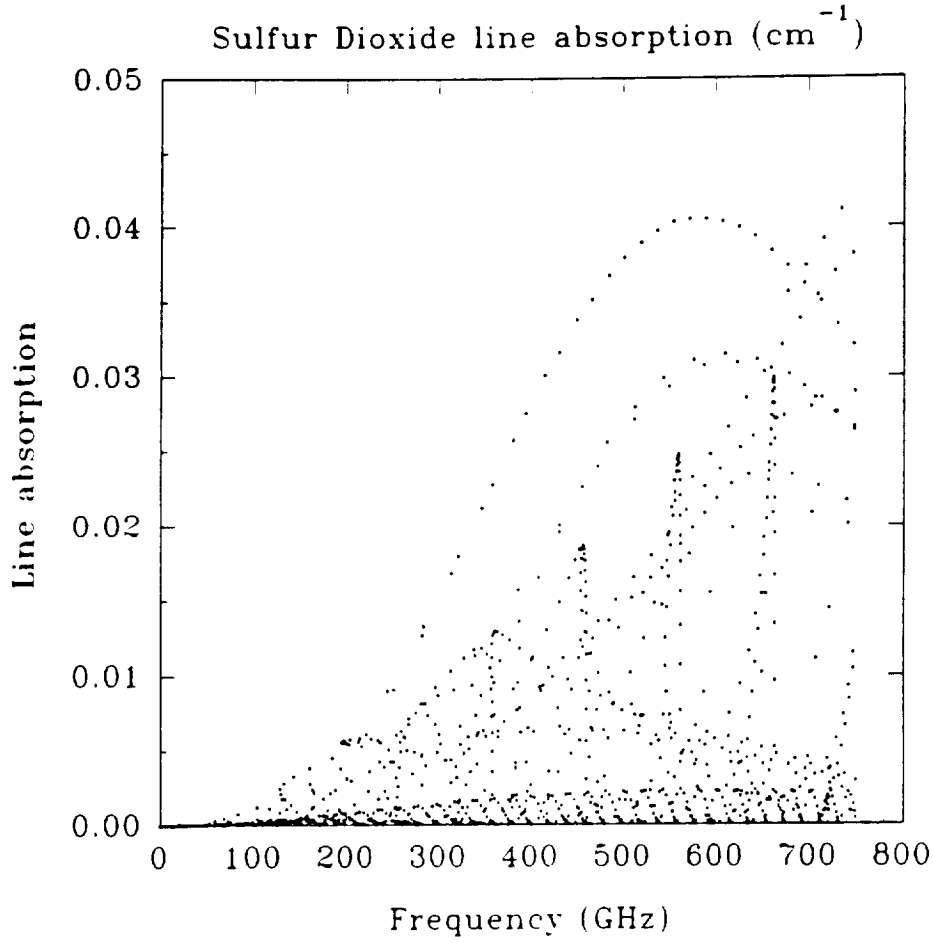

Figure 2.7 Representations of the absorption of sulfur dioxide at line centers.

broadening parameter of SO_2. Thus our VVW formalism includes the effects of both CO_2 broadening and SO_2 self-broadening when computing the absorption from the SO_2/CO_2 gaseous mixture, i.e., $\delta\nu = (\delta\nu_{SO_2/CO_2})\,P_{CO_2} + (\delta\nu_{SO_2/SO_2})\,P_{SO_2}$ where P_{CO_2} and P_{SO_2} are respectively the partial pressures of gaseous CO_2 and SO_2. A graphical representation of the 1200 SO_2 resonant lines used in our model is shown in Figure 2.7 for frequencies below 750 GHz.

All of our measurements of the absorptivity of gaseous SO_2 in a CO_2 atmosphere were performed at 296 K. As a result, we cannot experimentally determine the dependence of SO_2 opacity on temperature. However, we have determined a theoretical dependence of SO_2 opacity on temperature. This theoretical dependence (for the absorption at line center) is based on the work of Kolbe et al. (1976) in addition to the expected temperature dependence of the broadening parameter (see Townes and Schawlow, 1955). As a result, we expect the temperature dependence to be within the range of $T^{-4.0}$ to $T^{-3.0}$ (where $T^{-3.0}$ dependence is obtained for the absorptivity at line center and $T^{-4.0}$ is the temperature dependence very far from the line center). Note that our temperature dependence is well within the limits of the temperature variation reported by Steffes and Eshleman (1981) where a temperature dependence of $T^{-3.1(-4.3/-2.5)}$ was experimentally determined .

A careful investigation of the results reported in Figure 2.4 shows that our measured data are consistent with the results previously reported by Steffes and Eshleman (1981) in that the measured opacity is at least 50 % larger than that computed from the Van Vleck-Weisskopf (VVW) formalism. This deviation may be due to employing the same pressure broadening coefficient for all resonant lines of SO_2 used in the VVW formalism. However, since there is no direct measurement of the broadening parameter for each of the resonant lines employed in our model, the usage of the same pressure broadening coefficient for all resonant lines seems to be appropriate for this calculation. It is also worth noting that a similar deviation between the measured and calculated absorptivity has been detected in the study of other gases; particularly in the case of water vapor, where a deviation between the Van Vleck-Weisskopf calculation and experimental data is obtained at the "wings" of the H_2O lines. However, the reasons for such deviations are not fully understood.

However, an investigation of the results reported in Figures 2.5 and 2.6 reveals that our results at the higher frequencies are quite consistent with the results obtained using the VVW formalism, and seem to deviate from the f^2 dependence proposed by other researchers. Note that in Figure 2.5, the measured absorption at 5/31/90 does not completely overlap with the other three data points. This can be due to

the uncertainty in the mixing ratio of each reported data point (i.e., each of the four reported data points did not necessarily have the same mixing ratio). Another possibility is an error in the measurement of the absorption at 5/31/90.

These results show that the f^2 dependence of the SO_2 opacity proposed by Janssen and Poynter (1981) and adopted by Steffes and Eshleman (1981) for frequencies below 100 GHz and pressures greater than 1 bar is not valid. Our results indicate that the absorptivity dependence of SO_2 is slower than the f^2 previously reported by other researchers. Our results also demonstrate that the Van Vleck-Weisskopf formalism can be used to accurately model the absorptivity of SO_2/CO_2 gas mixture in the millimeter-wavelength region. In short, our new data indicate that previous results overestimated the absorption of gaseous SO_2 in the atmosphere of Venus and hence underestimated the SO_2 abundance within the atmosphere of Venus.

In summary, this work has demonstrated that the Van Vleck-Weisskopf formalism appears to provide a good estimate of the absorption of a SO_2/CO_2 gas mixture at wavelengths below 1.5 cm in contrast to previous findings which suggested a f^2 dependence of the absorption coefficient. In addition, a new method of measuring the absorptivity of gas mixtures has been described which characterizes the effects of dielectric loading inside the resonator. This new method eliminates any

additional inferred opacity due to variation in the coupling coefficient of the cavity and "true dielectric loading" upon the introduction of the gas mixture. These results are incorporated into a radiative transfer model (see Chapter 6) to infer a new upper limit on the abundance of gaseous SO_2 in the atmosphere of Venus based on existing microwave (1.3 cm) emission measurements. They are also used in the determination of the effects of gaseous SO_2 on the millimeter-wave spectrum of Venus.

CHAPTER 3

LABORATORY MEASUREMENTS OF THE OPACITY OF LIQUID SULFURIC ACID AT MILLIMETER WAVELENGTHS

3.1 Motivation for Experiment

Recent observations of the millimeter wave emission of Venus at 112 GHz (2.6 mm) have shown a 30 K variation in the observed flux emission as reported by de Pater et al. (1991). These emission variations may be attributed to variations in the abundance of absorbing constituents present in the atmosphere of Venus. Such constituents include gaseous H_2SO_4, SO_2, CO_2, and liquid sulfuric acid in the form of cloud condensate. (Detailed discussions of the presence of these constituents are given by Steffes and Eshleman (1982), Steffes (1985), and Steffes et al. (1990)) Among these constituents, gaseous CO_2 is considered to be the primary absorber in the atmosphere of Venus (Barrett, 1961). However, the CO_2

abundance variability is considered to be low and therefore cannot account for the measured variability in emission.

Recently, de Pater et al. (1991) suggested that this variability may be attributed to the variation in the abundance of the cloud condensate (i.e, liquid sulfuric acid). In order to evaluate this hypothesis, a knowledge of the dielectric properties of liquid sulfuric acid at millimeter wave frequencies is needed so as to determine the expected absorptivity from such a condensate and hence its effect on the emission spectrum of Venus. Estimation of the absorption of this condensate at millimeter wave frequencies is not straightforward since no laboratory measurements of the dielectric constant of liquid H_2SO_4 at millimeter wavelengths has been previously reported. Although the dielectric properties of liquid H_2SO_4 at microwave frequencies have been measured (Cimino, 1982), a simple extrapolation of these results into the millimeter wave region can lead to ambiguous results.

This chapter describes the methodology and the results of laboratory measurements of the millimeter wave properties of liquid sulfuric acid at 30-40 and 90-100 GHz, using two different concentrations of liquid H_2SO_4. These are the first measurements of the millimeter wave dielectric properties of liquid sulfuric acid to be reported. A characterization of the

frequency dependence of the complex dielectric constant of liquid sulfuric acid is also developed.

3.2 Experimental approach

The approach used in the measurement of the dielectric properties of liquid sulfuric acid at millimeter wave frequencies is similar to that described by Moore et al. (1991). The experiment employs a free space transmission setup shown in Figure 3.1. In this configuration, the sample is placed between the transmitting and receiving antennas. Optical lenses are used to focus the energy on the surface of the sample. The lenses and the two horn antennas are mounted on an adjustable rail to allow accurate positioning of these components with respect to the sample. Although the sample holder is designed to rotate to change the incidence angle of the transmitted wave, our measurements were performed at a normal incidence with respect to the sample.

In order to use this system for measuring the complex dielectric constant of liquids, a suitable cell had to be designed to hold the liquid sulfuric acid and to minimize the reaction of the acid with the cell walls. A sketch of the cell used is shown in Figure 3.2, where the cell walls are manufactured from high-grade Teflon. The thicknesses of the cell walls and the liquid sample are chosen so that an adequate signal level can be measured by the receiving

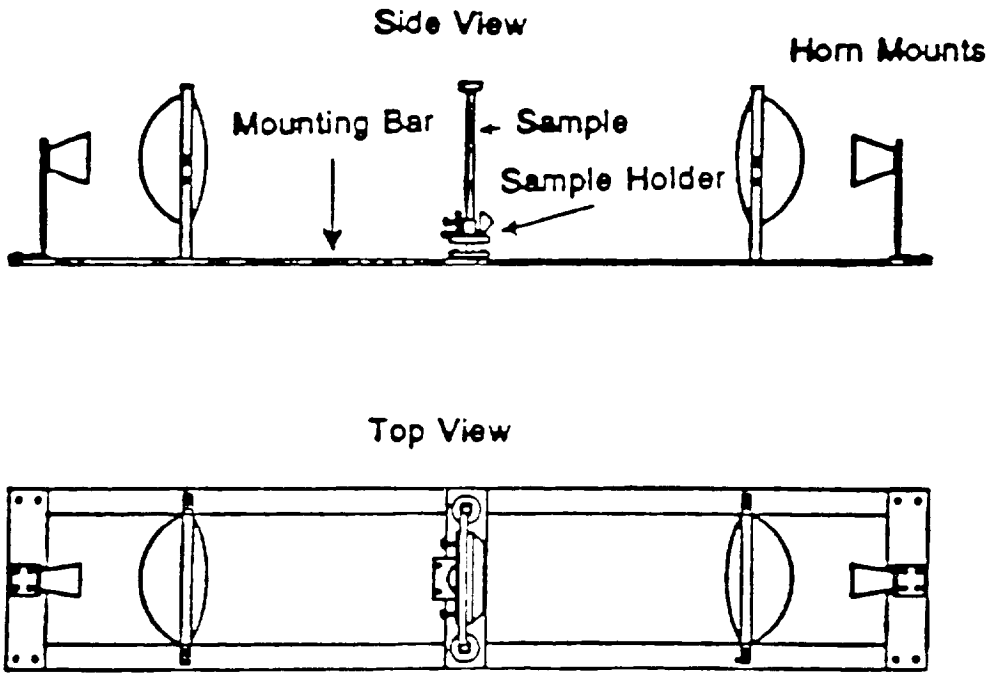

Figure 3.1 Sketch of the free space measurement system

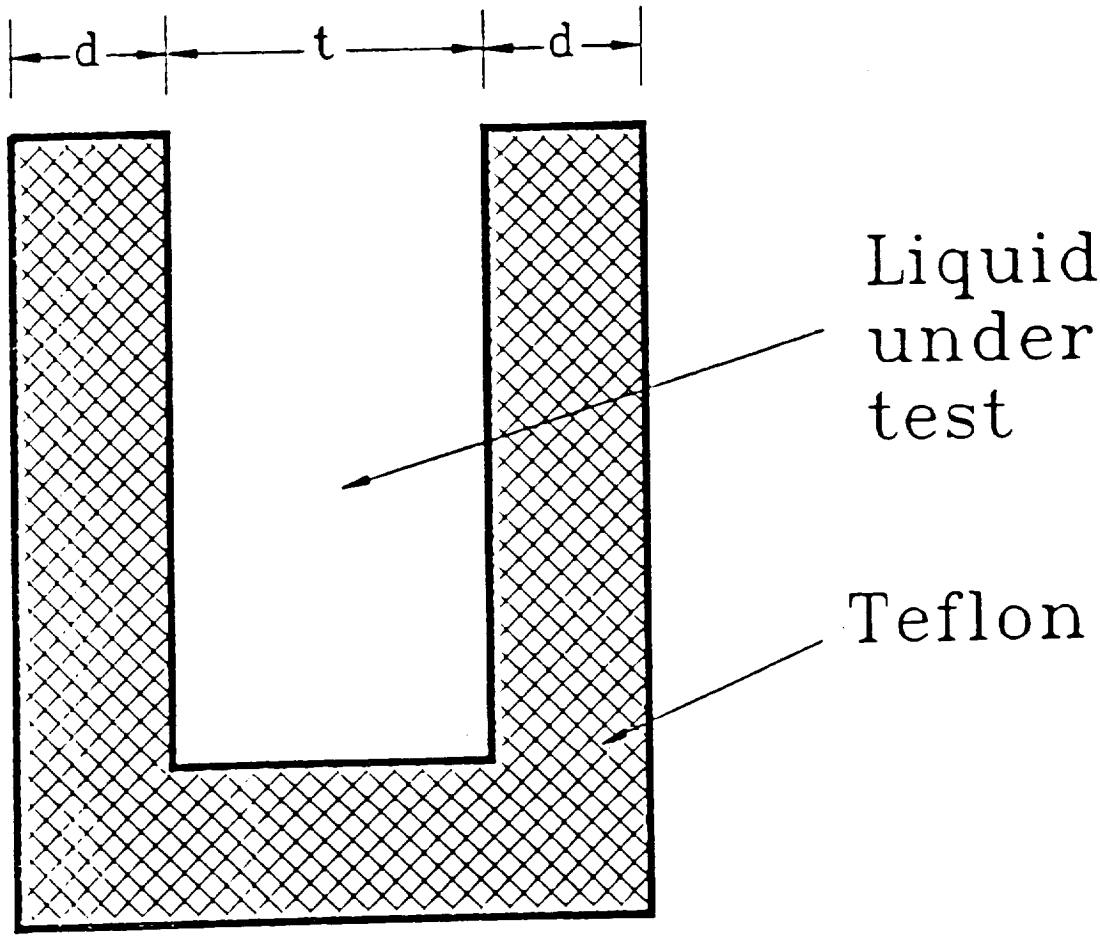

Figure 3.2 Sketch of the liquid cell used in the free space measurement of the dielectric constant of sulfuric acid.

antenna. A thickness of 1270μm was chosen for the walls and the liquid sample. In addition, the variation in the thickness of the cell walls is minimized in order to insure a uniform sample thickness (±25.0μm is achieved).

A block diagram of the electrical components used to measure the dielectric constant of liquid sulfuric acid between 90 and 100 GHz is shown in Figure 3.3. A similar system employing different antennas and lenses along with the appropriate power source is used for frequencies between 30.0 and 40.0 GHz. In both configurations, the system employs a digital computer to automate the measurement process and to control the Hewlett-Packard 8510 network analyzer used to measure the transmission coefficient of the liquid sample.

3.2.1 Experimental Procedure

The first step in the measurement process is the calibration of the system (without the sample). In addition, a check on the accuracy of the calibration process is performed by measuring the dielectric constant of a single sheet of material and comparing the measured values with published data. Once the calibration is satisfactory, the filled cell is mounted and measurement of the transmission coefficient of the liquid , $(S_{21})_{measured}$, as a function of frequency is performed. The results of such measurements are

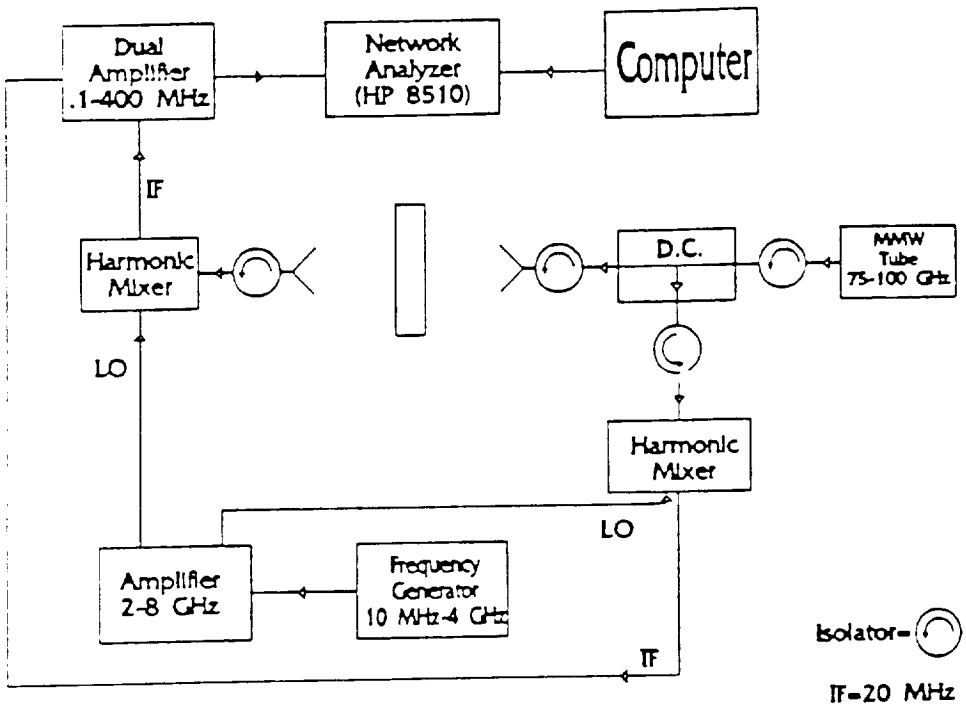

Figure 3.3 Block diagram of the free space measurement setup, as configured for measurements of the millimeter wave complex dielectric constant of liquid sulfuric acid.

then stored on a magnetic disk for later analysis.

As stated earlier, the measurement of the complex permittivity ($\epsilon_r = \epsilon'_r - j\epsilon''_r$) of liquid sulfuric acid was performed at two different frequency bands covering 30-40 and 90-100 GHz. The measurements of the complex dielectric constant of two samples of liquid sulfuric acid having 99% and 85% concentration by weight were performed. The latter concentration was equivalent to the estimated concentration of sulfuric acid in the clouds of Venus (Knollenberg and Hunten, 1980).

3.2.2 Determination of the Dielectric Constants

The determination of the complex dielectric constant of the liquid under test requires careful characterization of the geometry of the cell used and the determination of the theoretical transmission coefficient of that cell. A sketch of the liquid cell used in our setup is shown in Figure 3.4 where mediums I and III denote the teflon walls of thickness d, while medium II represents the liquid under test with thickness t. For the geometry shown in Figure 3.4, a composite scattering matrix representing the three media and the corresponding interfaces can be written as,

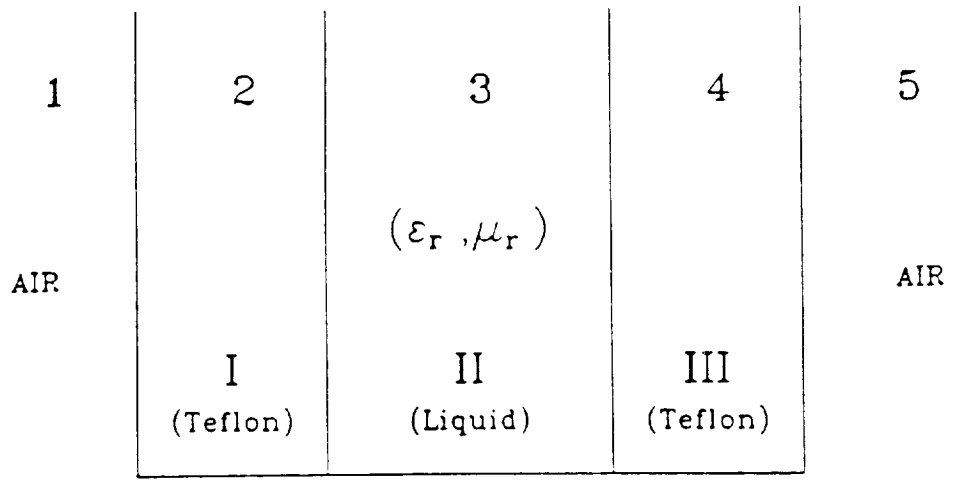

Figure 3.4 Detailed sketch of the liquid cell representing various media and their respective interfaces.

$$[S]_T = [S]_{12}[S]_I[S]_{23}[S]_{II}[S]_{34}[S]_{III}[S]_{45} \quad (3.1)$$

where $[S]_T$ is a 2x2 matrix relating the incoming and outgoing wave amplitudes in mediums 1 and 5 as shown Figure 3.4. Another important quantity is the propagation constant of an electromagnetic wave in medium i which can be expressed as

$$k_i = 2\pi f \frac{\sqrt{\mu_{ri}\epsilon_{ri}}}{c} \quad (3.2)$$

where f denotes the frequency, c is the speed of light in free space and ϵ_{ri} and μ_{ri} are the relative complex permittivity and permeability of medium i, respectively. These two complex quantities can be expressed as

$$\mu_{ri} = \mu'_{ri} - j\mu''_{ri} \quad (3.3)$$

and

$$\epsilon_{ri} = \epsilon'_{ri} - j\epsilon''_{ri} . \quad (3.4)$$

Since neither teflon nor liquid sulfuric acid possess magnetic properties, μ_{ri} is equal to μ_o.

The composite scattering matrix $[S]_T$ can then be written as a function of the propagation constants of the three media and their respective thicknesses. Since the dielectric constant of Teflon is well known ($\epsilon_{rI}=\epsilon_{rIII}=2.0-j.02$), $[S]_T$ can then be written as a function $\mathcal{F}$ such that

$$[S]_T = \mathcal{F}(k_{II}, t, d) \tag{3.5}$$

where k_{II} is the propagation constant in medium II as expressed in equation (3.2).

Once $[S]_T$ has been determined, one can solve for the propagation constant of medium II (k_{II}) by minimizing

$$(S_{21})_{measured} - (S_{21})_T \tag{3.6}$$

where $(S_{21})_{measured}$ is the measured transmission coefficient of the filled cell, while $(S_{21})_T$ is the theoretically calculated transmission coefficient obtained from the matrix $[S]_T$. This minimization process is carried out using a root finder program based on Newton's method and an initial guess for k_{II}. Once a satisfactory value of k_{II} has been reached in accordance with (3.6), the complex dielectric constant of the liquid under test can be determined using

$$\epsilon_{rII} = (k_{II}/k_o)^2 \tag{3.7}$$

where k_o denotes the propagation constant in free space.

3.3 Experimental Results

The measurement of the dielectric constant of distilled water at room temperature (T=296 K) was performed in order to check the accuracy of our measurement process. In this case,

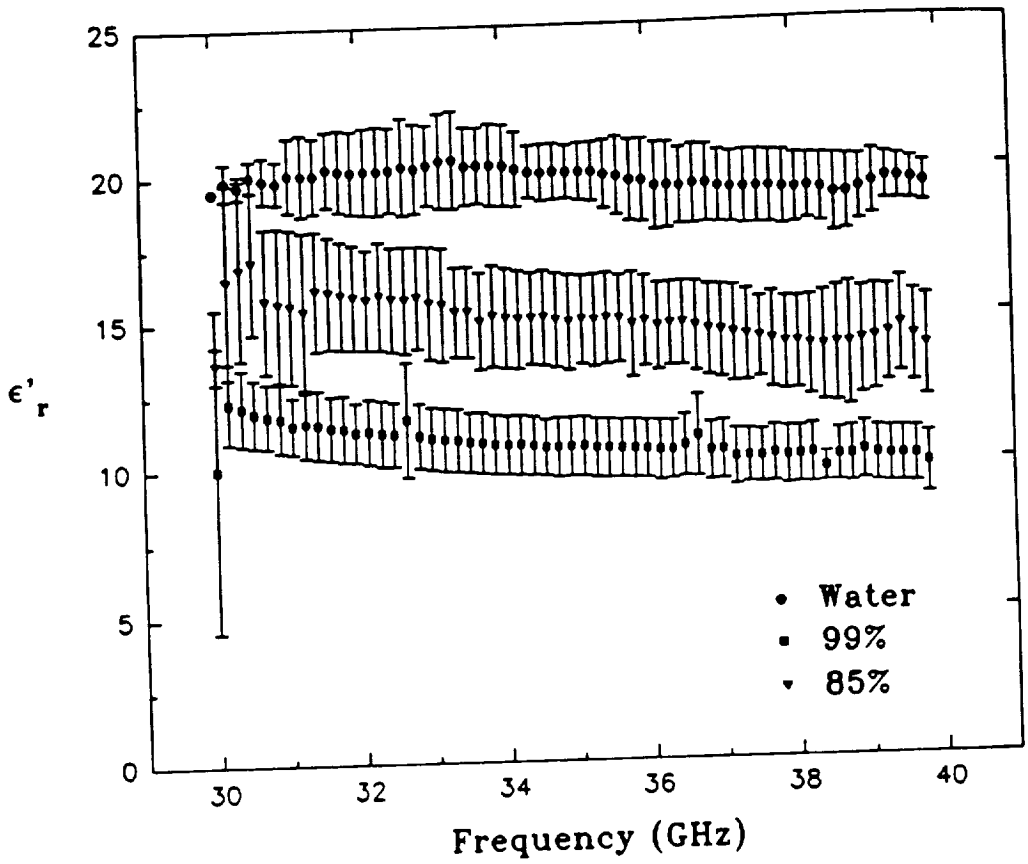

Figure 3.5 The measured real part of the complex dielectric constant of water and sulfuric acid for frequencies between 30 and 40 GHz at room temperature. Error bars indicate $\pm 1\sigma$ about the mean.

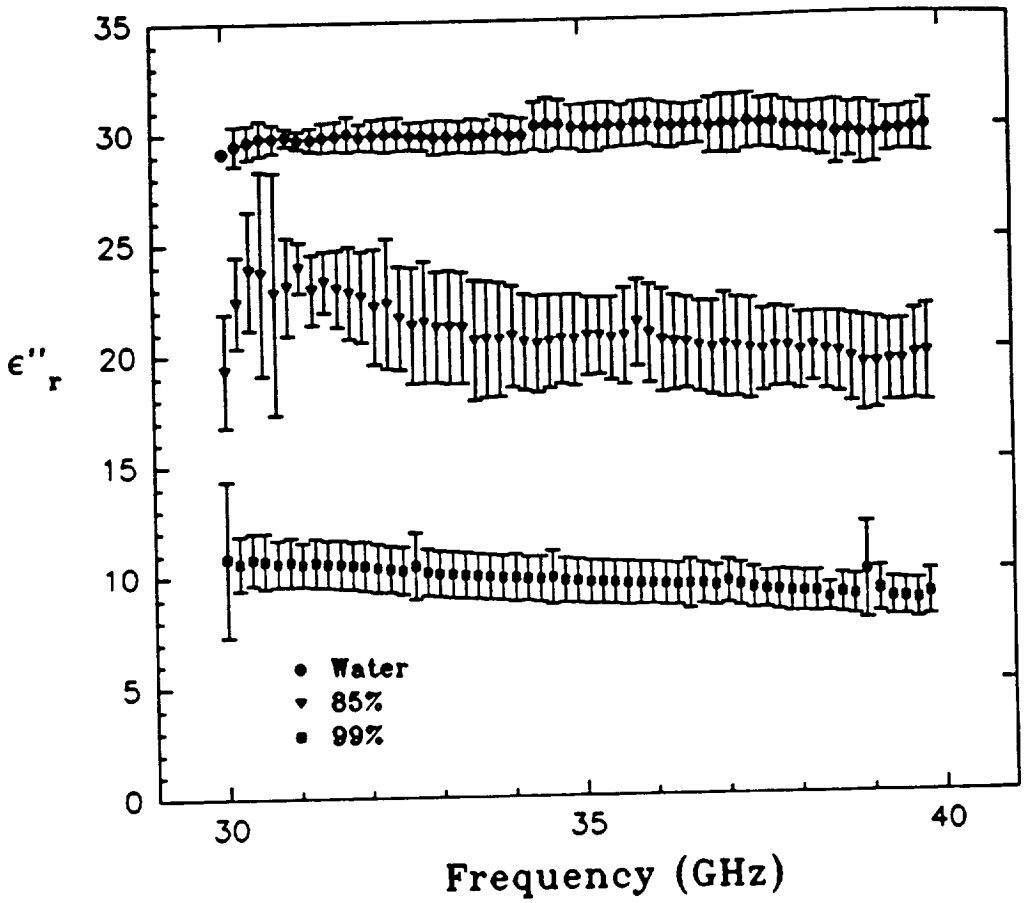

Figure 3.6 The measured imaginary part of the complex dielectric constant of water and sulfuric acid for frequencies between 30 and 40 GHz at room temperature. Error bars indicate $\pm 1\sigma$ about the mean.

a close agreement between our measurements and those previously reported (Oguchi, 1983) was obtained. The measured and reported complex dielectric constant of water are given in Table 3.1.

Table 3.1 Comparison between calculated and measured complex dielectric constant of water at 296 K.

	Measured		Reported*	
Freq (GHz)	ϵ'_r	ϵ''_r	ϵ'_r	ϵ''_r
32.0	21.6±2	29.9±.8	23.5	31.3
34.0	20.0±1.8	29.7±.82	22.0	29.9
36.0	19.4±1.49	29.0±1.02	21.7	28.6
38.0	19.2±1.18	28.5±1.06	20.5	28.0
92.0	7.78±.45	12.9±.23	8.2	13.2
94.0	7.79±.32	13.0±.3	8.0	13.0
96.0	7.6±.33	12.9±.28	7.8	12.92
98.0	7.58±.35	12.8±.28	7.62	12.73

* Oguchi, 1983.

The results of the measurements of the complex dielectric constant of liquid sulfuric acid at frequencies between 30.0 and 40.0 GHz are shown in Figures 3.5 and 3.6. Figure 3.5 shows the real part of the relative dielectric constant (ϵ'_{rII}) as a function of frequency for 99.0% and 85.0% concentrations (by weight) of sulfuric acid in addition to ϵ'_{rII} of water at

room temperature. Figure 3.6 shows the measured imaginary part of ϵ_{rII} (ϵ''_{rII}) as a function of frequency for the same liquids.

Similarly, the results of the measurements of the complex dielectric constant at 90.0-100.0 GHz are shown in Figures 3.7 and 3.8. The error bars shown in these four figures represent $\pm 1\sigma$ variations in the calculated values of ϵ'_{rII} and ϵ''_{rII} resulting from uncertainties in the thickness t of ± 25.0 μm. Hence these error bars do not include uncertainties due to instrumental errors which are of the order of an additional ±3% of the reported mean values. (The variation in the size of the error bars as function of frequency may be due to errors in the convergence of the root finder program used to determine the complex dielectric constant.)

3.4 Theoretical Characterization of the Dielectric Constant of Liquid Sulfuric Acid (H_2SO_4) at Millimeter-Wavelengths

In order to investigate the effects of cloud condensates on the millimeter wave emission of Venus, a knowledge of the complex dielectric constant of liquid sulfuric acid is necessary over a wider frequency range. Although our measurements were performed over a relatively narrow frequency range (i.e., 30-40 and 90-100 GHz), a theoretical characterization of the dielectric constant at other wavelengths can be performed. Brand et al. (1953) measured the

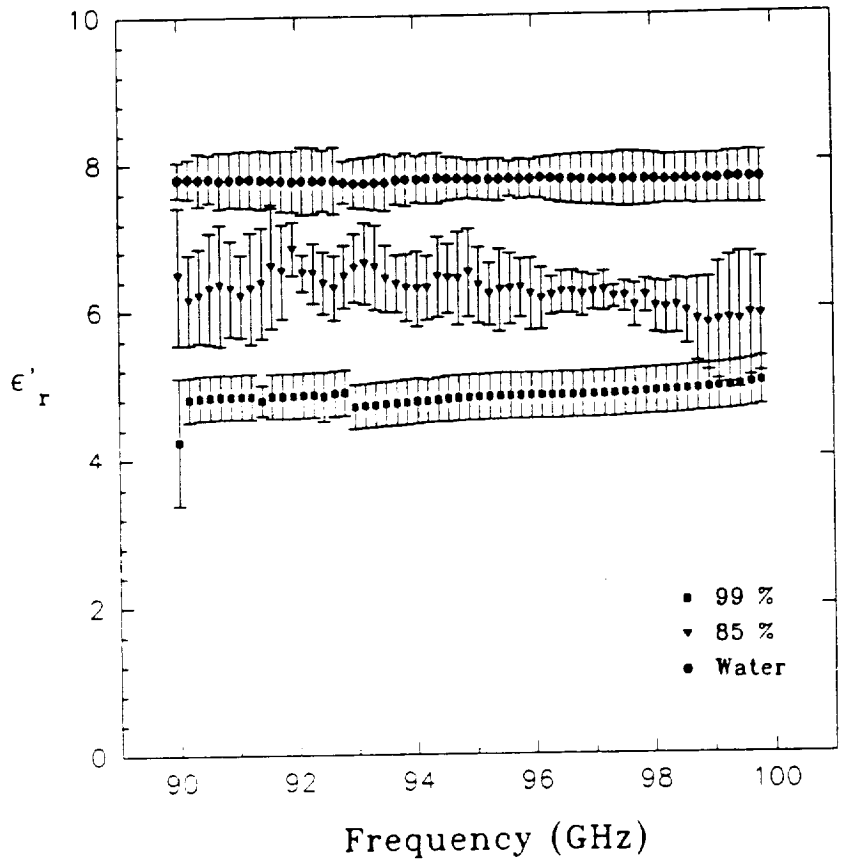

Figure 3.7 The measured real part of the complex dielectric constant of water and sulfuric acid for frequencies between 90 and 100 GHz at room temperature. Error bars indicate $\pm 1\sigma$ about the mean.

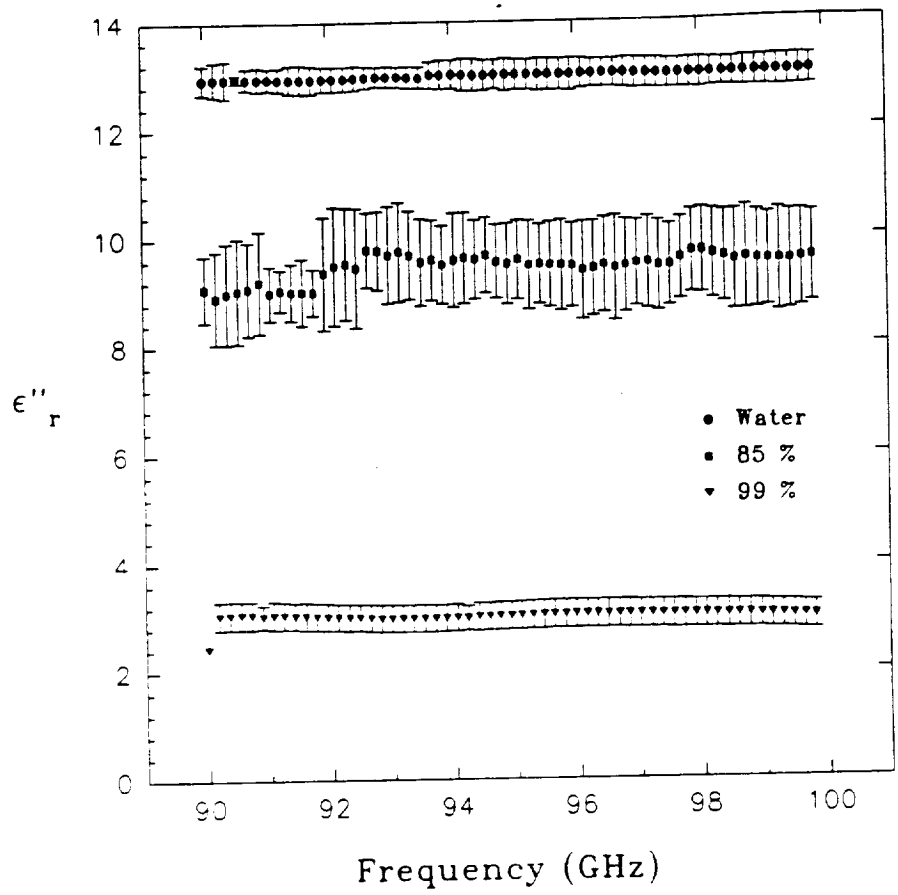

Figure 3.8 The measured imaginary part of the complex dielectric constant of water and sulfuric acid for frequencies between 90 and 100 GHz at room temperature. Error bars indicate ±1σ about the mean.

dielectric constant of liquid sulfuric acid with concentrations ranging between 96 and 100 % at microwave frequencies. A best fit expression for their data was also developed which is consistent with a model of the liquid having multiple relaxation times. As a result, we have developed a best fit model for our measured data based on a semi-empirical equation developed by Cole and Cole (1941);

$$\epsilon_r = \epsilon_{r\infty} + \frac{\epsilon_{rs} - \epsilon_{r\infty}}{1 + (jw\tau)^{1-\alpha}} \qquad (3.8)$$

where ϵ_r ($\epsilon_r = \epsilon'_r - j\epsilon''_r$) is the complex dielectric constant, $\epsilon_{r\infty}$ is the real part of the dielectric constant at $w=\infty$, ϵ_{rs} is the real part of ϵ_r at d.c., τ is the relaxation time (this relaxation time is defined as the time it takes the induced polarization to fall to 1/e of its maximum value after the removal of a constant applied electric field), and α is a constant between 0 and 1. Equation (3.8) can be rewritten as per King and Smith (1981) so that,

$$\epsilon'_r = \epsilon_{r\infty} + (\epsilon_{rs} - \epsilon_{r\infty}) \frac{1 + w\tau^{1-\alpha} \sin(\alpha \frac{\pi}{2})}{1 + 2(w\tau)^{1-\alpha} \sin(\alpha \frac{\pi}{2}) + (w\tau)^{2(1-\alpha)}} \qquad (3.9)$$

and,

$$\epsilon_r'' = (\epsilon_{rs} - \epsilon_{r\infty}) \frac{(w\tau)^{1-\alpha} \cos(\alpha \frac{\pi}{2})}{1+2(w\tau)^{1-\alpha} \sin(\alpha \frac{\pi}{2}) + (w\tau)^{2(1-\alpha)}} \quad . \qquad (3.10)$$

In order to employ the above two equations to model our measured data, the values of ϵ_{rs}, $\epsilon_{r\infty}$, τ and α must first be determined. For the case of ϵ_{rs}, its value is determined based on the static dielectric constant of water and 100 % sulfuric acid and the mole fraction of the concentration of interest. That is,

$$\epsilon_{rs} = \epsilon_{rs_{H_2O}} \frac{m_{H_2O}}{m_T} + \epsilon_{rs_{100\% H_2SO_4}} \frac{m_{H_2SO_4}}{m_T} \qquad (3.11)$$

where $\epsilon_{rs_{H_2O}}$ and $\epsilon_{rs_{H_2SO_4}}$ are the static dielectric constants of H_2O and 100% H_2SO_4 and m_{H_2O}/m_T and $m_{H_2SO_4}/m_T$ are the mole fractions of H_2O and H_2SO_4 respectively. For the 85% (by weight) liquid sulfuric acid used in our measurements, a value of 87.5 is obtained for ϵ_{rs} (ϵ_{rs}=80.4 for water and ϵ_{rs}=95.0 for sulfuric acid, see Brand et al., 1953). The other three parameters are determined by best-fitting the measured data with equations (3.9) and (3.10). As a result, our expression for the complex dielectric constant of 85% liquid sulfuric acid is given by,

$$\epsilon_r = 3.3 + \frac{(87.5-3.3)}{1+(jw(1.7x10^{-11})^{(1-.09)}} \quad . \qquad \textbf{(3.12)}$$

A comparison between our measured data and the theoretically determined complex dielectric constant of liquid sulfuric acid are shown in Figures 3.9 and 3.10. In Figure 3.9, ϵ'_r is plotted against frequency while Figure 3.10 represents ϵ''_r versus frequency for 85% liquid sulfuric acid. A closer examination of the two plots reveals that our data agrees well with the values obtained from the developed model. As a result, this new model will allow us to determine the expected dielectric constant of liquid sulfuric acid at frequencies other than the ones reported in this work. This new formalism will be later incorporated into a radiative transfer model to investigate the effects of liquid H_2SO_4 on the millimeter-wave emission of Venus.

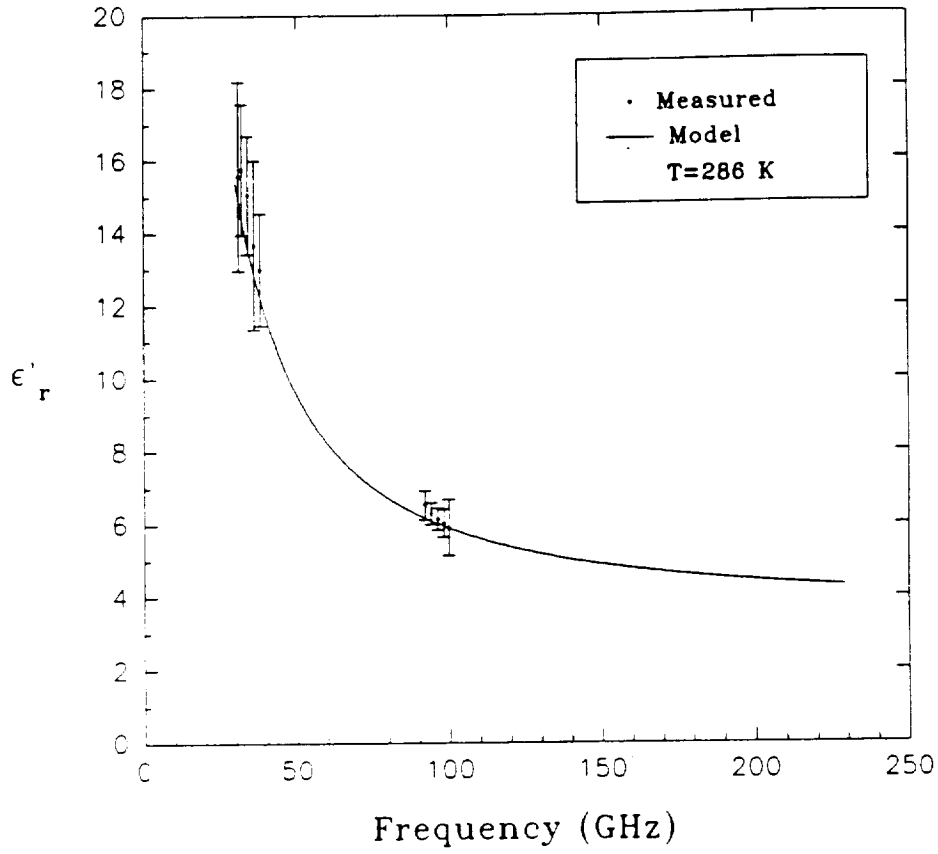

Figure 3.9 Comparison between the measured and calculated real part of the complex dielectric constant of liquid sulfuric acid at room temperature.

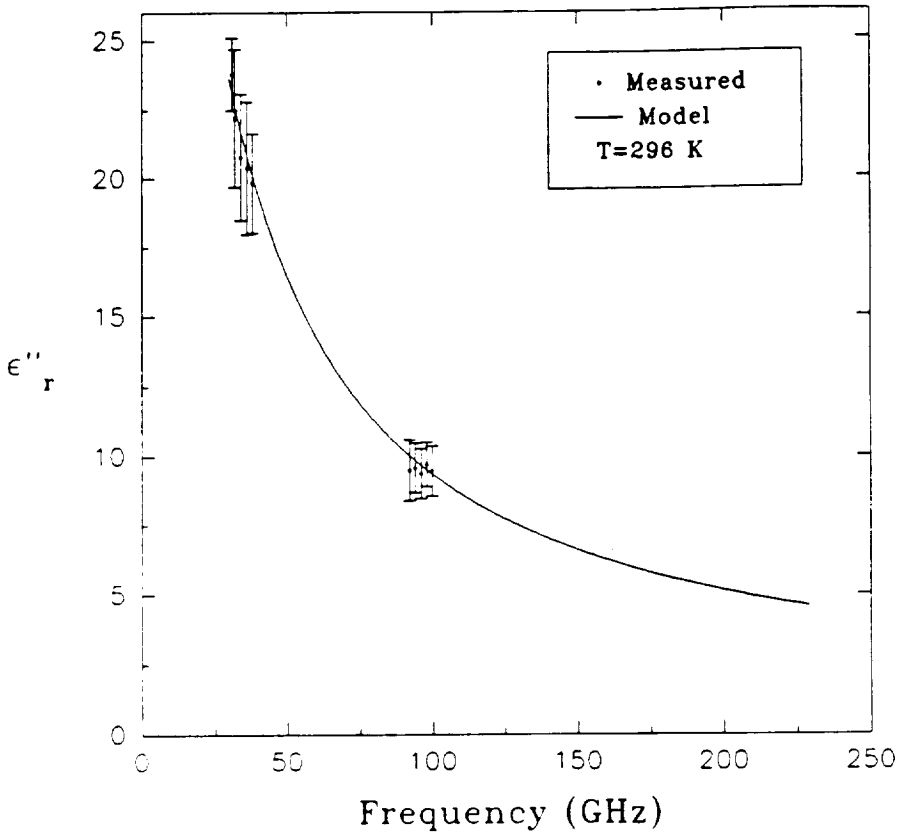

Figure 3.10 Comparison between the measured and calculated imaginary part of the complex dielectric constant of liquid sulfuric acid at room temperature.

CHAPTER 4

VAPOR PRESSURE OF GASEOUS SULFURIC ACID (H_2SO_4)

4.1 Introduction and Motivation

The laboratory measurement of the partial pressure of gaseous sulfuric acid in equilibrium with liquid H_2SO_4 is of great importance in modeling the abundance of gaseous sulfuric acid which is found in the middle atmosphere of Venus. First, the laboratory measurement of the vapor pressure of H_2SO_4 provides data needed for more accurate calibration of the microwave opacity measurements of gaseous H_2SO_4 made by Steffes (1985). As a result, the calibrated opacity can then be used to infer the expected abundance of gaseous sulfuric acid from measurements of microwave opacity in the atmosphere of Venus. In addition, the measurement of the partial pressure of gaseous H_2SO_4 is used to determine the saturation abundance of gaseous sulfuric acid thus providing an upper limit for the abundance of gaseous sulfuric acid in the atmosphere of Venus.

In the past, several researchers have attempted to determine the partial pressure of gaseous sulfuric acid but their results have not been consistent. For example, Esposito (1983) used the theoretically-derived vapor pressure model of Gmitro and Vermeulen (1964) for determining saturation abundances of gaseous H_2SO_4, SO_3, and H_2O (the vapors which accompany liquid sulfuric acid) in the Venus atmosphere. However, because laboratory measurements by Ayers et al. (1980) showed that the Gmitro and Vermeulen model overestimated the partial pressures of these constituents by a factor of about 10, Esposito simply scaled the Gmitro and Vermeulen results by that factor for his model. While laboratory data from Ayers et al. (1980) and Steffes (1985) showed that the vapor pressures of gases accompanying liquid sulfuric acid were indeed much lower than the Gmitro and Vermeulen model, neither was able to directly measure the partial pressure of the individual gaseous constituents. The Ayers et al. experiment measured the acidity of the vapor above 98% concentration of liquid sulfuric acid. However, the relative proportion of this acidity which was due to gaseous H_2SO_4 (as opposed to that due to SO_3) was calculated from the Gmitro and Vermeulen model and was not directly measured. Steffes (1985) measured volumes of liquid sulfuric acid solutions which vaporized to equilibrate an evacuated chamber in order to infer the vapor pressures of the accompanying

gases. However, he too used the theoretical results from Gmitro and Vermeulen in determining the relative proportion of gaseous H_2SO_4 and SO_3. Consequently, Steffes (1985,1986) estimated that about 47% of the gaseous H_2SO_4 that vaporized from a liquid sulfuric acid reservoir at 575 K dissociated to form gaseous SO_3 and H_2O. Although this estimate resulted in adequate results for an upper limit on gaseous sulfuric acid vapor pressure, a direct measurement of the dissociation factor (and hence the partial pressure of gaseous H_2SO_4) is necessary in order to unambiguously determine the abundances of these gases and thus to infer their microwave properties.

An apparatus capable of measuring the partial pressure of gaseous H_2SO_4 for temperatures between 480 and 610 K has been developed. Using this apparatus, we have been able to measure the partial pressure of gaseous sulfuric acid for two liquid concentrations (99% and 95.9% by weight). From the measured pressure we have been able to develop a new best-fit expression for the partial pressure of gaseous H_2SO_4 as a function of the temperature between 480 and 610 K. In addition, the resulting measurements have enabled us to compute the dissociation factor of gaseous H_2SO_4 (i.e. the percentage of gaseous H_2SO_4 that dissociated to form gaseous SO_3 and H_2O) along with a new expression for the equilibrium constant, K_p. This new value of the equilibrium constant is used with the results from Ayers et al. (1980) to determine

the partial pressure of H_2SO_4 for temperatures between 330 to 480 K (see appendix A).

The result of our measurements are used to infer the saturation abundance of gaseous sulfuric acid in the atmosphere of Venus. In addition, our results are applied to previous laboratory results (Steffes, 1985) so as to obtain a corrected expression for the microwave absorptivity (normalized by the number mixing ratio) of gaseous H_2SO_4 in a CO_2 atmosphere at 2.24 GHz. The results of the corrected microwave absorptivity in addition to the measured partial pressure of sulfuric acid are used by Jenkins and Steffes (1991) to determine the abundance of gaseous H_2SO_4 in the middle atmosphere of Venus.

A detailed description of the laboratory apparatus used in the measurement of the partial pressure of sulfuric acid and the measurement technique used are described in Appendix A.

4.2 Application of the Measured Vapor Pressure of H_2SO_4 to the Atmosphere of Venus

A direct application of the measured partial pressure of gaseous H_2SO_4 (see Appendix A) is the correction of previous laboratory measurements of the microwave absorptivity (normalized by the mixing ratio) of gaseous sulfuric acid in a CO_2 atmosphere at 2.2 GHz. The original data was reported by

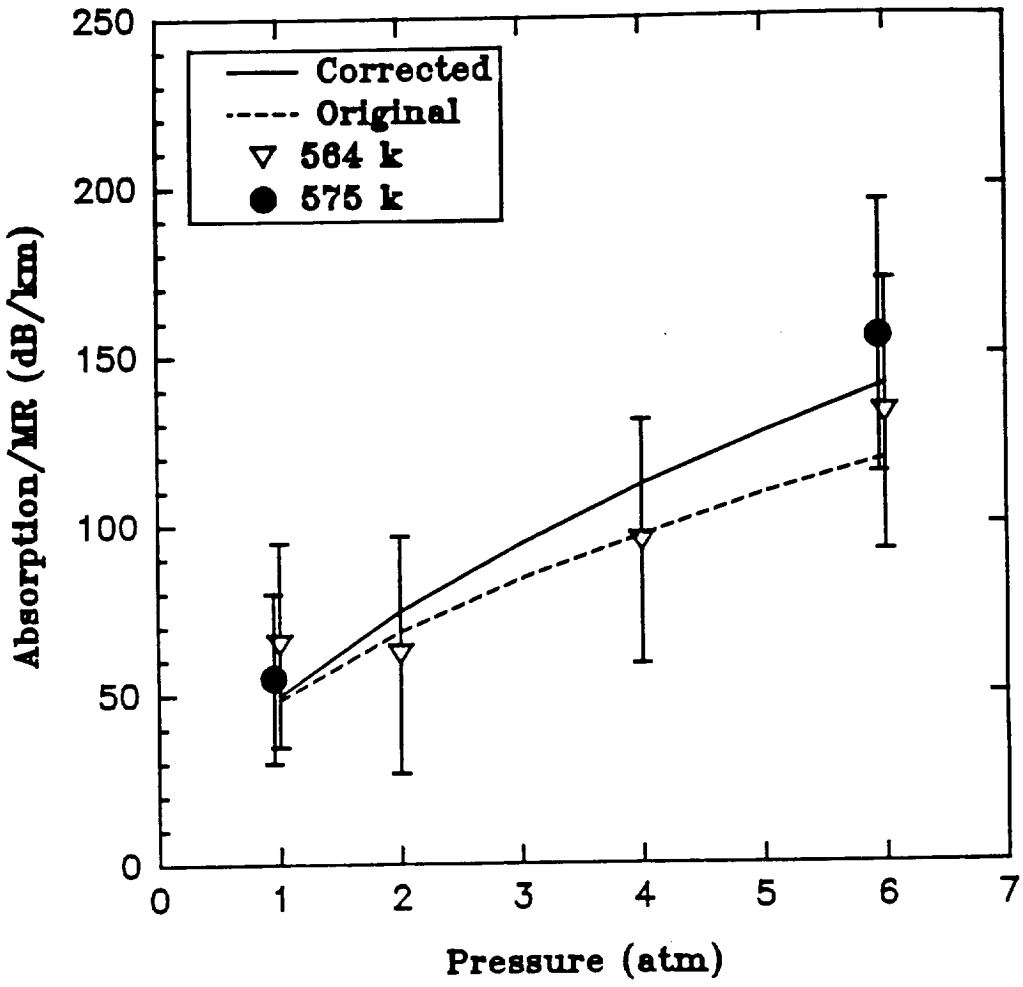

Figure 4.1 Corrected measurements of the microwave absorptivity of gaseous sulfuric acid at 2.24 GHz. Solid line represents a best-fit multiplicative expression for the absorptivity while the dashed line is the original expression (Steffes, 1985).

Steffes (1985) in which he used the partial pressure resulting from an assumed 47% dissociation factor when developing an expression for the microwave opacity of gaseous sulfuric acid. (His measurements were conducted at 575 and 564 K which are well within our temperature range). As a consequence of our direct measurements of the partial pressure of gaseous sulfuric acid, the absorptivity measured by Steffes (1985) has been readjusted to account for the variation of the dissociation factor with temperature. The resulting plot of the corrected absorptivity is shown in Figure 4.1 where the solid line represents a best-fit multiplicative expression for the absorptivity given as,

$$\alpha_{13}\ (dB\ km^{-1}) \simeq 9.25\times10^{9}\ q\ (\ P\ )^{.58}\ (\ T\ )^{-3} \qquad \textbf{(4.1)}$$

where q is the volume mixing ratio of gaseous sulfuric acid, P is the pressure in atm, and T is the temperature in Kelvins. The error bars shown in Figure 4.1 represent ± 1σ errors in the absorptivity measurements but do not include uncertainties in the mixing ratio.

Another important application of our results is shown in Figure 4.2. In this figure, the dashed line represents the saturation abundance of gaseous sulfuric acid based on our measurements of the partial pressure of H_2SO_4 and the pressure-temperature profile of Venus reported by Seiff et al. (1980). In addition, the solid line represents the abundance of

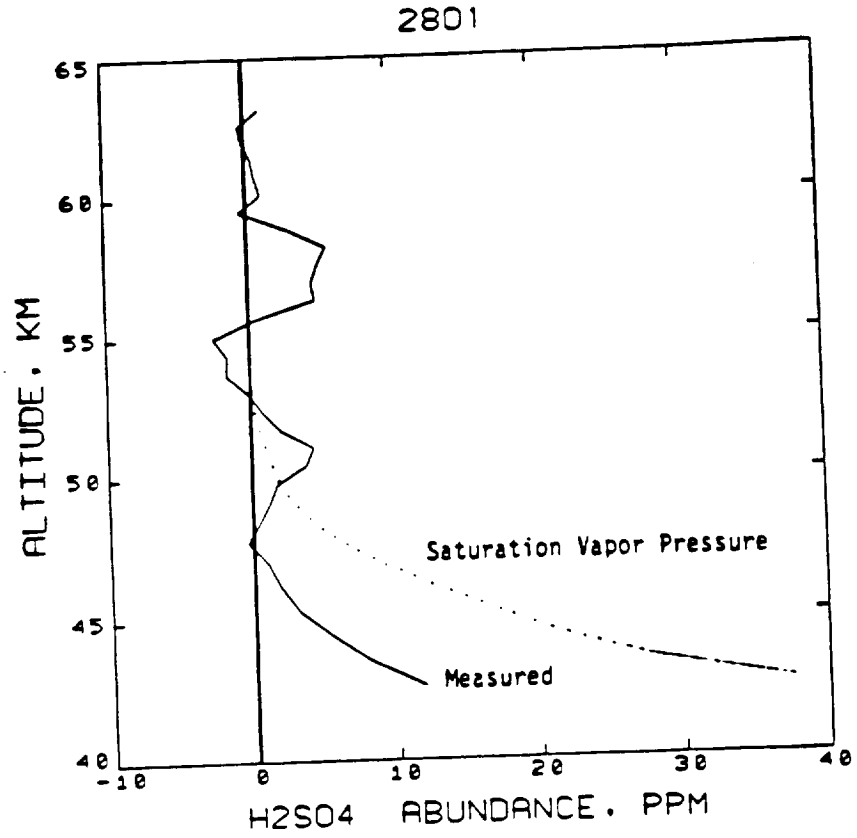

Figure 4.2 An abundance profile for gaseous sulfuric acid in the atmosphere of Venus after Jenkins and Steffes (1991). The dashed line represents saturation abundance of gaseous H_2SO_4 in the atmosphere of Venus.

gaseous H_2SO_4 in the Venus atmosphere inferred from a 13 cm absorptivity profile obtained from the Pioneer-Venus radio occultation studies of Jenkins and Steffes (1991), using our corrected expression for the 13 cm absorptivity of sulfuric acid (equation 4.1).

In short, our results have been used to correct previously reported measurements of the microwave absorption of gaseous H_2SO_4. This provides a more accurate result for the microwave absorption of sulfuric acid within the atmosphere of Venus. The resulting abundance profiles of gaseous sulfuric acid can then be used to study the effects of this gas on the chemistry and the millimeter-wave emission of Venus.

CHAPTER 5

MEASUREMENT OF THE OPACITY OF GASEOUS SULFURIC ACID (H_2SO_4) AT W-BAND (94.1 GHZ)

5.1 Motivation

As discussed in the previous chapters, a complete understanding of the millimeter-wavelength emission from Venus requires an accurate determination of the opacities of the major absorbers in the Venus atmosphere. Recent observations of the millimeter-wave emission from Venus at 112 GHz (2.6 mm) have shown significant variations in the continuum flux emission (de Pater et al., 1991) which may be attributed to the variability in the abundances of absorbing constituents in the Venus atmosphere. Such constituents include gaseous H_2SO_4, SO_2, and liquid sulfuric acid (cloud condensates). Recently, Fahd and Steffes (1991) have shown that the effects of liquid H_2SO_4 and gaseous SO_2 cannot completely account for this measured variability in the millimeter-wave emission of Venus.

To fully understand potential sources of this variation, one needs to study the effects of gaseous sulfuric acid on the millimeter-wave emission of Venus.

Unfortunately, little (if any) laboratory work has been performed to measure the opacity of gaseous H_2SO_4 at millimeter-wavelengths for Venus-like conditions. In addition, the simple extrapolation of the microwave opacity of H_2SO_4 measured by Steffes (1985,1986) to higher frequencies is not straightforward and could lead to erroneous results.

To investigate the role of gaseous H_2SO_4 in the atmosphere of Venus, we have measured the opacity of gaseous H_2SO_4 in a CO_2 atmosphere at 550, 570, and 590 K from 1 to 2 atmospheres total pressure at 94.1 GHz. This work represents the first time that a measurement of the millimeter-wave opacity of a H_2SO_4/CO_2 gaseous mixture has been conducted for Venus-like conditions. We have also developed a modeling formalism to calculate the expected opacity of this gaseous mixture at other frequencies based on our measured results and the results reported by Steffes (1985,1986). Comparisons between the measured and the theoretically derived opacities of H_2SO_4/CO_2 mixture are also presented.

5.2 Laboratory Configuration

The experimental system used to measure the millimeter-wave opacity of gaseous H_2SO_4 in a CO_2 atmosphere consists of two major subsystems: The planetary atmospheric simulator and the millimeter-wave subsystem as diagrammed in Figure 5.1.

The planetary atmospheric simulator subsystem consists of a glass cell (which contains the gaseous mixture), two pressure gauges, a thermocouple display unit, a CO_2 tank and an oil diffusion vacuum pump. In this subsystem, the glass cell (length=27") is placed into a temperature controlled oven with a maximum temperature of 600 K. The temperature of the oven is electronically controlled, with a temperature variation of less than ± 5 K. A calibrated thermocouple unit is inserted into the glass cell in order to display the system's temperature. Liquid sulfuric acid is deposited into a custom made flask prior to the start of the measurements. The pressure and vacuum status of the planetary atmospheric subsystem are monitored via two gauges. Gauge P (0-80 psig) with a display resolution of 1 psig and an accuracy of ± 3 psig is used to measure the internal pressure of the glass cell resulting from the introduction of the H_2SO_4/CO_2 gaseous mixture into the system. Gauge V is a thermocouple vacuum gauge that is able to measure pressures between 0-800 Torr with 1 Torr display resolution and an accuracy of 1% of full scale. It is used to monitor the vacuum status of the glass

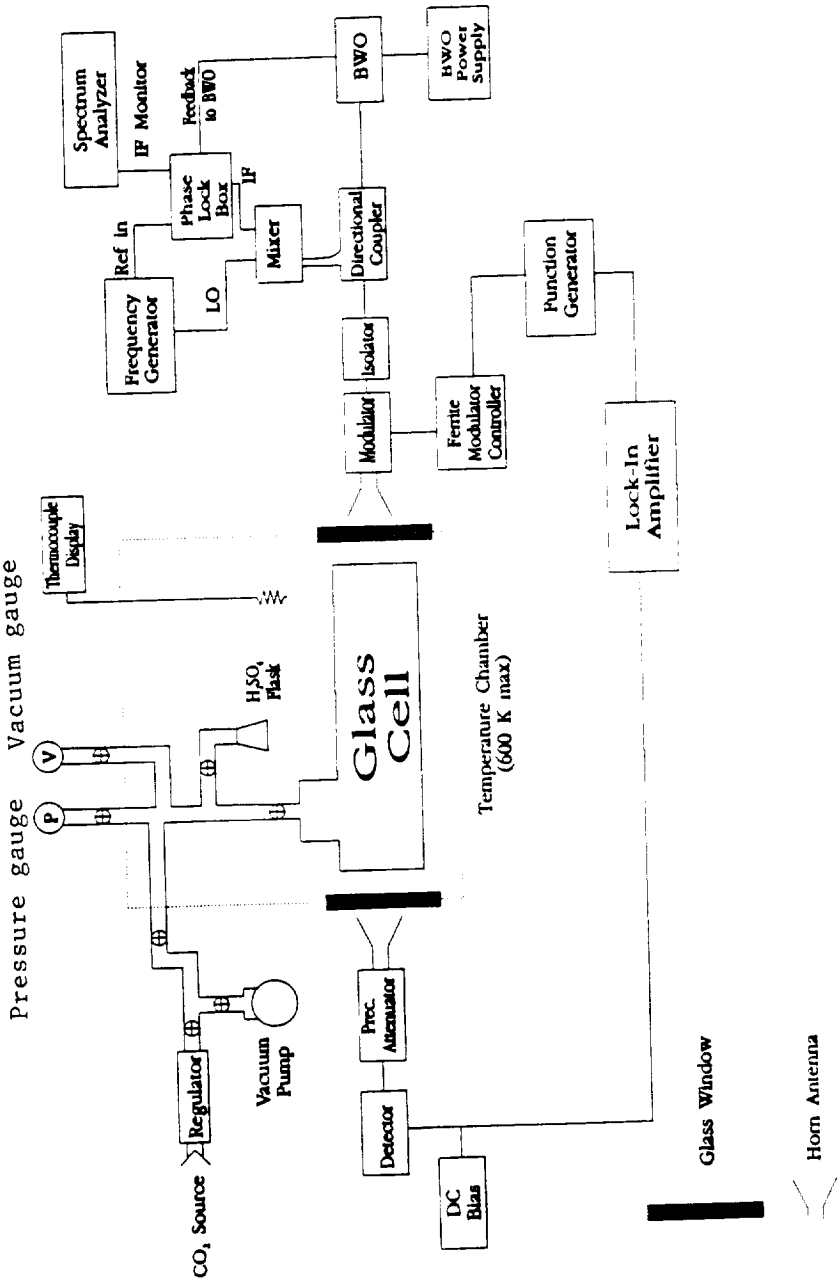

Figure 5.1 Block diagram of the atmospheric simulator as configured for measurements of the millimeter-wave absorption of gaseous H_2SO_4 under Venus atmospheric conditions at 94.1 GHz.

cell. Two Pyrex-66 glass windows are installed on the two sides of the oven to allow the propagation of the electromagnetic energy. A network of 3/8" stainless-steel tubing and valves connect the components of the planetary atmospheric subsystem so that each component may be isolated from the system as necessary. An oil diffusion pump is used to evacuate the glass cell prior to the introduction of the gaseous mixture.

The millimeter-wave subsystem (also shown in Figure 5.1) consists of a Siemens backward wave oscillator (BWO) powered by a MicroNow power supply. The BWO is electrically isolated from the waveguide apparatus by use of a polyester sheet and nylon screws on the waveguide flange of the BWO. (this is necessary to insure phase locking stability). Enroute to the glass cell, the signal is first sampled by a 10dB directional coupler. The sampled signal passes into a harmonic mixer as part of the phase locking system. The majority of the signal goes on through an isolator, which prevents reflections to the BWO, and is then electronically chopped by a ferrite modulator before entering the cell. The received power is detected by a schottky barrier point contact diode detector at 94 GHz. Power changes are measured as voltage changes at the detector. In order to give the detector the most linear response, the diode is biased with a current of 10 mA. The detector's output is measured with a lock-in amplifier where the modulation

reference comes from a function generator which drives the ferrite switch. The modulation frequency is 100 Hz. The output of the lock-in amplifier is fed into a digital voltmeter.

Phase locking stabilizes the frequency output of the BWO. The -10dB port of the directional coupler feeds the BWO output into the harmonic mixer where it is heterodyned with the local oscillator (LO). A synthesized signal generator (2-18 GHz) serves as the LO and as the reference signal for the phase-locked loop. The intermediate frequency (IF) from the mixer is fed into the phase detector. The phase-locked loop functions only when the LO harmonic is below the BWO frequency, i.e., setting the LO to 9.368 GHz gives 9.368 GHz x 10= 93.680 GHz + 420 MHz IF = 94.1 GHz. An IF monitor output on the phase detector allows viewing the locked waveform with a spectrum analyzer.

In order to minimize the effect of any reflections from the cell wall, the radius of the cell must be chosen greater than the radius of the first Fresnel zone (the Fresnel zone is defined as that volume surrounding a ray path through which another ray can travel and arrive at the receiver having travelled no more than 1/2 wavelength farther than the primary ray; Bullington, 1957). Thus, it follows that

$$R_c > \left[\frac{\lambda r}{2}\right]^{1/2} \quad , \qquad (5.1)$$

where R_c is the radius of the cell, λ is the wavelength (in this case 3 mm), and r is the separation distance between the two horns (1 m). Using the above equation, a minimum cell radius of 1.52" is required. A glass cell with a radius of 2.5" is used in the experimental setup.

5.2.1 Measurement Procedure

The measurement of the millimeter-wave opacity of gaseous H_2SO_4/CO_2 can be summarized as follows: The oven is first heated to the desired temperature. Once the desired temperature is reached, the glass cell is evacuated. By using gauge V as a vacuum monitor, we are able to check the status of the glass cell in order to insure that no major leaks are present. Although the chamber is not leak proof, we are able to maintain a leak rate within the system of less than 1 Torr/hour. The variable attenuator is then set to a predetermined attenuation and the resulting detector voltage is recorded. (The millimeter-wave subsystem is usually turned on for a period of ten hours prior to the beginning of the experiment. This extended time period allows the BWO to warm up and become more stable.) Next, the valve connecting the H_2SO_4 flask and the glass cell is opened allowing the sulfuric acid vapor to equilibrate with the evacuated glass cell. Once

equilibrium is reached, the flask's valve is closed and a visual check is made to verify that the remaining liquid acid is clear. Gaseous CO_2 is then introduced in the system at a slow rate so as not to cause any condensation. When the total internal pressure (measured by gauge P) reaches 2 atm, the CO_2 tank is shut off and the two gases are allowed to mix for a specified time period. The attenuation on the variable attenuator is then decreased until the output voltage is equal to the detector voltage of the evacuated glass cell. The opacity of the gaseous mixture can then be inferred from the change in the calibrated attenuator setting. The total internal pressure is then reduced to 1 atm and the measurement process is repeated. This approach has the advantage that the same gas mixture is used for the measurement at various pressures (at each temperature point). Thus, even though some uncertainties may exist due to the mixing ratio of the initial mixture, the mixing ratios at subsequent pressures will be the same, and the uncertainties for any pressure dependence will only be due to the accuracy limits of the absorptivity measurements and not to uncertainties in the mixing ratio.

5.3 Experimental Uncertainties

In general, the main source of experimental uncertainties in the transmission measurements are the fluctuation in the output power of the source. However, our system is phase

locked so as to minimize frequency and output power deviations. Frequency stabilization due to the phase locking system is approximately ± 20 KHz and power variation is less than ± .02 dB. In order to incorporate the effect of frequency and power fluctuation in our error bars, two measurements are taken for each data point and statistics are developed to compute the 1 σ variation in the measured absorptivity (the number of data points collected was limited due to the availability of some of the equipment).

Additional instrumental uncertainties include uncertainties in the measured pressure and temperature. In the case of pressure measurements, the accuracy was limited by the quality of the two pressure gauges used. The 0-800 Torr gauge has an accuracy of 1% of the full scale while the 0-80 psig gauge has an accuracy of ± 3 psig. The temperature accuracy of the thermocouple used was ± 5 K (temperature uncertainty is shown as horizontal error bars in Figure 5.2). The accuracy of the variable attenuator is also incorporated in our total uncertainties. The uncertainties due to the mixing ratio have been determined for the three temperatures used in our measurements. Using the expression developed by Spilker (1990) for mixing ratio accuracy, mixing ratios of 1.25% ± 0.13% ,0.87% ± 0.087% and 0.59% ± 0.06% are obtained at 590, 570, and 550 K respectively (in this calculation the partial pressure of H_2SO_4 is obtained using equation (5.2)). These

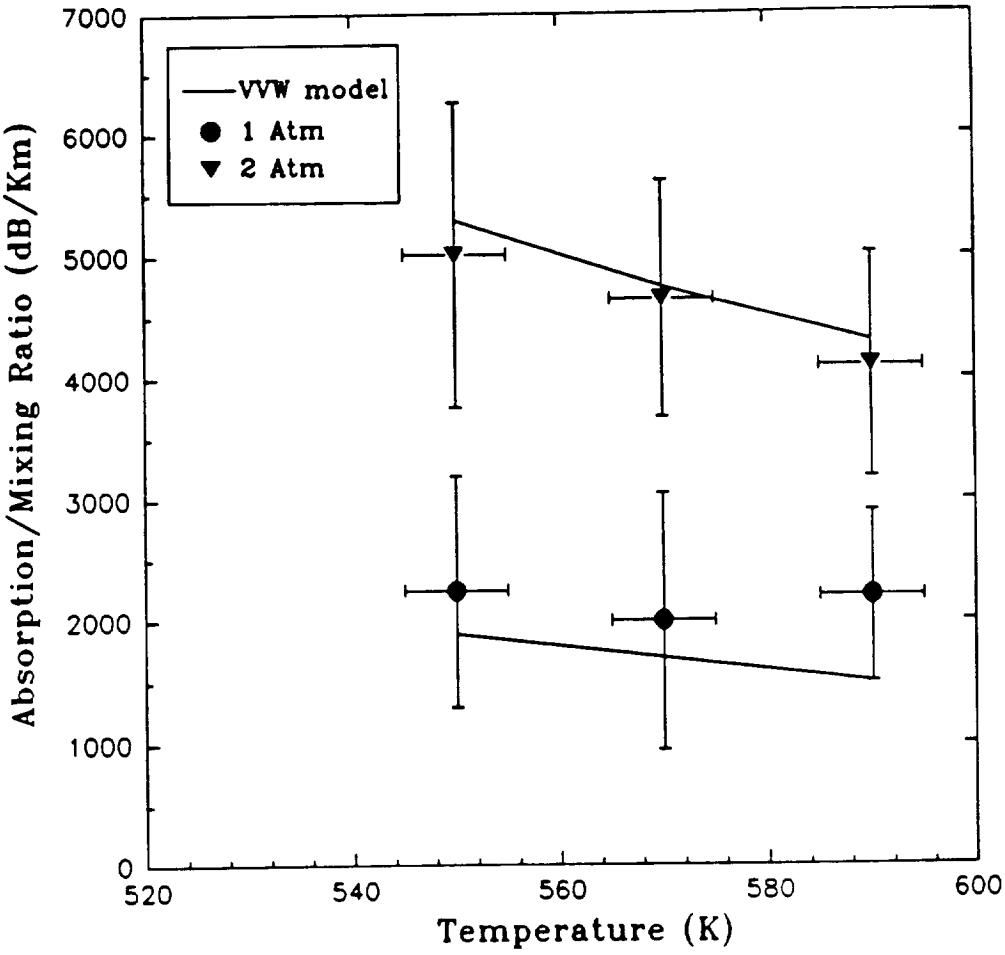

Figure 5.2 Laboratory measurements of the normalized absorptivity (dB/km) of gaseous H_2SO_4 in a CO_2 Atmosphere at 94.1 GHz. Solid curves are the theoretically calculated absorption from the VVW formalism.

mixing ratios uncertainties are also included in the vertical error bars shown in Figure 5.2.

Additional experimental uncertainties include the detector's noise which was characterized from variations in the measured output voltage. The resulting total uncertainties due to noise and instrumental uncertainties are shown in Figure 5.2 as ±1 σ variations about the mean. Finally, an estimate reflecting the effects of multiple reflections from the glass plates on the measured absorption has been added to the error bars of Figure 5.2.

5.4 Experimental Results and Theoretical Characterization of H_2SO_4 Absorption

Measurement of the opacity of gaseous H_2SO_4 in a CO_2 atmosphere has been performed at 94.1 GHz and at temperature of 550 K, 570 K, and 590 K. These temperatures were chosen so as to allow enough H_2SO_4 vapor in the glass cell. The experiment was conducted at total pressures of 2 and 1 atm for each temperature. For a specific pressure and temperature, the expected vapor pressure of H_2SO_4 can be computed by (see appendix A),

$$\ln p = 6.65 - \frac{6100}{T} \qquad (5.2)$$

where p is the sulfuric acid vapor pressure (atm) and T is the temperature in K. Using the above expression, a mixing ratio

of 1.23%, .87% and .59% occurs respectively at 590, 570 and 550 K.

The measured absorption (dB/km) of H_2SO_4/CO_2 at 94.1 GHz is shown in Figure 5.2 where it is plotted as a function of temperature for 2 and 1 atm. (note that the reported absorptions are normalized to their respective mixing ratios). Using the measured data, a best fit multiplicative expressions has been developed to predict the absorption of H_2SO_4/CO_2 at 94.1 GHz,

$$\alpha = 2x10^{11} p^{.98} q\, T^{-2.9} \qquad dB/km \qquad \textbf{(5.3)}$$

where q is the H_2SO_4 number mixing ratio, P is the total pressure in atmospheres, and T is the temperature in Kelvins (in the above equation, the pressure and temperature exponents are fitted to the measured data).

Although the developed expression is valid for the conditions at which the measurements were performed (i.e. 94.1 GHz), care must be taken when projecting the absorption of H_2SO_4 at frequencies far from 94.1 GHz. To accurately determine the expected absorptivity at other frequencies, we have used the Van Vleck-Weisskopf (VVW) formalism to calculate the opacity of the H_2SO_4/CO_2 gaseous mixture. In this formalism, the absorptivity due to a single resonant line, at frequency f, can be computed as per Townes and Schawlow (1955),

$$\alpha = \alpha_{max} f^2 \nu_o^{-2} \delta\nu^2 \left[\left((\nu_o - f)^2 + \delta\nu^2 \right)^{-1} + \left((\nu_o + f)^2 + \delta\nu^2 \right)^{-1} \right] \quad (5.4)$$

where f is the frequency in GHz, ν_o is the resonant line frequency, and $\delta\nu$ is the line width. In our VVW model, we totaled the contribution from 2359 resonant lines reported by Pickett et al. (private communication, 1991). These lines cover the frequency between 1.5 and 450 GHz. A graphical representation of the resonant lines and their respective line intensities, I_{ab}, are shown in Figure 5.3 along with an expanded view of the lines between 1.5 and 40 GHz.

In order to fully implement the VVW formalism, an appropriate broadening parameter, $\delta\nu$, must be determined. Previously, Janssen and Poynter (private communication, 1987) used a value of 3 MHz/Torr in their model (their model used a different set of resonant lines) but their results were inconsistent with the measured microwave absorptivity of Steffes (1985,1986). In addition, no measurements of the broadening parameter of H_2SO_4 by CO_2 have been reported. To solve this problem, we adjusted the broadening parameter in the VVW formalism so that the calculated opacity matches the measured absorptivity at 94.1 GHz and the microwave absorption at 2.24 GHz and 8.42 GHz reported by Steffes (1985). As a result, a broadening parameter of 1.55 MHz/Torr was found to fit the above data and seem to provide close agreement between the measured and calculated values of the absorptivity of H_2SO_4

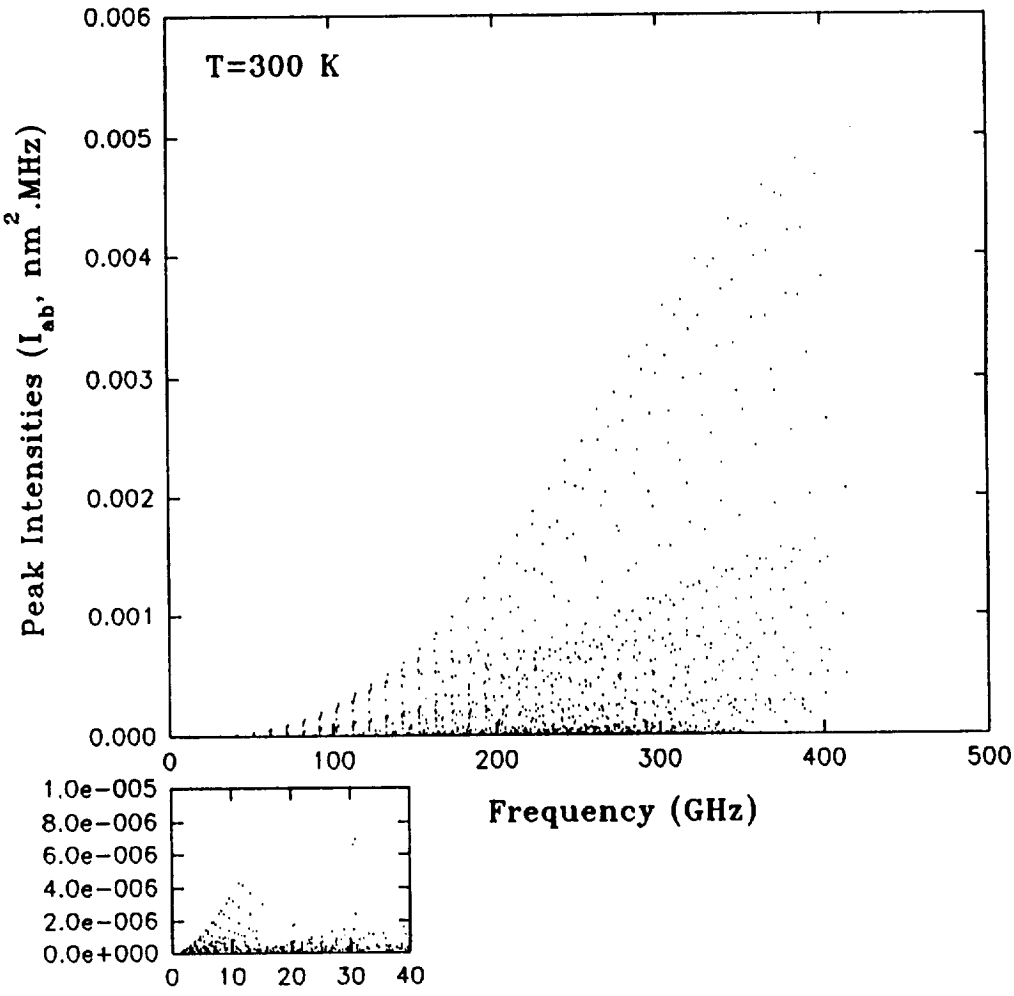

Figure 5.3 Diagram of the peak intensities at 300 K of the 2359 resonant lines used in the VVW formalism.

in a CO_2 atmosphere.

A comparison between the calculated and measured opacities of H_2SO_4/CO_2 are shown in Figures 5.2, 5.4, and 5.5 where the discrete data points in Figures 5.4 and 5.5 are obtained from Steffes (1985). In Figure 5.4, the calculated absorption of H_2SO_4/CO_2 mixture at 2.24 GHz and temperatures of 564 and 575 K are compared with the previously published work. Similarly, Figure 5.5 shows the results at 8.42 GHz and temperatures of 550 and 520 K. A careful examination of these results indicates that the calculated opacities of H_2SO_4 using the VVW formalism with a broadening parameter of 1.55 MHz/Torr agree well with the measured microwave and millimeter-wave opacities of the gaseous mixture. This finding is quite important since it demonstrates for the first time that the VVW formalism can be used to accurately predict the opacity of H_2SO_4/CO_2 gas mixture over a wide frequency range. As a result, we can use the developed model to predict the opacity of H_2SO_4 at other specified conditions and in particular, we can employ the VVW formalism in our radiative transfer model to study the effects of this gaseous mixture on the emission from Venus.

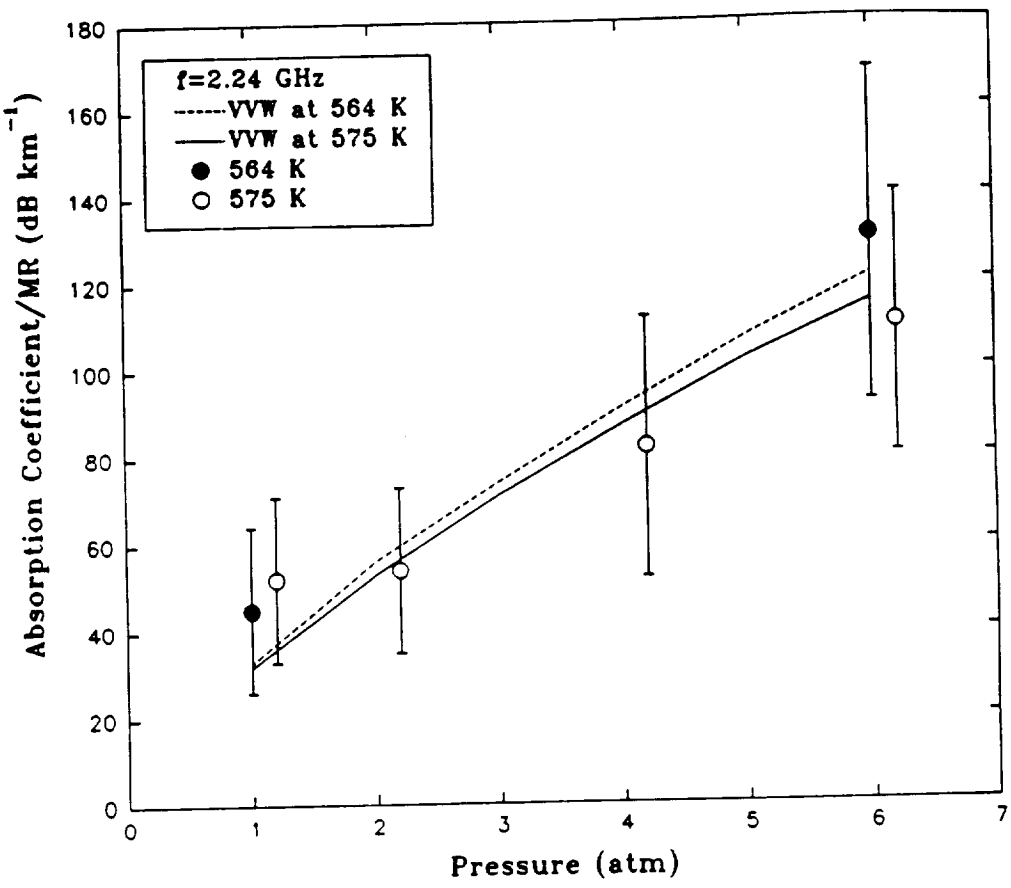

Figure 5.4 Comparison between the measured absorption (normalized by mixing ratio) of H_2SO_4 (Steffes, 1985,1986) and the calculated absorption from the VVW formalism at 2.24 GHz.

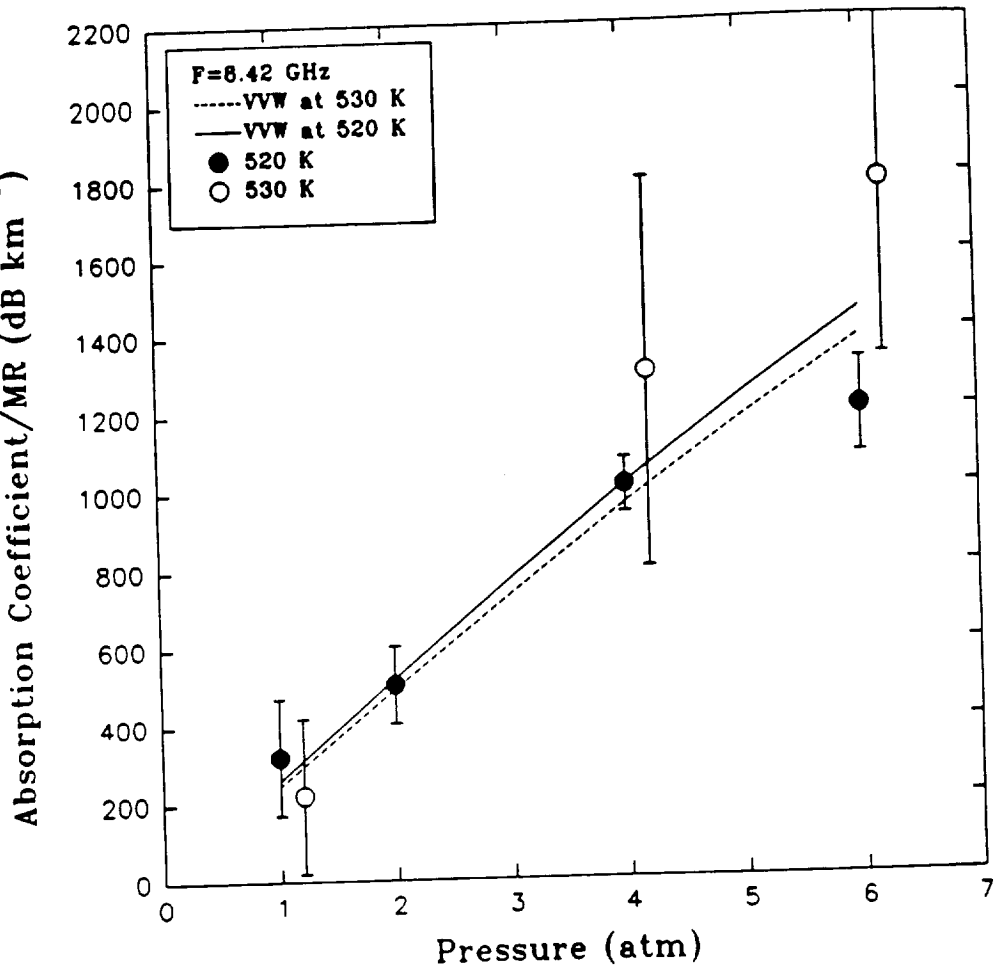

Figure 5.5 Comparison between the measured absorption (normalized by mixing ratio) of H_2SO_4 (Steffes, 1985,1986) and the calculated absorption from the VVW formalism at 8.42 GHz.

CHAPTER 6

MODELING OF THE ATMOSPHERE OF VENUS

6.1 Development of the Radiative Transfer Model

In the previous chapters, detailed descriptions regarding laboratory measurements of the millimeter-wave opacity of constituents of the Venus atmosphere were presented. In order to study the effect of these constituents (and other possible absorbers) on the millimeter-wavelength emission from Venus, a radiative transfer model has been developed. This model incorporates the results of our measurements in addition to other data that is pertinent to the atmosphere of Venus.

In the classic theory of radiative transfer, the radiated energy of a black body (also known as brightness) in units of Watts per square meter per hertz per steradian ($Wm^{-2}Hz^{-1}Sr^{-1}$), is related to its physical temperature through the Planck function given as (Liou, 1980),

C-2

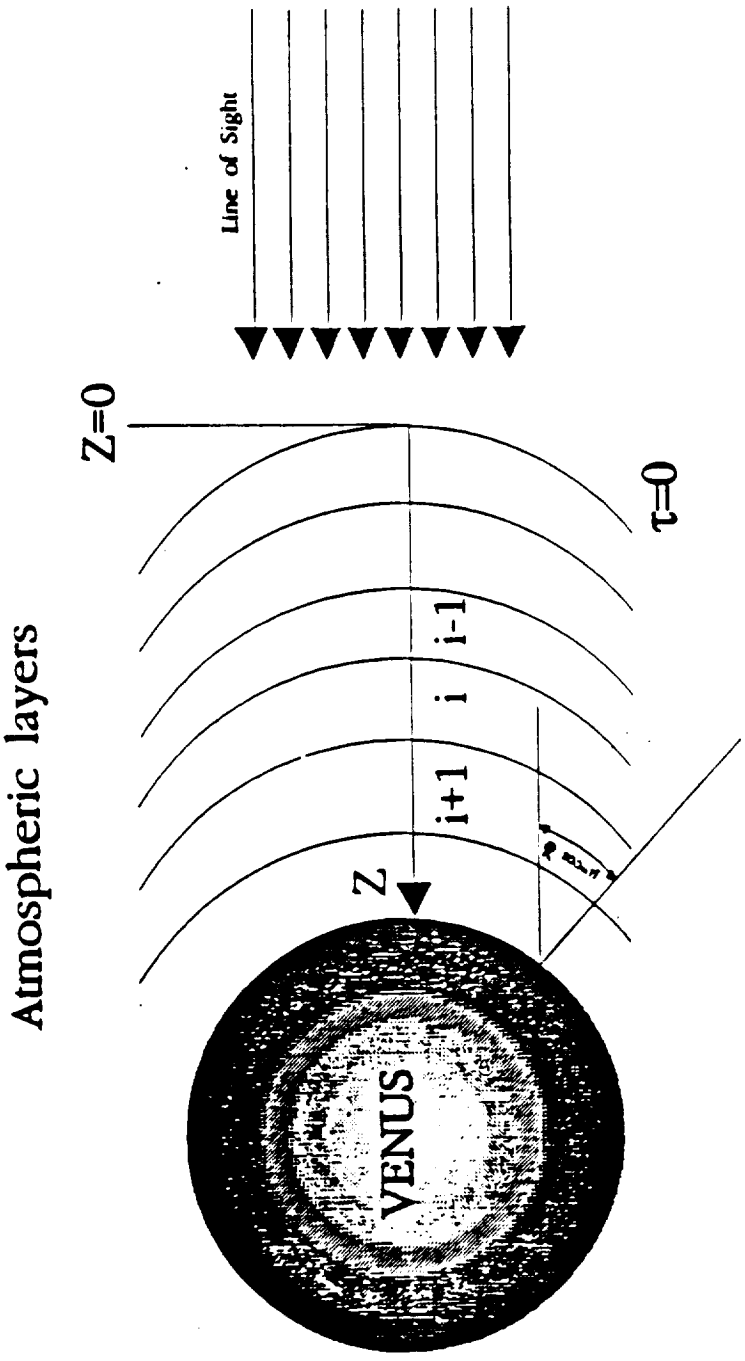

Figure 6.1 Sketch of the geometry of the planet Venus.

$$B_\nu(T) = \frac{2h\nu^3}{c^2\left[\exp\left(\frac{h\nu}{kT}\right)-1\right]} \qquad \textbf{(6.1)}$$

where ν is the frequency, c is the speed of light, h is Planck's constant (6.63×10^{-34} J s) and k is Boltzman's constant (1.38×10^{-23} J/k). The geometry of the planet Venus used in the radiative transfer model is shown in Figure 6.1 where the zenith angle at a given point ,γ, is defined as the angle between the normal to the surface and an observer's line of sight to that point. The quantity μ is defined as the cosine of the zenith angle γ. In general, the total brightness emitted at the top of the atmosphere (Z=0) along a path in the direction of μ is given as (Liou, 1980);

$$B_\nu(T,\mu) = B_\nu(T_S)\, e^{-\int_0^{z_{Surface}} \alpha_\nu(z')\frac{dz'}{\mu}} + \int_0^{z_{Surface}} B_\nu(T(z))\, e^{-\int_0^{z} \alpha_\nu(z')\frac{dz'}{\mu}}\, \alpha_\nu(z)\, \frac{dz}{\mu} \qquad \textbf{(6.2)}$$

where z is the depth as measured from the top of the atmosphere, and $\alpha_\nu(z)$ is the total absorption coefficient of all absorbing constituents at depth z and frequency ν. The total brightness can also be written as function of the weighing function $W_\nu(z,\nu)$ which describes the locations within the atmosphere which contribute most to the total brightness,

$$B_\nu(T,\mu) = \int_0^{Z_{surface}} B_\nu(T(z))\, W_\nu(z,\nu)\, \frac{dz}{\mu} \qquad (6.3)$$

Another expression which is usually employed in radiative transfer modeling is the vertical optical depth, τ, defined as,

$$\tau_\nu(Z) = \int_0^Z \alpha_\nu(Z')\, dZ' \,. \qquad (6.4)$$

Upon substituting equation (6.4) into (6.2), we obtain an alternate form of the radiative transfer equation,

$$B_\nu(T,\mu) = B_\nu(T_S)\, e^{-\frac{\tau_1}{\mu}} + \int_0^{\tau_1} B_\nu(T(\tau'))\, e^{-\frac{\tau}{\mu}}\, \frac{d\tau'}{\mu} \qquad (6.5)$$

where τ_1 is the optical depth at the planet's surface.

Radio emission from planets is usually given as a brightness temperature, T_B, which is the temperature at which a blackbody would radiate an intensity of electromagnetic radiation identical to that of the planet at a specific frequency. The brightness is related to the brightness temperature via Planck's function;

$$T_B = \frac{h\nu}{k \ln\left(\frac{2h\nu^3}{Bc^2}+1\right)} \quad . \tag{6.6}$$

6.2 Disk Average Brightness

The disk average brightness of a planet, $B_\nu(T_D)$, can be obtained by integrating equation (6.5) over all angles of incidence thus,

$$B_\nu(T_D) = 2\int_0^1 B_\nu(T,\mu)\,\mu\,d\mu \quad . \tag{6.7}$$

Upon substituting equation 6.5 into 6.7 we obtain,

$$B_\nu(T_D) = 2\int_0^1 B_\nu(T_S)\,e^{-\tau_1/\mu}\,\mu\,d\mu + 2\int_0^1\int_0^{\tau_1} B_\nu[T(\tau')]e^{-\tau'/\mu}d\tau' d\mu \tag{6.8}$$

where the first term is the brightness of the surface observed at the top of the atmosphere reduced by the absorption of the intervening layers by a factor $e^{-\tau_1/\mu}$. The second term of equation (6.8) corresponds to the brightness emanating from within the atmosphere of Venus.

For a simple spherical planet, the integration may be simplified to a single exponential integral (Goodman, 1969) so that,

$$B_\nu(T_D) = 2B_\nu(T_S)\,E_3(\tau_1) - 2\int_0^{\tau_1} B_\nu(T(\tau'))\,dE_3(\tau') \tag{6.9}$$

where,

$$E_n(\tau) = \int_1^\infty \frac{1}{y^n} e^{-\tau y} dy \qquad (6.10)$$

and $y=1/\mu$. In the developed model, the weighting function at a particular frequency is computed via $W_\nu(z) = T(z)\, dE_3(\tau(z))$.

Numerical implementation of the radiative transfer model has been achieved where the integral in equation (6.9) is evaluated by dividing the atmosphere into discrete layers as shown in Figure 6.1. The average pressure, temperature, and altitude at each discrete layer (each layer has a thickness of 1 km.) are determined using the pressure-temperature profile described by Seiff et al. (1980). The integration is evaluated starting at the top of the atmosphere (Z=0) and is terminated at the surface of the planet. The brightness at each layer is evaluated in addition to the corresponding optical depth of that particular layer. The contributions from each layer are then added to yield the total brightness and hence the disk-averaged brightness temperature of the planet.

6.3 Parameters of the Radiative Transfer Model

To fully implement a radiative transfer model, several variables must be included in the model. Such variables include the pressure-temperature profile of the atmosphere of the planet, the expected opacities of the major atmospheric

constituents, and the distribution of these absorbing constituents within the atmosphere.

6.3.1 Pressure-Temperature Profile of Venus

Several pressure-temperature profiles of Venus have been developed using data from entry probes released in the atmosphere of Venus in the late seventies. Seiff et al. (1980) developed such profiles using the collected data from the four Pioneer-Venus entry probes. In our model, the profile obtained from the sounder probe (released over the equator of Venus) is employed. A plot of this pressure and temperature profile is shown in Figure 6.2 as function of altitude. In addition, a standard disk radius of 6120 km is used for Venus (the standard disk radius includes the physical radius of the planet in addition to the height of the atmosphere).

6.3.2 Gaseous CO_2 Absorption

Gaseous carbon dioxide (CO_2) is considered to be the major absorber in the atmosphere of Venus. The absorption from CO_2 can be attributed to the collisions of CO_2 molecules in the atmosphere of Venus. Ho et al. (1966), determined the following expression for the absorptivity, α, of a mixture of CO_2 and N_2 under high pressure;

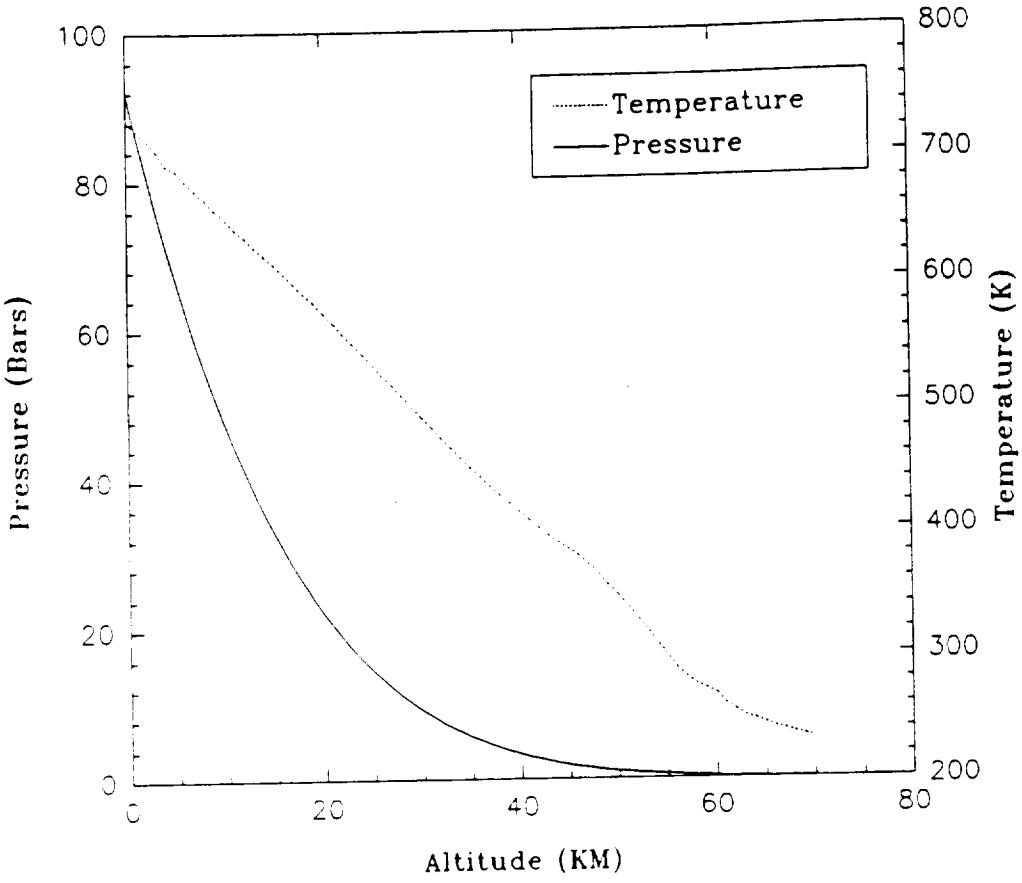

Figure 6.2 Pressure-Temperature profile of the atmosphere of Venus.

$$\alpha = 1.15x10^{8}\left[q_{CO_2}^2 + .25q_{CO_2}q_{N_2} + .0054q_{N_2}^2\right]f^2p^2T^{-5} \quad dB/km \tag{6.11}$$

where p is the pressure in atmospheres, T is the temperature in K, f is the frequency in GHz, and q is the number mixing ratio. For the atmosphere of Venus, CO_2 composes about 96% of the atmosphere while N_2 corresponds to about 3.0 % (Steffes, 1982). In the development of the radiative transfer model, the above expression is used to compute the opacity of gaseous CO_2 in the atmosphere of Venus. A plot of the expected absorption of CO_2 in the atmosphere of Venus is shown in Figure (6.3), where the absorption (1/km) is plotted as a function of altitude for 30, 50, 75, 100, and 125 GHz, based on the T-P profile of Seiff et al., (1980).

6.3.3 SO_2-CO_2 Absorption

As we demonstrated in Chapter 2, the results from the measured opacity of gaseous SO_2 in a CO_2 atmosphere indicate that the Van Vleck-Weisskopf formalism can be used to determine the opacity of sulfur dioxide for Venus-like conditions at wavelengths shortward of 1.5 cm. This key finding differs from previous results of Steffes and Eshleman (1981) and Janssen and Poynter (1981) which suggested that the microwave opacity of SO_2 had an f^2 dependence. As a result of our finding, we have incorporated the VVW formalism in our radiative transfer model to infer the expected opacity of

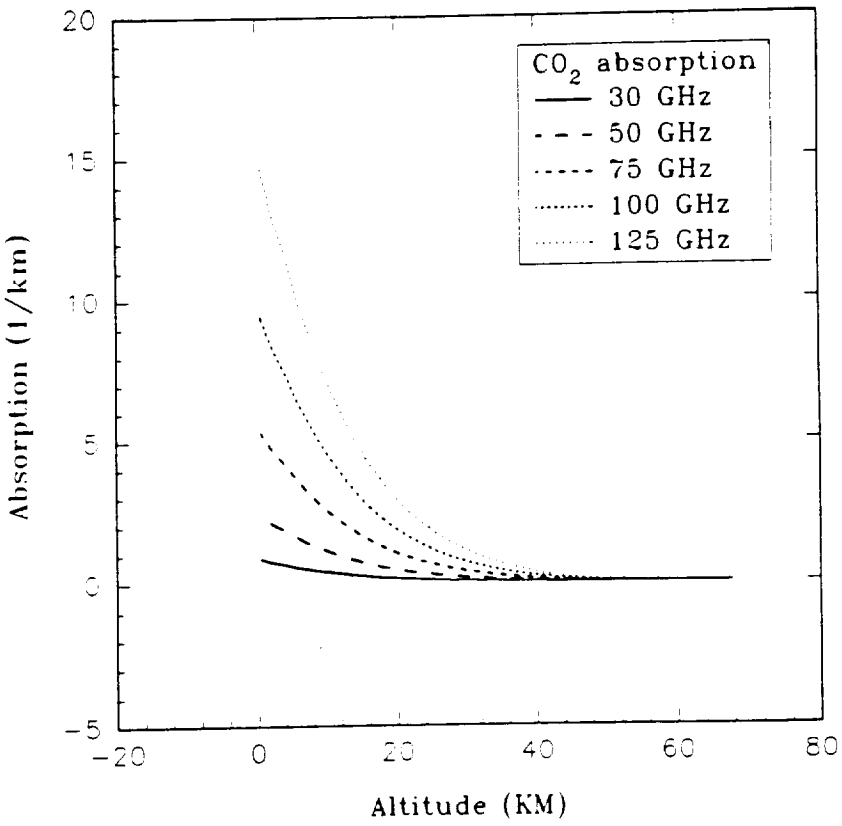

Figure 6.3 Expected absorption of gaseous CO_2 in the atmosphere of Venus based on the results of Seiff et al. (1980) and the results of Ho et al. (1966).

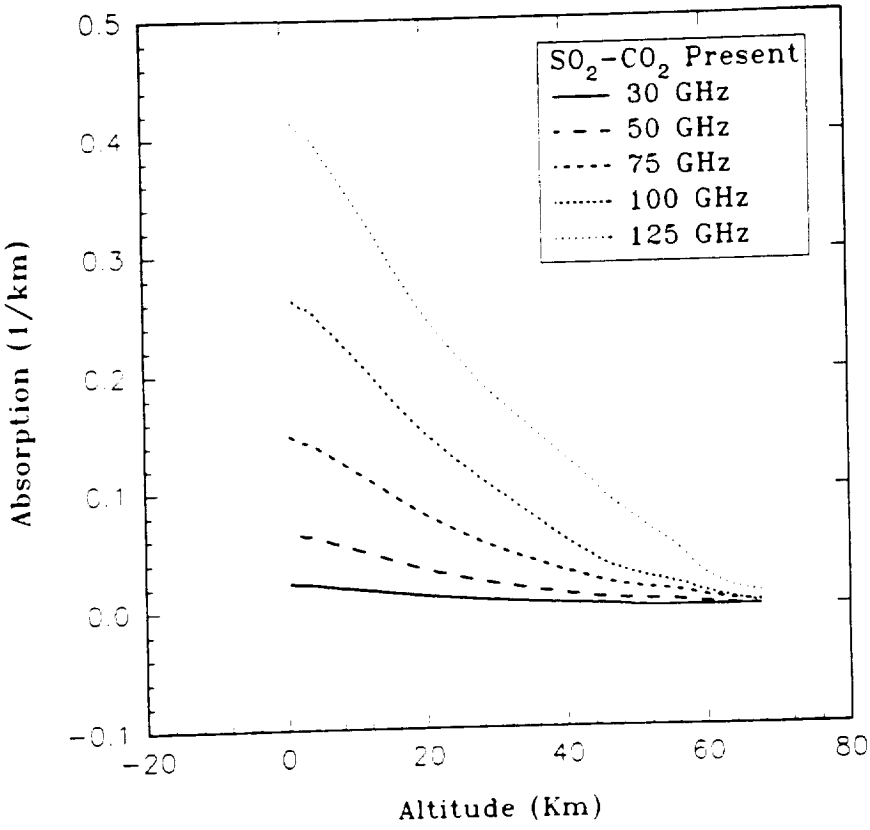

Figure 6.4 Absorption profiles for gaseous SO_2 in a CO_2 atmosphere according to the VVW formalism and the T-p profile of Seiff et al. (1980) (SO_2 abundance: 62 ppm).

gaseous SO_2 under Venus-like conditions. Typical absorption profiles of gaseous SO_2 in a CO_2 atmosphere are shown in Figure (6.4) where the absorption of gaseous sulfur dioxide (1/km) is plotted versus altitude for a specific T-p profile of Venus at 30, 50, 75, 100, and 125 GHz, assuming an SO_2 abundance of 62 ppm.

6.3.4 Liquid Sulfuric Acid Condensates

As discussed in Chapter 3, liquid sulfuric acid is known to exist in the form of clouds within the atmosphere of Venus where the more dense lower cloud layer extends between altitudes of 48 and 50 km, (Knollenberg and Hunten, 1980). However, its effects on the millimeter-wave emission from Venus are not fully understood. To fully understand its role on the emission of Venus, its absorptivity must be determined so as it can be employed in a radiative transfer model.

In general, when an electromagnetic wave propagates through a cloud layer, it is scattered and absorbed by cloud particles. For a plane wave with a wavelength λ, incident upon a spherical particle with radius a, the absorption cross-section is given as,

$$Q_a = \frac{Absorbed\ \ Power\ \ (W)}{Incident\ \ Power\ \ density\ \ (W/m^2)} \qquad \textbf{(6.12)}$$

and the scattering cross-section is given by,

$$Q_s = \frac{Scattered\ \ Power\ \ (W)}{Incident\ \ Power\ \ density\ \ (W/m^2)} \quad . \qquad \textbf{(6.13)}$$

For a dielectric sphere with a complex relative permittivity ϵ_r, the absorption and scattering cross-sections are respectively (Ulaby, 1980),

$$Q_a = \frac{\lambda^2}{2\pi} \sum_{n=1}^{\infty} (2n+1)\left(|a_n|^2 + |b_n|^2\right) \qquad \textbf{(6.14)}$$

and,

$$Q_s = \frac{\lambda^2}{2\pi} \sum_{n=1}^{\infty} (2n+1)\, Re\,(a_n + b_n) \qquad \textbf{(6.15)}$$

where Re signifies "real part of", and a_n and b_n are the Mie coefficients which are function of ϵ_r and a. For the case where the droplet dimension is much smaller than λ, the absorption and scattering cross-sections are reduced to what is referred to as the Rayleigh approximation where,

$$Q_s = \frac{2\lambda^2}{3\pi}\, \chi^6 |k|^2 \qquad \textbf{(6.16)}$$

and,

$$Q_a = \frac{\lambda^2}{\pi} \chi^2\, Im(-k) \qquad \textbf{(6.17)}$$

where Im signifies "the imaginary part of", and k is a complex quantity related to the complex index of refraction $\hat{n}$, by

$$k = \frac{\hat{n}^2-1}{\hat{n}^2+2} = \frac{\epsilon-1}{\epsilon+2} \quad , \tag{6.18}$$

and

$$\chi = \frac{2\pi a}{\lambda} \quad . \tag{6.19}$$

Thus, if $|\hat{n}\chi| < .5$, the absorption and scattering cross-sections can be evaluated using the Rayleigh approximation while if $|\hat{n}\chi| > .5$, the Mie coefficients must be used (Ulaby et al. 1980).

For a typical cloud layer, the volume extinction coefficient (K_e) is the sum of the absorption and scattering coefficients (Ulaby et al., 1980);

$$\alpha_{cloud} = \sum_{n=1}^{N_v} [Q_a(r_i) + Q_s(r_i)] = K_e = K_a + K_s \tag{6.20}$$

where N_v is the number of particles per unit volume and r_i is the radius of the i^{th} particle. K_a and K_s are the volume scattering and volume absorption coefficients respectively (i.e., the total scattering (absorbing) cross-section per unit volume).

For the case of the Venus atmosphere, extensive studies of the physical parameters of the cloud condensates have been performed using data from several entry probes. Knollenberg and Hunten (1980), determined conservative upper limits of 25 microns for droplet size and 50 mg/m^3 for cloud bulk density.

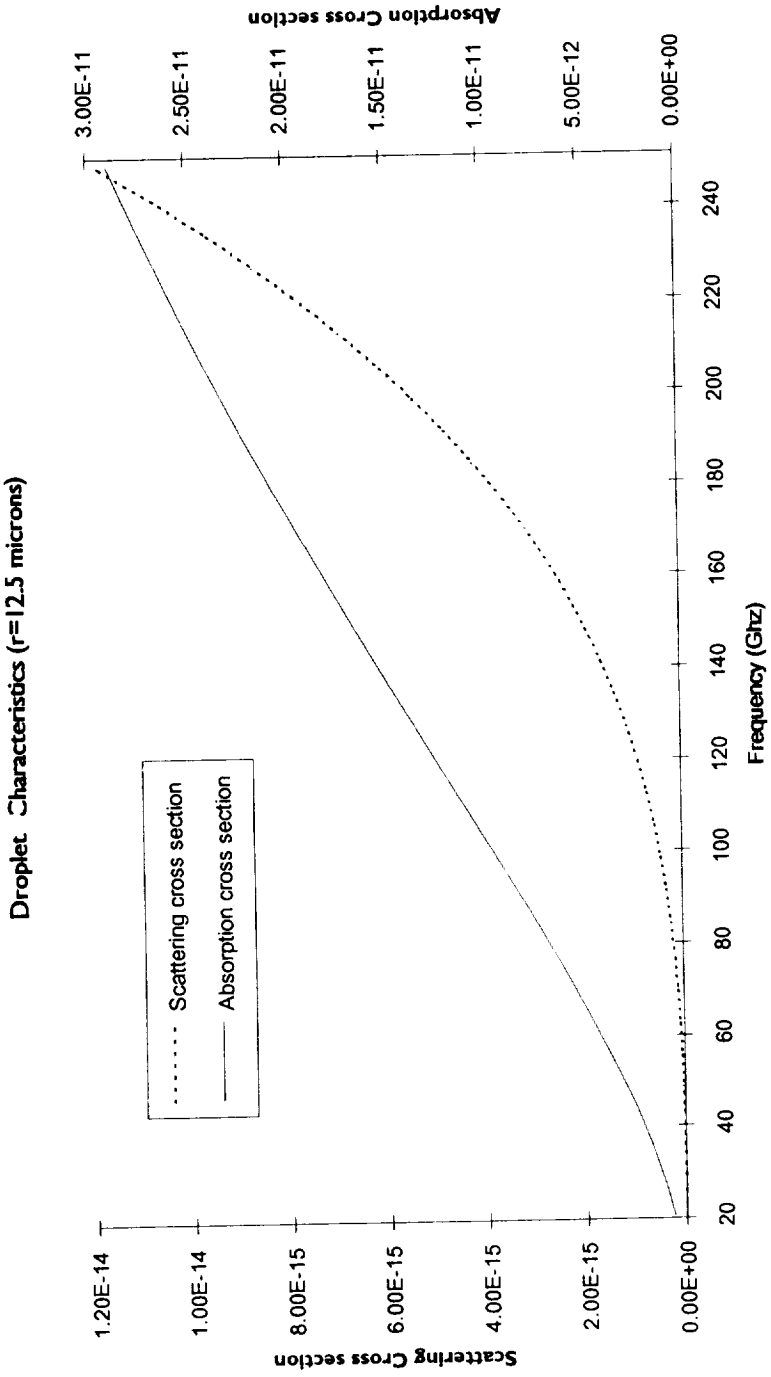

Figure 6.5 Comparison of the scattering and absorbing cross-section of liquid sulfuric acid droplets with radius of 12.5 microns at room temperature (296 K).

Using this information and our results regarding the complex dielectric constant of sulfuric acid (see Chapter 3), the scattering and absorption cross-sections for such a condensate have been computed. Plots of the computed cross-sections are shown in Figure (6.5). An examination of the results indicates that the absorption cross-section is many orders of magnitude greater than the scattering cross-section for 25 micron particles at the temperature and with composition characteristic of the lower cloud deck of Venus. Since the absorption cross-section is much greater than the scattering cross-section, the volume extinction coefficient can be approximated by (Battan, 1973),

$$\alpha_{cloud} = \frac{246\, M\epsilon''}{\rho\, \lambda \left[(\epsilon_r'+2)^2 + (\epsilon_r'')^2 \right]} \quad (dB/km) \qquad \textbf{(6.21)}$$

where ρ is the density of the liquid sulfuric acid and M is the bulk density of the cloud (bulk density= total mass occupied by cloud particles per unit volume) in the same units, λ is the wavelengths in km and ϵ_r' and ϵ_r'' are the real and imaginary parts (respectively) of the complex dielectric constant of the liquid.

Using our model for the complex dielectric constant of H_2SO_4, the expected opacity (1/km) of liquid sulfuric acid has been computed using equation (6.21). The results of this calculation are shown in Figure 6.6. In this figure, the real

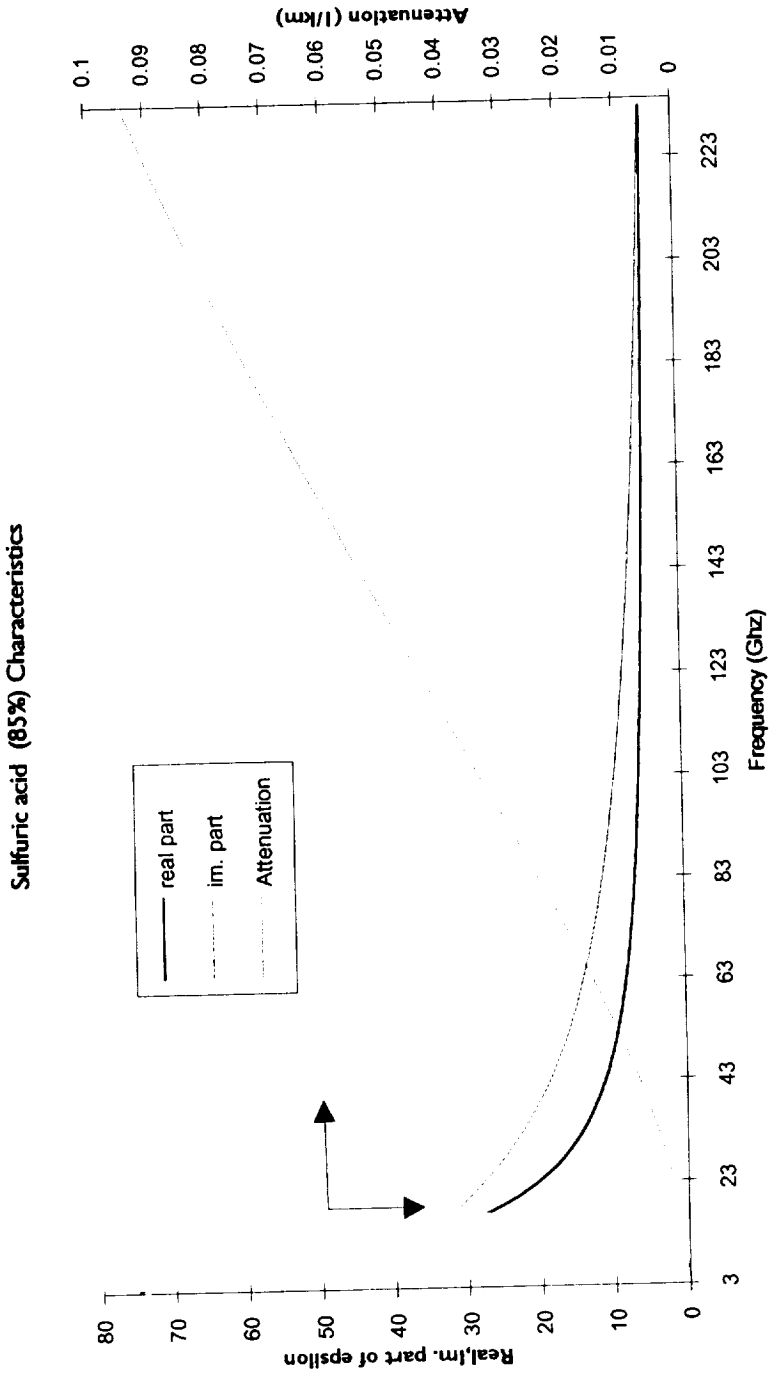

Figure 6.6 Expected absorption (1/km) and dielectric properties of an 85 % (by weight) liquid sulfuric acid solution with a bulk density of 50 mg/m^3 and a droplet radius of 12.5 microns.

and imaginary parts of the complex dielectric constant of sulfuric acid are also plotted in addition to the expected absorption of H_2SO_4 for a typical cloud layer in the atmosphere of Venus. Results from equation (6.21) will be incorporated into the radiative transfer model in order to investigate the effects of sulfuric acid cloud condensates on the millimeter-wave emission from Venus.

6.3.4.1 Scattering Effects of the Cloud Condensates

Although the scattering cross-section of a single H_2SO_4 droplet is much smaller than its absorbing cross-section, the effect of the bulk density of the condensates must be evaluated when computing the back-scattering from a cloud layer. This backscattering effect can cause a cooler brightness temperature due to reflection of the cold sky. To investigate the significance of this phenomenon on the emission of Venus, we have computed the expected transmission and reflection coefficients for a typical cloud layer in the atmosphere of Venus.

For a cloud made up of discrete homogeneous layers and assuming that radiation is scattered in only the forward and backward directions, the transmission and reflection

coefficients of a layer with thickness dz are given as (Gasiewski, 1990),

$$t_{ec} = \frac{\overline{w}}{1+\sqrt{1-\overline{w}^2}\coth(\alpha_c dz)} \qquad (6.22)$$

and

$$t_{ec} = \frac{\sqrt{1-\overline{w}^2}\,csch(\alpha_c dz)}{1+\sqrt{1-\overline{w}^2}\coth(\alpha_c dz)} \qquad (6.23)$$

respectively, where α_c is the total power attenuation from the cloud which in the case of Venus includes the absorption from gaseous CO_2 and liquid sulfuric acid. The quantity α_c can be written as (Gasiewski, 1990),

$$\alpha_c = \sqrt{k_a^2 + 2k_a k_{sb}} \qquad (6.24)$$

where k_{sb} is the back-scattering coefficient. The quantity $\overline{w}$ is referred to as back-scattering albedo given as,

$$\overline{w} = \frac{k_{sb}}{k_a + k_{sb}} \quad . \qquad (6.25)$$

The back-scattering coefficient, k_{sb}, can be determined from the scattering-coefficient, k_s, and the phase fraction asymmetry, g, of the clouds as,

$$k_{sb} = k_s\left(\frac{1-g}{2}\right) \quad . \tag{6.26}$$

For a spherical droplet, the asymmetry phase function is equal to zero. In this case:

$$k_{sb}=\frac{k_s}{2} \tag{6.27}$$

which indicates that the scattered wave is equally divided in a forward and a backward direction.

Since the cloud is made up of several discrete layers, a composite transmission and reflection coefficient can be computed based on the transmission and absorption coefficients of two adjacent layers (a and b) by (Paltridge and Platt, 1976) where,

$$r_{ab} = r_a+\frac{t_a^2 r_a}{1-r_a r_b} \tag{6.28}$$

and,

$$t_{ab} = \frac{t_a t_b}{1-r_a r_b} \quad . \tag{6.29}$$

Using the above two equations, we have determined the composite reflection and transmission coefficient for the H_2SO_4 cloud layer of Venus. A mass density of 50 mg/m^3 with droplet diameters of 25 microns are used in our computation. The results reported in Chapter 3 concerning the complex dielectric constant of H_2SO_4 are also used in the calculation.

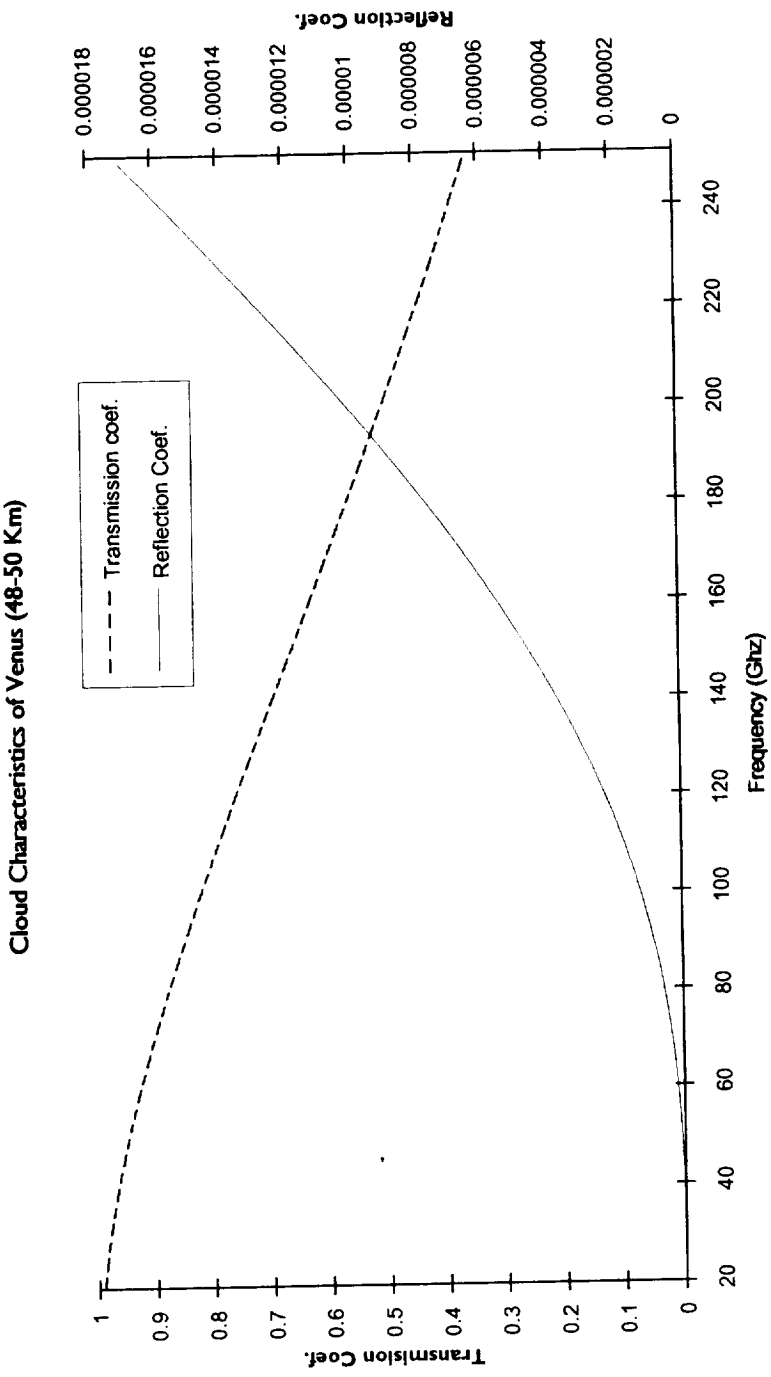

Figure 6.7 Transmission and reflection coefficient for the H_2SO_4 cloud layer in the atmosphere of Venus.

A graphical representation of the results is shown in Figure 6.7 where the transmission and reflection coefficient are plotted as a function of frequency for a cloud layer with thickness of 2 km. An examination of the results indicate that the cloud layer is mostly transmissive and the reflection coefficient is very small. Thus, back-scattering does not have a major role in the observed variations in the millimeter-wave emission from Venus.

6.3.5 Gaseous H_2SO_4-CO_2 Absorption

As reported in Chapter 5, the VVW formalism provides an accurate means for computing the expected absorptivity from gaseous sulfuric acid in a CO_2 atmosphere at microwave and millimeter-wavelengths. This important finding allows us to integrate the opacity of H_2SO_4/CO_2 gaseous mixture in our radiative transfer model so as to investigate its effect on the millimeter wavelength emission from Venus.

Using the VVW formalism, we have computed several absorption profiles of H_2SO_4/CO_2 gaseous mixture using the pressure-temperature profile of Seiff et al. (1980) and a gaseous abundance of 25 ppm. The absorption profiles are shown in Figure 6.8 for frequencies of 30, 50, 75, 100, 102.5, 113, 125, and 143 GHz. In addition, we have plotted the absorptivity of this gaseous mixture versus frequency for a single pressure and temperature point which is relevant to the

atmosphere of Venus (in this case, the pressure and temperature are for 42 Km altitude). An examination of this profile, shown in Figure 6.9, reveals that the absorption appears to go through several local peaks . This result is quite interesting since it demonstrates for the first time that the expected absorptivity is not a monotonically increasing function. This phenomenon well explains the results of Figure 6.8 where the absorption at 102 GHz is larger than the absorption at 125 GHz for altitudes above 42 km.

6.3.6 H_2O Vapor

Although water vapor is known to exist in the atmosphere of Venus, discrepancies regarding its abundance are still unresolved. Estimates using the Pioneer-Venus gas chromatography (PVGC) experiment (Oyama, 1979) place the H_2O concentration on the order of several thousand ppm. Other measurements of H_2O vapor range from 20 to 200 ppm. Recently, Lewis and Grinspoon (1990) concluded that a mean water abundance of 50 ±20 ppm and a near-surface water vapor abundance of 10 ±4 ppm provide a conservative upper limit on the water vapor abundance in the atmosphere of Venus.

In order to include the effects of H_2O vapor in the radiative transfer model, a knowledge of the opacity of water vapor in a CO_2 atmosphere is needed. For this, the results

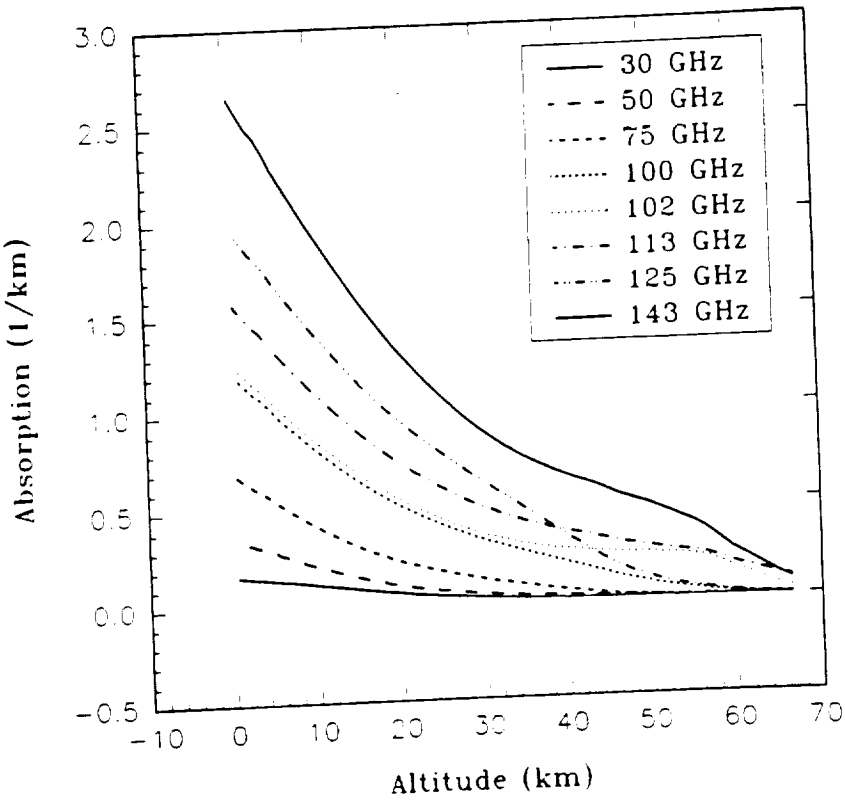

Figure 6.8 Absorption profiles due to gaseous H_2SO_4 as function of altitudes with an H_2SO_4 abundance of 25 ppm.

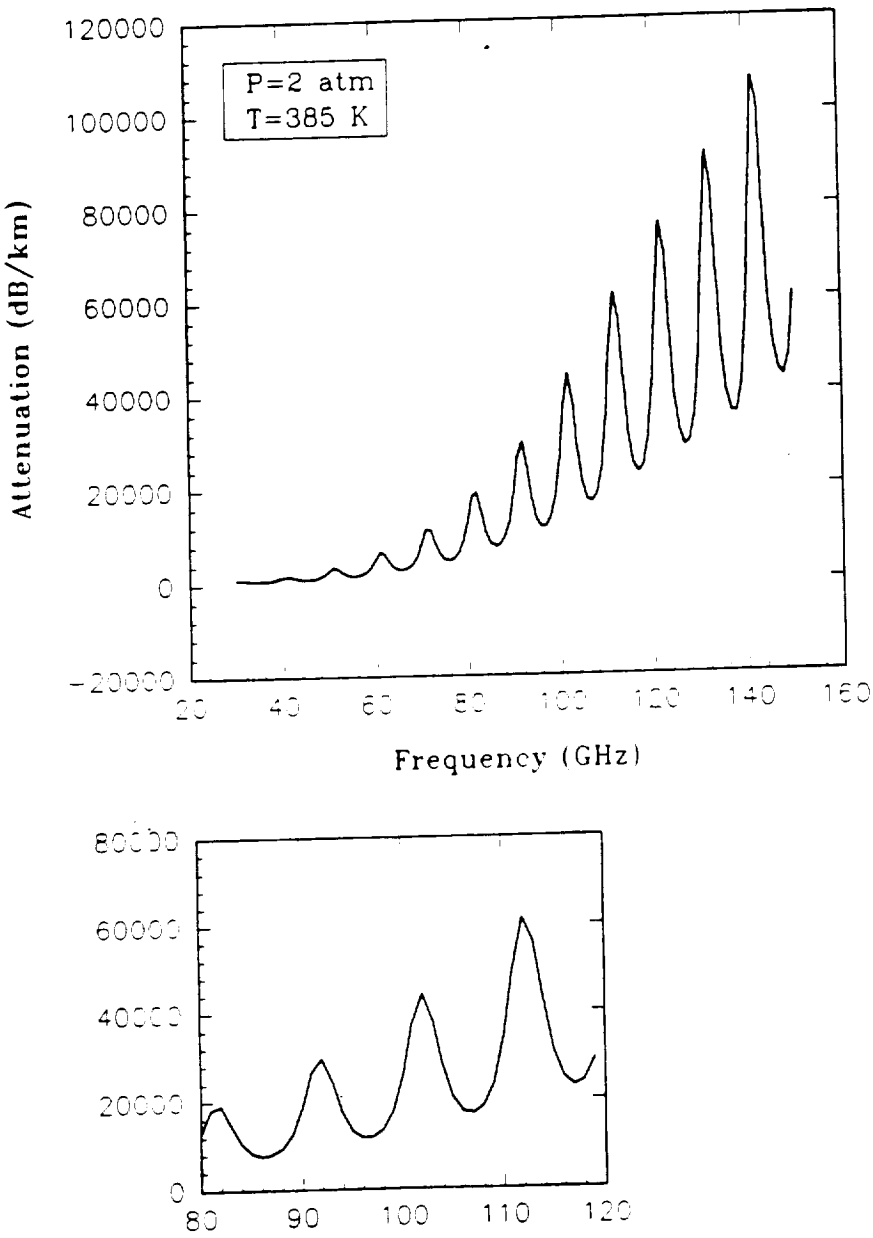

Figure 6.9 Absorption of gaseous H_2SO_4 (normalized by mixing ratio) as function of frequency for a typical pressure-temperature point in the Venus atmosphere.

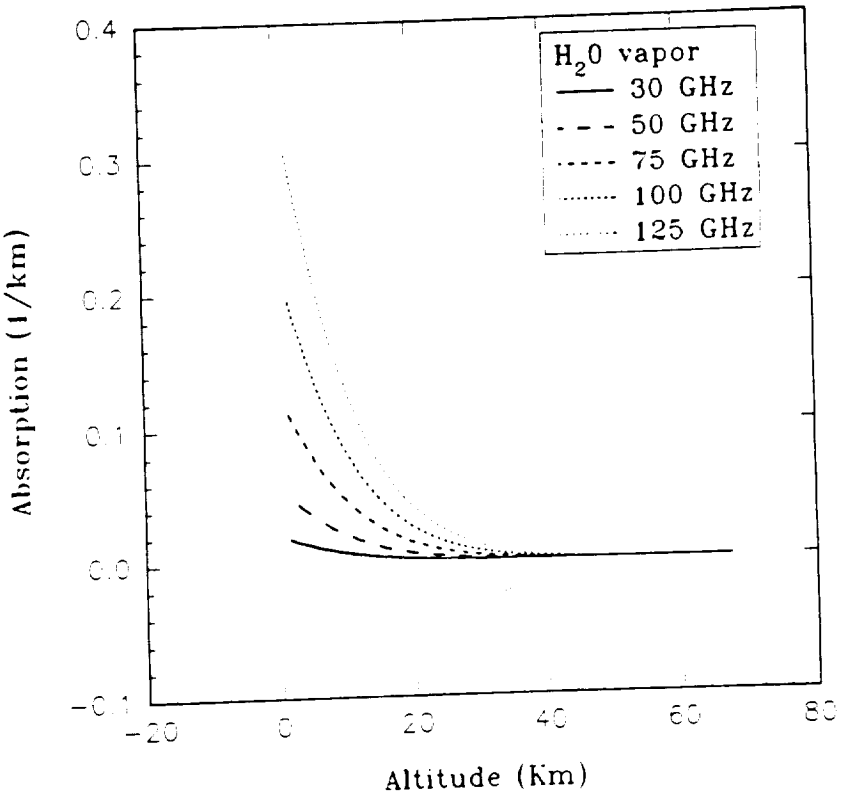

Figure 6.10 Absorption profiles of H_2O in a CO_2 atmosphere as per Waters(1976) and the T-p profile of Venus as reported by Seiff et al. (1980).

reported by Waters (1976) are used for the opacity of water vapor at frequencies below 300 GHz. The H_2O absorption model includes the contributions from ten rotational lines of H_2O vapor with frequencies up to 448 GHz. While strong H_2O resonant lines exist above 448 GHz, their contribution is estimated to be less than 10 % of the absorptivity computed using the ten rotational lines at frequencies between 100 and 300 GHz (Waters, personal communication 1992). In addition, Dryagin et al. (1966) measured the absorption of water vapor between 100 and 200 GHz and their results agree well with the calculated absorptivity of H_2O vapor using the ten lowest water-vapor absorption transitions. Since the water absorptivity reported by Waters is for terrestrial conditions (i.e., nitrogen and oxygen broadening), we have modified his expression to include the CO_2 broadening effect present in the atmosphere of Venus. A typical spectrum of the expected absorption from H_2O in a CO_2 atmosphere is shown in Figure 6.5 where the absorption of H_2O vapor at 30, 50, 75, 100, and 125 GHz is plotted as function of altitude of Venus using an abundance of 70 ppm.

6.4 Modeling Results

In the previous sections, we have determined the expected absorption from the major constituents in the atmosphere of

Venus. We now turn our attention to the effects of these constituents on the millimeter-wave emission from Venus.

A) Sensitivity to CO_2:

Gaseous CO_2 composes 96 % of the atmosphere of Venus, its expected absorption is well characterized by the work of Ho et al. (1966) as reported in section 6.3.2. Using the developed radiative transfer model, the brightness temperature (K) of Venus based only on gaseous CO_2 opacity is shown in Figure 6.11 for frequencies between 30 and 150 GHz.

B) Sensitivity to SO_2-CO_2:

To investigate the effect of gaseous SO_2 on the emission of Venus, an appropriate abundance profile must be employed. In our radiative transfer model, we have used a uniform SO_2 mixing ratio at altitudes below 48 km and an exponential depletion above the cloud base. Based on this assumption and the findings regarding the opacity of SO_2, the radiative transfer model is used to compute the expected brightness temperature of Venus considering only the effects of CO_2 and SO_2 at the 1.35 cm wavelength where the brightness temperature of Venus has been accurately measured by several researchers. (most recently by Steffes et al. (1990) who reported an equivalent disk temperature of 507±22 K at 22.25 GHz). Since the effects of other non-CO_2 gaseous absorbers at 1.35 cm on

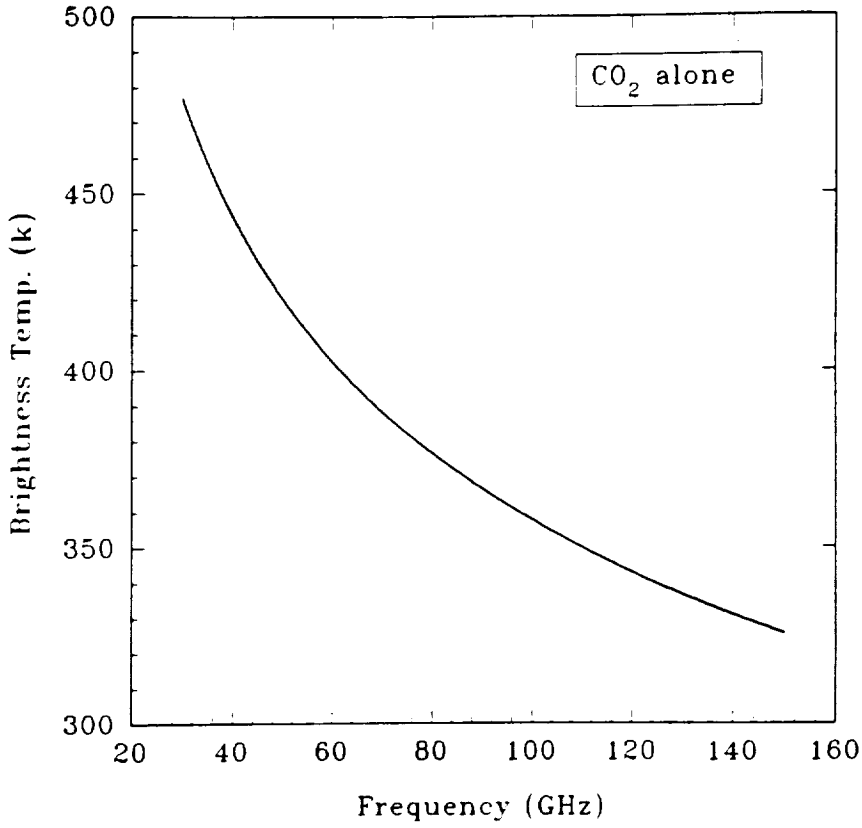

Figure 6.11 Computed brightness temperature of Venus assuming that gaseous CO_2 is the only atmospheric constituent.

the total opacity of the atmosphere of Venus are minimal (Steffes, 1986), an accurate estimate of the abundance of gaseous SO_2 based on the microwave absorption of Venus at 1.35 cm can be made. Using the measured brightness temperature at 1.35 cm. (507±22 K) and the model developed for SO_2 absorption, we infer a uniform mixing ratio of 62 ppm (+183, -62) at altitudes below 48 km.

Using this developed profile, we can then use our radiative transfer model to compute the expected brightness temperature of Venus at millimeter-wavelengths based on the presence of CO_2 and SO_2 alone. A plot of the brightness spectrum is shown in Figure 6.12 for an SO_2 abundance of 62 ppm below 48 km. In addition, the brightness temperature for several frequencies are listed in Table 6.1.

C) Sensitivity of Liquid H_2SO_4:

Results from the radiative transfer model indicate that liquid H_2SO_4 does indeed affect the brightness temperature of Venus at millimeter-wavelengths (refer to Table 6.1). For instance, at 112 GHz, a decrease in brightness temperature of 2 K is obtained for uniform cloud layer in the 48-50 km altitude range where droplets sizes of 25 micron are assumed with a bulk density of 50 mg/m^3. However this decrease in brightness temperature is much less than the reported variation in emission of Venus. This indicates that variations

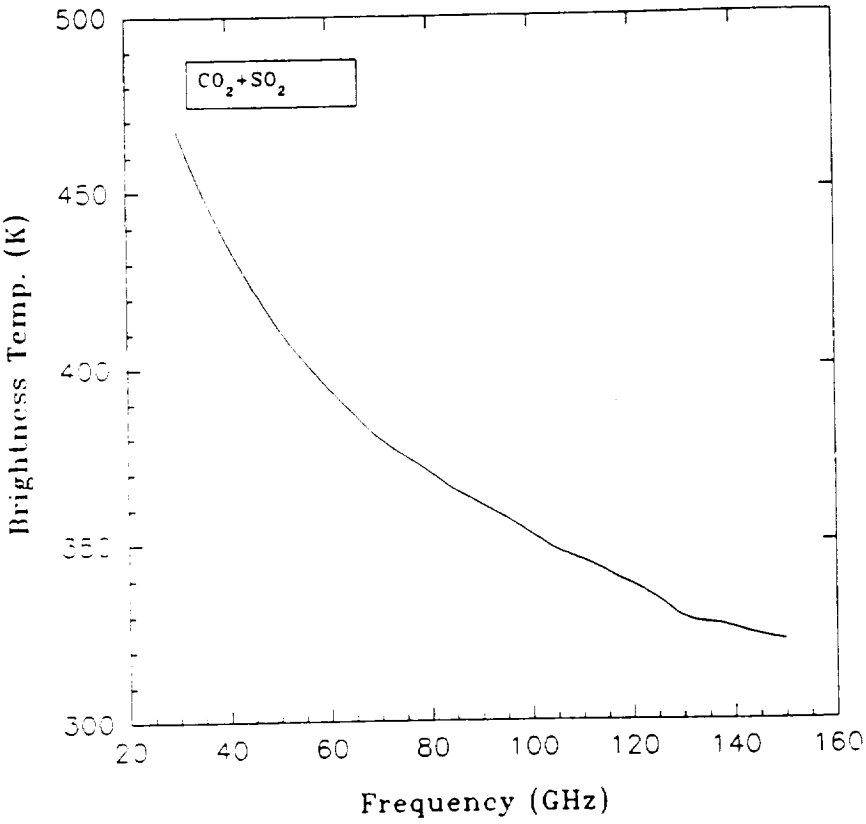

Figure 6.12 Expected brightness temperature of Venus based on the presence of CO_2 and SO_2 with an SO_2 abundance of 62 ppm below 48 km and exponentially decreasing above 48 km.

Table 6.1 Calculated brightness temperature of Venus at discrete frequencies.

Freq (GHz)	Brightness Temperature (k)					
	CO_2	$+SO_2$	$+H_2O$	H_2SO_4 (liq.)	H_2SO_4 (25ppm)	H_2SO_4 10ppm
30	477	467	467	466	457	463
40	444	435	435	433	425	430
50	420	412	412	410	400	406
60	402	394	394	392	382	388
70	388	380	380	378	368	373
80	377	370	370	368	358	363
90	367	361	361	359	350	354
100	358	353	353	351	343	347
102	356	351	351	349	334	341
106	353	347	347	346	341	344
112	349	344	344	342	328	334
125	340	334	334	333	329	331
140	331	326	326	325	321	323
150	326	322	322	321	320	320
160	321	316	316	316	313	314
170	316	314	314	313	311	312
180	312	310	310	309	307	308
190	308	305	305	305	303	304
200	305	301	301	301	300	300
210	301	299	299	299	297	298
220	298	296	296	296	295	295
230	295	294	294	294	292	293

in the abundance of liquid H_2SO_4 are not the major source of the observed brightness temperature variations.

However, by using our model of the complex dielectric constant of liquid H_2SO_4 and the radiative transfer model, we have demonstrated that liquid H_2SO_4 does have an effect on the millimeter-wave emission of Venus (see Table 6.1) and its presence must be included in any future modeling of the emission of Venus.

D) Sensitivity to H_2O vapor:

The expected absorption of H_2O vapor is included in the radiative transfer model in order to study its effects on the millimeter-wave emission of Venus. As a result, we have found that water vapor has a minimal effect on the calculated brightness temperature of Venus at millimeter wavelength (see Table 6.1). A plot of the computed brightness temperature of Venus with CO_2, SO_2 and H_2O is shown in Figure (6.13) using an abundance profile of 70 ppm at 30 km and an abundance that decreases linearly above and below 30 km.

E) Sensitivity to H_2SO_4 vapor:

The expected opacity of gaseous H_2SO_4 in a CO_2 atmosphere is also included in the radiative transfer model. This opacity is based on the VVW model of H_2SO_4 absorption as discussed in Chapter 5. An abundance profile of 25 ppm between 38 and 48 km

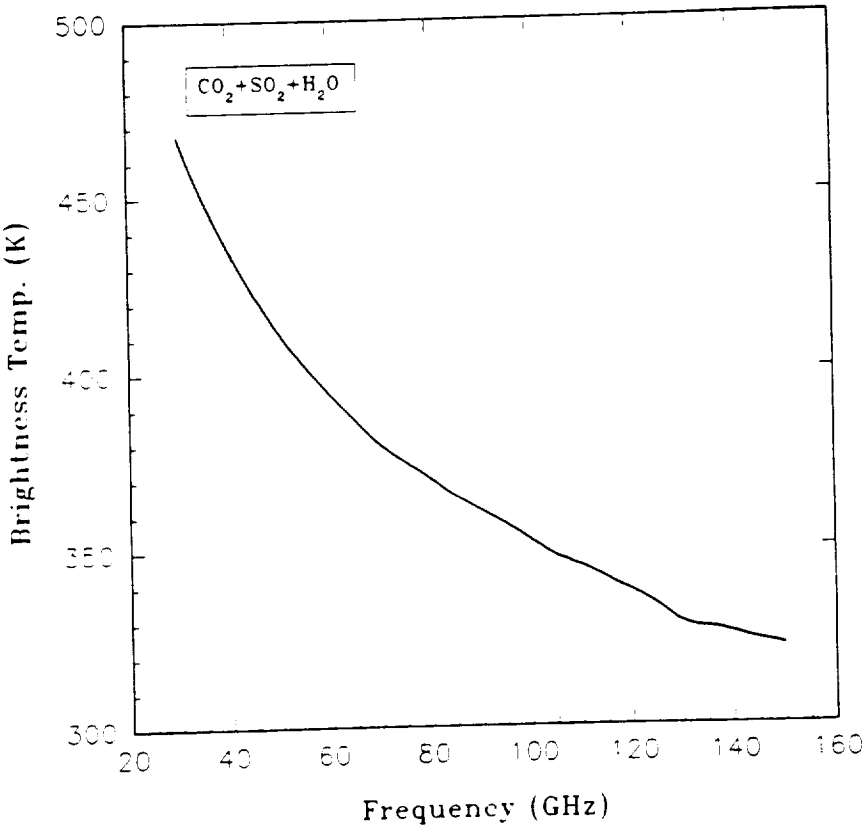

Figure 6.13 Calculated brightness temperature of Venus based only on CO_2, SO_2 and Water vapor.

is also used in our model. (This abundance of H_2SO_4 gas is based on the work of Jenkins and Steffes (1991), who reported average abundances on that order for the equatorial regions of Venus based on Pioneer Venus radio occultation studies. Note, however, that they reported abundances variations from 0 to 30 ppm, depending on location.) Above 48 km, the abundance profile follows the saturation abundance of H_2SO_4 as determined from the T-p profile of Venus and the partial pressure of H_2SO_4 (see appendix A). Below 38 km, the abundance is assumed to be zero.

A plot of the resulting brightness temperature spectrum of Venus between 30 and 230 GHz is shown in Figure (6.14), where a comparison between the brightness temperature with H_2SO_4 abundance of 25 and 10 ppm is shown.

F) Millimeter-wave spectra of Venus:

A plot of the calculated millimeter-wave spectrum of Venus based on the presence of one or more constituents is shown in Figure (6.15) for frequencies between 30 and 230 GHz. The abundance profile of each constituent used to develop this brightness temperature profile is summarized in Table 6.2.

A closer examination of the reported spectrum of Venus reveals several important features:

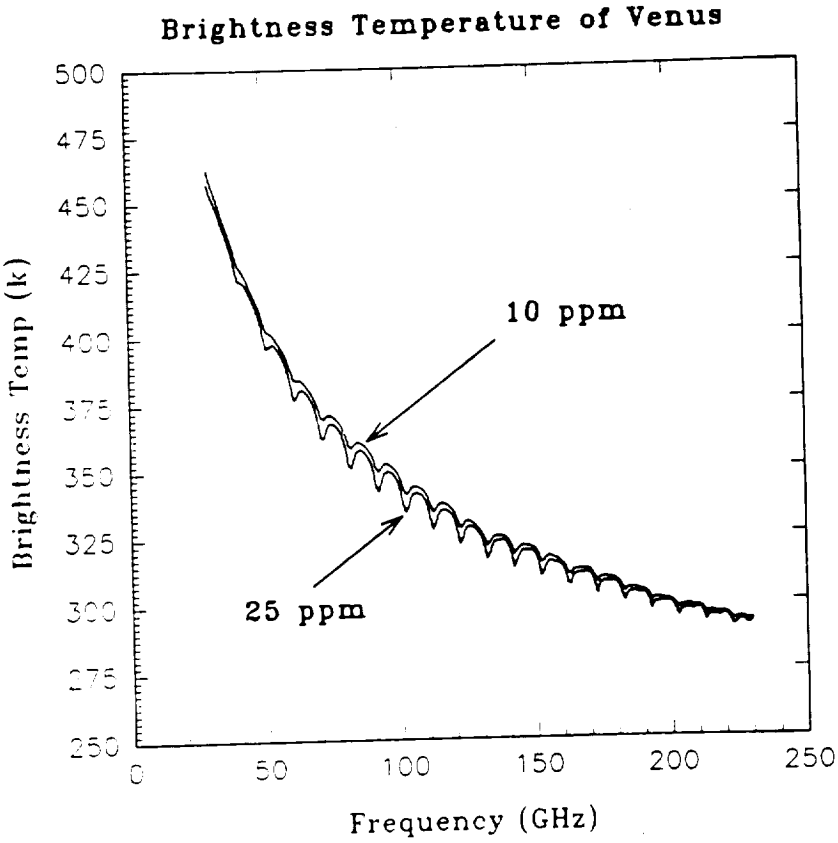

Figure 6.14 Calculated brightness temperature of Venus for H_2SO_4 abundances of 25 and 10 ppm for frequencies between 30 and 230 GHz.

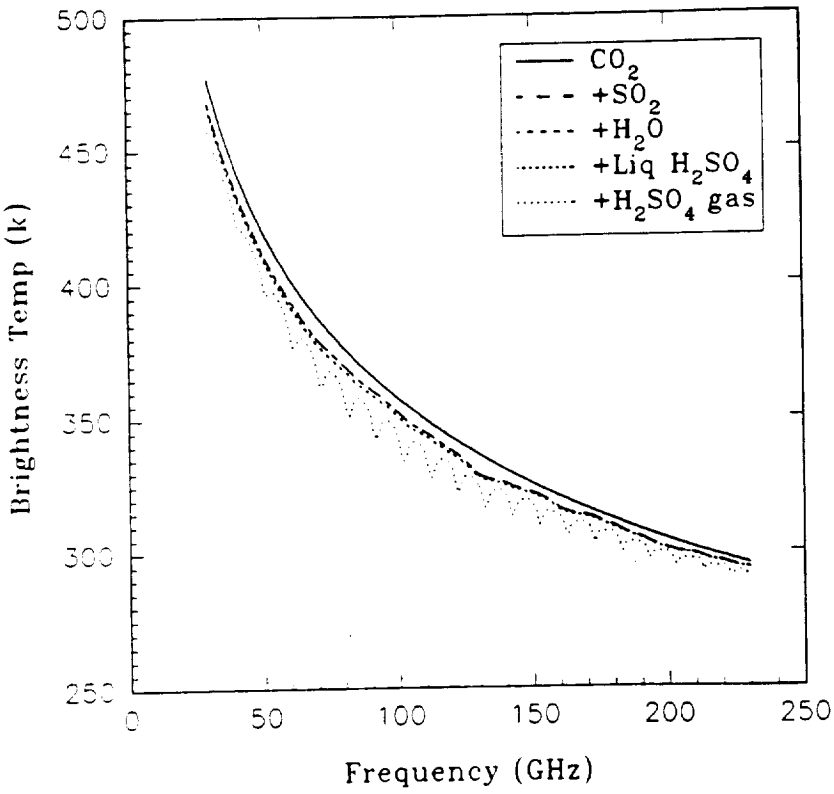

Figure 6.15 Comparison of the effects of atmospheric constituents on the brightness temperature of Venus between 30 and 230 GHz.

Table 6.2 Abundance profiles for each of the constituents present in the atmosphere of Venus.

Atmospheric Constituents	Abundance Profile
CO_2	96 % and 3% N_2
Gaseous SO_2	62 ppm below 48 km and exponentially decreasing above 48 km.
Water Vapor	70 ppm at 30 km. and decreases linearly below and above 30 km.
H_2SO_4 (liquid)	85% concentration by weight. Droplets diameter of 25 microns and a bulk density of 50 mg/m_3.
Gaseous H_2SO_4	25 ppm between 38 and 48 km, zero ppm below 38 km. Abundance follows saturation abundance above 48 km.

a) Gaseous SO_2 does affect the brightness temperature of Venus. However, variations in its abundance cannot completely account for the measured 30 K variation in emission measured by de Pater et al. (1991). In addition, gaseous SO_2 seems to have the biggest effect on the brightness temperature at frequencies below 180 GHz as noted in Table 6.1. This frequency dependence of the change in brightness temperature can be well explained by carefully examining Figures 6.16 and 6.17 which show the weighting functions of the atmosphere of Venus at several frequencies. (Note that the abrupt discontinuities in the weighting function are due to the

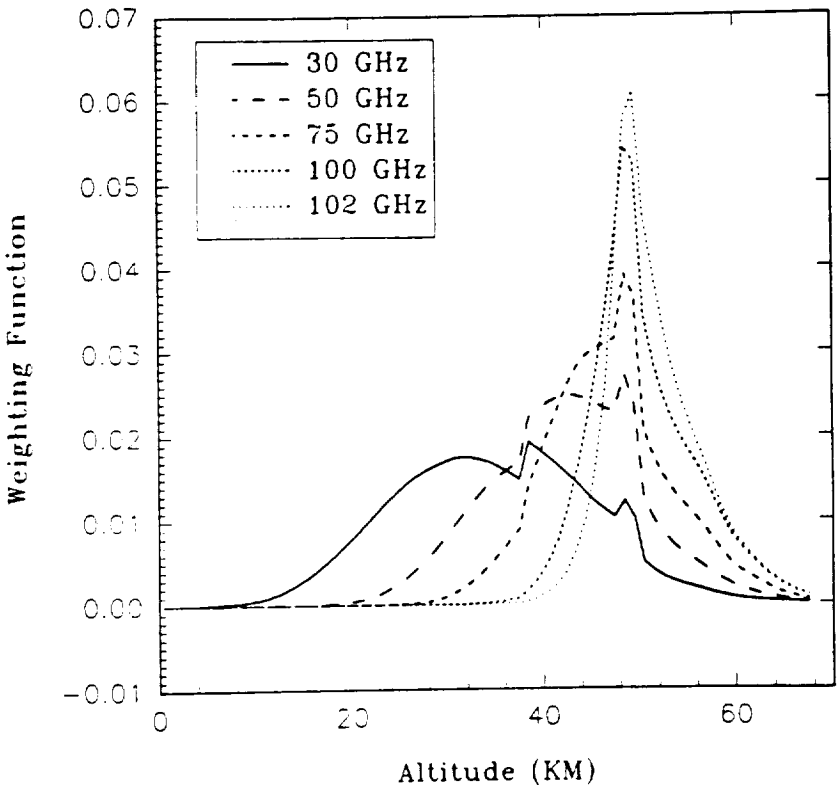

Figure 6.16 Calculated weighting functions of the atmosphere of Venus as function of altitude at 30,50,75,100 and 102 GHz.

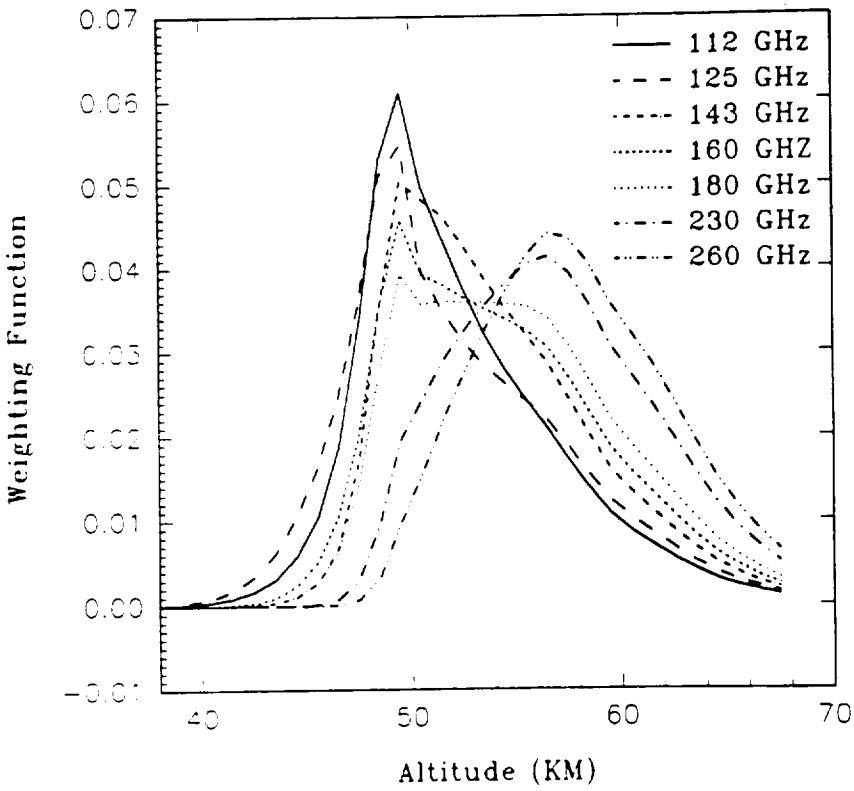

Figure 6.17 Calculated weighting functions of the atmosphere of Venus as function of altitude at 112, 125, 143, 160, 180, 230, 260 GHz.

addition of one or more atmospheric constituents.) Also note that at frequencies below 180 GHz, most of the emission from the atmosphere of Venus is emanating from a portion of the atmosphere where gaseous SO_2 is abundant, in this case below 48 km. At frequencies above 180 GHz, the weighting function shifts up in altitude which means that the emission is due to the absorption of the constituents present above 50 km, predominately gaseous CO_2.

b) The addition of water vapor to SO_2 and CO_2 has little effect on the brightness temperature of Venus. This is indicated by the fact that the brightness temperature profile of Venus with SO_2 and CO_2 alone completely overlays the brightness temperature profile obtained when water vapor is added (see Figure 6.15).

c) The presence of liquid sulfuric acid as a cloud condensate does have an impact on the calculated brightness temperature of Venus as shown in Table 6.1. Specifically, for frequencies between 30 and 120 GHz, a drop of 2 K is observed due to the addition of H_2SO_4 condensate to the atmosphere of Venus. Between 120 and 150 GHz, a drop of 1 K is observed. Above 150 GHz, the drop in the brightness temperature is barely noticeable. This effect is also noticed in Figure 6.15 where a complete overlay of the brightness spectra with and without

liquid sulfuric acid is observed at frequencies above 150 GHz.

d) Aside from gaseous CO_2, gaseous H_2SO_4 seem to have the biggest effect on the calculated brightness temperature of Venus. Specifically at 112 GHz, the brightness temperature with CO_2+SO_2+H_2SO_4(liq)+H_2O is 342 K. When gaseous H_2SO_4 is added to the atmosphere of Venus, a drop of 14 K is observed (see Table 6.1). However, at 106 GHz, a drop of only 5 K is obtained. This abrupt change in the brightness temperature between 106 and 112 GHz can be easily explained by the shape of the absorption profile of gaseous H_2SO_4 reported in Figure 6.9. From this profile, we see that at 112 GHz the absorption goes through a local maximum which tend to greatly decrease the calculated brightness temperature. At 106 GHz, the profile goes through a local minimum which yields a smaller change in the brightness temperature of Venus. This phenomenon is quite noticeable for frequencies between 50 and 180 GHz where several "dips" in the calculated brightness temperature are observed. Above 180 GHz, the magnitude of these dips decrease and the effect of the presence of gaseous H_2SO_4 in the atmosphere on the brightness temperature is minimized. This is consistent with the weighting function at 180 GHz which shows that most of the emission is emanating from altitudes above 50 km. Thus, at frequencies above 180 GHz, most of the observable

absorption in the atmosphere of Venus is due to the presence of gaseous CO_2.

e) Comparisons with radio observation of Venus:

Although many researchers have observed the radio emission from Venus at microwave frequencies (Steffes et al. 1990, Janssen and Poynter, 1981), very few have observed the emission from Venus at millimeter-wavelengths. de Pater et al. (1991) observed the millimeter-wave emission of Venus at 112 GHz and their observations showed a variation of 30 K in the emission between the night and day side of Venus.

Table 6.3 Comparison between observed and computed brightness temperature of Venus.

Frequency (GHz)	Computed Brightness Temperature (k)	Observed Brightness Temperature (k)
13.3	557	561±19[1]
18.46	519	520±17[1]
22.2	499	507±22[1]
112.2	328[2],343[3]	Max=365[a] Min=335[a]

[1] Steffes et al. 1990.
[2] 25 ppm H_2SO_4
[3] 0 ppm H_2SO_4
[a] de Pater et al. 1991.

Table 6.3 summarizes recent observations of Venus. The observed emissions are also compared with our calculated brightness temperature from the radiative transfer model. The results reported in Table 6.3 indicates that our radiative transfer model agrees with the measured values. This is quite important since we can now state that the observed variations by de Pater et al. (1991) are most likely due to variations in the abundance of gaseous sulfuric acid and not to liquid sulfuric acid as previously suggested.

CHAPTER 7

SUMMARY AND CONCLUSIONS

7.1 Uniqueness of Work

This research provides new information which is essential to the understanding of the millimeter-wave spectrum of Venus. In addition, this research provides contributions to both planetary science and millimeter-wave measurement techniques. In the laboratory measurements area, our measurement of the dielectric constant of liquid sulfuric acid represents the first time that its absorption coefficient has been determined at millimeter-wavelengths. The results of the measurement of the opacity of SO_2 under Venus-like conditions are very significant in that they present the first time that the opacity of sulfur dioxide has been measured at millimeter-wavelengths under simulated Venus conditions. In addition, our results have shown that the f^2 dependence of the opacity of SO_2

is not valid and that the Van Vleck-Weisskopf formalism seems to accurately model the opacity of SO_2 at frequencies above 20 GHz. As a result, an updated abundance profile of SO_2 has been determined. The measurements of the dissociation factor of H_2SO_4 have provided a direct technique for measuring the partial pressure of gaseous sulfuric acid. The results from the latter measurements are used to determine the saturation abundance of H_2SO_4 in the atmosphere of Venus. Finally, our measurement of the millimeter-wave opacity of gaseous H_2SO_4/CO_2 under Venus-like conditions represents the first laboratory measurement of the opacity of this gaseous mixture at 94 GHz.

Several contributions toward microwave and millimeter-wavelength measurement techniques have resulted from our research. This includes an innovative technique of measuring the opacity of a gaseous mixture while minimizing the effects of dielectric loading on the quality factor of the resonator used. In addition, the measurement of the dielectric constant of liquid sulfuric acid has demonstrated the ability of a free space transmission system for conducting such measurements.

Although the development of the radiative transfer model is not entirely new, the incorporation of our measured results into the model provides for the first time the ability to accurately interpret the millimeter-wavelength emission of Venus. Results of the radiative transfer model indicate that gaseous SO_2 does have a significant effect on the emission of

Venus. In addition, the presence of H_2SO_4 cloud layer does affect the emission of Venus in that the cloud effect is comparable with that of gaseous SO_2. However, we have found that the presence of SO_2 and liquid H_2SO_4 cannot completely account for the measured variations in the observed emission at 112 GHz. Another important finding is that water vapor does not significantly affect the emission at millimeter-wavelengths. Lastly, we have demonstrated that variations in the abundance of gaseous sulfuric acid is the most likely cause of the measured variation in the millimeter-wave emission.

These results, in conjunction with the reported observations of Venus, have allowed us to develop a new abundance profiles for the atmospheric constituents of Venus. Revised limits on the abundances of gaseous SO_2 and H_2SO_4 have been determined. This type of information is crucial in the development of theories regarding the evolution of Venus which in turn may help in the study of planet earth.

Finally, this research has resulted in the publication of two papers:

1) Fahd, A. K., and P. G. Steffes, Laboratory measurements of the millimeter-wave properties of liquid sulfuric acid (H_2SO_4), J. Geophysical Research : Planets, 96, E2, 17471-17476, 1991.

2) Fahd, A. K., and P. G. Steffes, Laboratory measurements of the opacity of gaseous sulfur dioxide under Venus-like conditions, Icarus, accepted for publication, March, 1992.

In addition, this research has been presented as several conference reports:

1) A.K. Fahd and P.G. Steffes, "Laboratory Measurements of the Opacity of Gaseous Sulfuric Acid (H_2SO_4) at 94 GHz.", Bulletin of the American Astronomical Society, vol. 22, 1991. Presented at 23rd Annual Meeting of the Division for Planetary Sciences of the American Astronomical Society, Palo-Alto, November 4,1991.

2) A.K. Fahd and P.G. Steffes, "Laboratory Measurements of the Opacity of Gaseous Sulfur Dioxide (SO_2) at 94 GHz," Bulletin of the American Astronomical Society, vol. 22, 1991. Presented at 23rd Annual Meeting of the Division for Planetary Sciences of the American Astronomical Society, Palo-Alto, November 4, 1991.

3) A.K. Fahd and P.G. Steffes, "Laboratory Measurements of the Millimeter-Wave Properties of Liquid Sulfuric Acid (H_2SO_4) Between 90 and 100 GHz," Bulletin of the American Astronomical Society, vol. 22, pg. 1035, 1990.

Presented at the 22nd Annual Meeting of the Division for Planetary Sciences of the American Astronomical Society, Charlottesville, Virginia, October 22, 1990.

4) A.K. Fahd and P.G. Steffes, "Laboratory Measurements of the 1.3 and 13.3 cm Opacity of Gaseous SO_2 under Simulated Conditions of the Middle Atmosphere of Venus," Bulletin of the American Astronomical Society, vol. 22, pg. 1032, 1990. Presented at the 22nd Annual Meeting of the Division for Planetary Sciences of the American Astronomical Society, Charlottesville, Virginia, October 22, 1990.

5) A.K. Fahd and P.G. Steffes, "Laboratory Measurements of the Dissociation Factor of Gaseous Sulfuric Acid (H_2SO_4)," Bulletin of the American Astronomical Society, vol. 21, pg. 927, 1989. Presented at the 21st Annual Meeting of the Division for Planetary Sciences of the American Astronomical Society, Providence, Rhode Island, November 1, 1989.

7.2 Suggestion for Future Work

Although we are in a better position to explain the observed variation in the millimeter-wave emission from Venus, several important ideas can be further explored to better understand the millimeter-wave spectrum of Venus:

A) Conduct a more accurate measurement of the temperature dependence of the opacity of gaseous SO_2: This can be achieved by conducting laboratory measurements using a configuration similar to the one described in this work but at different temperatures (specifically, at a range of temperatures that are characteristic of the atmosphere of Venus). As a result of this proposed measurement, one could develop a more accurate temperature dependence for the SO_2 opacity, and hence a better estimate on the abundance of sulfur dioxide in the atmosphere of Venus.

B) Develop a laboratory apparatus to be used in conjunction with a mass spectrometer to investigate the presence of gaseous H_2SO_4 dimers at certain pressures and temperatures. The presence of these dimers can greatly influence the measured partial pressure of gaseous H_2SO_4 which can yield to erroneous determination of the saturation abundance of gaseous H_2SO_4 in the atmosphere of Venus (see Appendix A).

C) Conduct radio observations of the emission of Venus at 112 and 106 GHz so as to confirm the presence of the reported "dip" in the brightness temperature of Venus as reported in Chapter 6.

D) Development of a Fourier Transform Spectrometer which can be mounted on existing millimeter and submillimeter antennas. The development of such an apparatus will make it easier to study broad spectral features of Venus.

APPENDIX A

A.1 Measurement of the Vapor Pressure of Sulfuric Acid (H_2SO_4)

The apparatus developed for the measurement of the dissociation factor of gaseous sulfuric acid is shown in Figure A.1. In this setup, a large chamber (of known volume, in this case 34.8 Liters) was constructed using Pyrex glass as shown in Figure A.2. The reasons for choosing glass are its ability to withstand high temperatures in addition to the ability of monitoring the status of the sulfuric acid vapor to make sure that the vapor does not condense during the pressure measurement. The top of the glass vessel is sealed using a stainless steel plate. In order to form a good seal at the glass lip, a high temperature Viton O-ring is sandwiched between the glass and the plate.

Throughout the setup, stainless steel tubes are used to minimize the acid-metal reaction at high temperatures. In addition, all stainless steel tubing was submerged in a sulfuric acid solution for an extended period of time prior to the experiment. This process helped minimize the amount of impurities (within the stainless steel tubing) which could

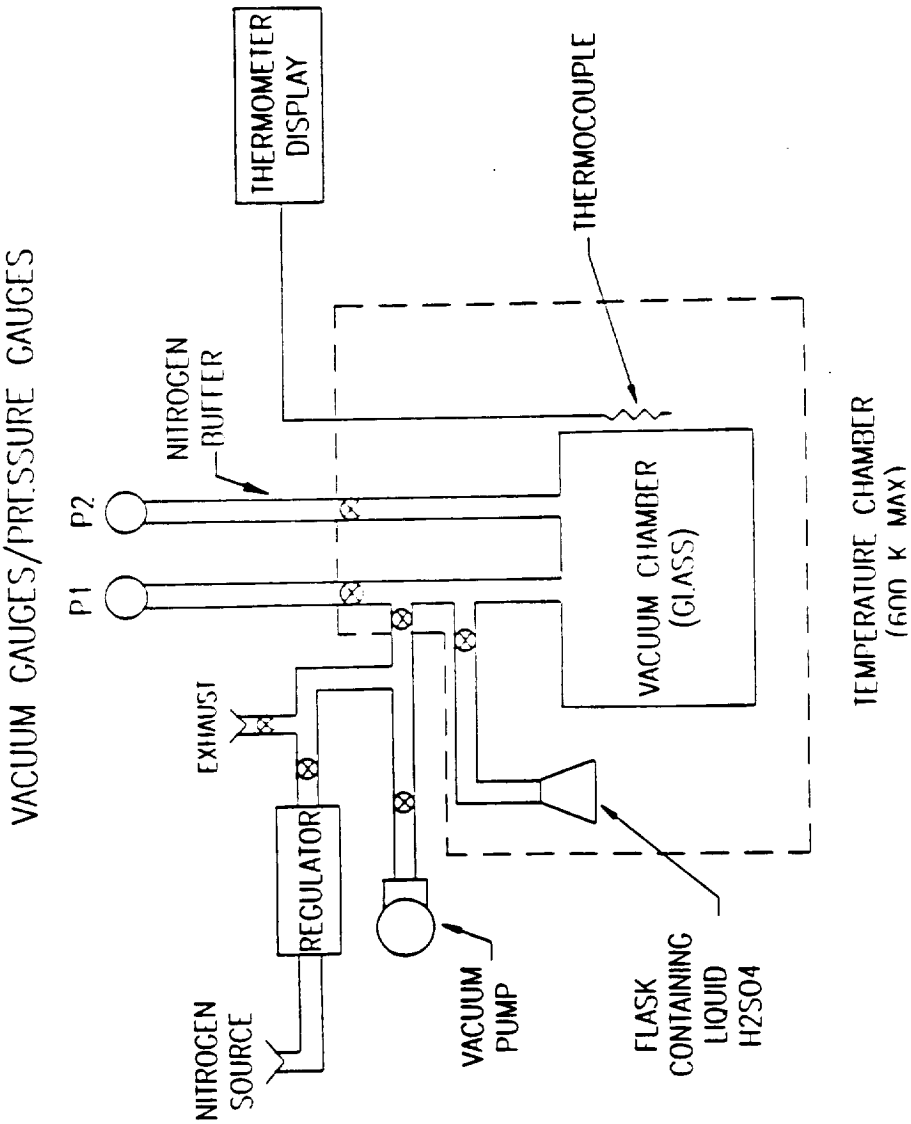

Figure A.1 Laboratory apparatus used to measure the dissociation factor of gaseous sulfuric acid.

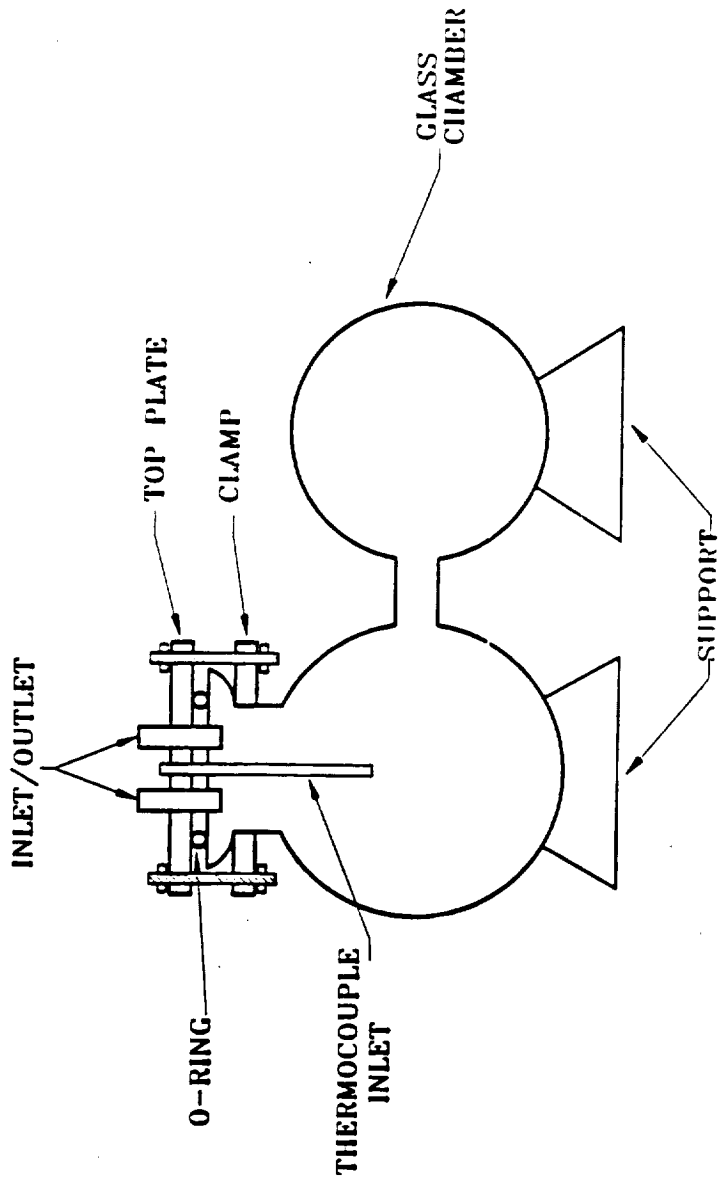

Figure A.2 Cross sectional view of the vacuum chamber used in the setup.

react with the sulfuric acid producing inaccurate results. A custom made Pyrex flask was designed so that the liquid sulfuric acid could be introduced and extracted from the system with ease. The flask is filled with a precisely known volume of liquid sulfuric acid at room temperature where for volumes less than 1 ml, repeatable accuracies of better than .01 ml have been obtained.

The complete system is contained inside a temperature controlled oven. The system employs two vacuum gauges, P1 and P2 where gauge P1 is used to measure pressures in the 0-20 Torr range while gauge P2 is used to measure pressures ranging from 0 to 800 Torr with 1 Torr increments. A small amount of nitrogen is used in the experimental setup as a buffer so as to prevent any sulfuric acid vapor from coming in direct contact with gauge P2. The laboratory measurements were conducted on two different concentrations of liquid sulfuric acid (99% and 95.9% by weight) at distinct temperatures ranging between 480 to 603 K (Table A.1).

The measurement procedure can be summarized as follows: The oven is first heated to the desired temperature. Once this temperature is reached, the chamber is evacuated. By using gauge P1 as a vacuum monitor, we are able to check the status of the vacuum chamber in order to insure that no major leaks are present. Although no leak-proof vacuum was obtained, we were able to maintain a leak rate within the system of less

than .8 Torr/hour. The minimization of these leaks has a major effect on the calculation of the dissociation factor since any substantial leaks in the system can alter the measured pressure. The nitrogen buffer valve is then opened and the resulting pressure (due only to nitrogen gas) is recorded. The system is then evacuated and the buffer is refilled with equal amount of nitrogen. The remaining nitrogen in the system is evacuated and the flask (containing liquid sulfuric acid) valve is opened allowing the sulfuric acid liquid to reach vapor pressure equilibrium with the evacuated chamber. Once equilibrium is reached, the flask valve is closed and a visual check is made to verify that the remaining liquid acid is clear. After the flask is closed, the valve connecting gauge P2 (containing a small amount of nitrogen as a buffer) is opened and the system is allowed to reach equilibrium. The resulting chamber pressure is then recorded.

Throughout this process, the system temperature was maintained to within ± 5 K so as to minimize the effects of temperature variation on the results. Once the chamber pressure was recorded, the oven was shut off and the gaseous sulfuric acid was evacuated from the chamber. The system is then allowed to cool overnight to its original room temperature. At that point, the remaining volume of liquid sulfuric acid is measured and the evaporated liquid volume is determined.

A.2 Determination of the Dissociation Factor and the Partial Pressure of Gaseous Sulfuric Acid (H_2SO_4)

The dissociation factor of gaseous H_2SO_4 can be inferred from a number of quantities actually measured during the experiment. Let V_{Liquid} (ml) denote the volume (at room temperature) of liquid H_2SO_4 and liquid H_2O (since we are not using a 100 % concentration by weight) that evaporates from the flask during the experiment. Thus, V_{Liquid} can be expressed as a function of V_{H_2O} and $V_{H_2SO_4}$,

$$V_{Liquid} = \mathcal{F}\ (V_{H_2SO_4}\ ,\ V_{H_2O}) \qquad \textbf{(A.1)}$$

The percent concentration of the liquid sulfuric acid (by weight) can be defined as follows:

$$PCM = \frac{V_{H_2SO_4}\ \rho_{H_2SO_4}}{V_{H_2SO_4}\ \rho_{H_2SO_4} + V_{H_2O}\ \rho_{H_2O}} \qquad \textbf{(A.2)}$$

(i.e. PCM=.99 for 99 % concentration by weight), where ρ_{H_2O} is the density of H_2O (1 g/ml) and $\rho_{H_2SO_4}$ is the density of liquid sulfuric acid. From equations (A.1) and (A.2) one can solve for V_{H_2O} and $V_{H_2SO_4}$,

$$V_{H_2O} = \frac{V_{Liquid}\ \rho_{Liquid}\ (1-PCM)}{\rho_{H_2O}} \qquad \textbf{(A.3)}$$

and

$$V_{H_2SO_4} = \frac{V_{Liquid}\ PCM\ \rho_{Liquid}}{\rho_{H_2SO_4}} \qquad \textbf{(A.4)}$$

where ρ_{Liquid} is the density of the liquid mixture. Thus by using equations (A.3) and (A.4) one can calculate the volume of liquid H_2SO_4 and liquid H_2O that evaporated from the liquid solution. This calculation is necessary since the liquid solution used in the experiment is not 100 % sulfuric acid and any additional pressure that is due to dissolved water must be accounted for. The pressure due to the vaporized liquid water can be found by calculating the number of evaporated moles and using the ideal gas law as follows,

$$\eta_{Water} = V_{H_2O}\ \frac{\rho_{H_2O}}{16} \qquad \textbf{(A.5)}$$

where η_{water} is the number of the evaporated moles of water. The pressure due to η_{water} , P_{water}(atm), can then be calculated from,

$$P_{water} = \frac{\eta_{water}\ R\ T}{V_{Chamber}} \qquad \textbf{(A.6)}$$

where R is the ideal gas constant (.08205 l. Atm/mole K.), T is the temperature of the chamber in K and $V_{Chamber}$ (liters) is the volume of the vacuum chamber.

The net pressure expected from the evaporated sulfuric acid molecules (P_{Net}), can be written as,

$$P_{Net} = P_{Result} - P_{Water} - P_{Nitrogen} \qquad \textbf{(A.7)}$$

where P_{Result} is the measured pressure from gauge P2 and $P_{Nitrogen}$ is the pressure in the system due only to the nitrogen buffer. Thus P_{Net} can be thought of as the pressure due to H_2SO_4 and any additional SO_3 and H_2O molecules that dissociate from the evaporating sulfuric acid. As a result, equation (A.7) can be written as,

$$P_{Net} = P_{H_2SO_4} + P_{SO_3} + P_{H_2O} \qquad \textbf{(A.8)}$$

where P_{H_2O} in equation (A.8) is a different quantity than that determined in equation (A.6). The application of the ideal gas equation to P_{Net} yields,

$$P_{Net}\ V_{Chamber} = \eta_{Total}\ R\ T \qquad \textbf{(A.9)}$$

where η_{Total} is the total number of moles of gas that result from the evaporated sulfuric acid liquid. It can be written as,

$$\eta_{Total} = \eta_{H_2SO_4}\ (1+D) \qquad \textbf{(A.10)}$$

where $\eta_{H_2SO_4}$ is the number of moles of liquid sulfuric acid which vaporized while the flask was open and D is the dissociation factor defined as,

$$D = \frac{P_{SO_3}}{P_{H_2SO_4} + P_{SO_3}} \qquad \textbf{(A.11)}$$

The quantity $\eta_{H_2SO_4}$ can be obtained from the volume of the liquid sulfuric acid and its density,

$$\eta_{H_2SO_4} = V_{H_2SO_4} \frac{\rho_{H_2SO_4}}{98} \qquad \textbf{(A.12)}$$

The determination of the dissociation factor can then be calculated using equations (A.4,A.9,A.10,A.12),

$$D = \frac{98\ P_{NeT}\ V_{Chamber}\ (PCM + \rho_{H_2SO_4}\ (1 - PCM)) - (V_{Liquid}\ PCM\ \rho_{H_2SO_4}\ R\ T)}{V_{Liquid}\ PCM\ \rho_{H_2SO_4}\ R\ T} \qquad \textbf{(A.13)}$$

Thus if the chamber volume, the system temperature, the density of liquid sulfuric acid, the pressure resulting from the evaporated liquid acid, and the amount of the evaporated liquid are known, then a direct application of equation (A.13) will give the dissociation factor of the gaseous sulfuric acid. Once the calculated dissociation factor D is determined, the partial pressure of gaseous H_2SO_4 can then be calculated. This can be performed by using equation (A.8) and the fact that P_{H_2O} is equal to P_{SO_3},

$$P_{Net} = P_{H_2SO_4} + 2\ P_{SO_3} = P_{H_2SO_4} + 2\ P_{H_2O} \qquad \textbf{(A.14)}$$

by combining equations (A.11) and (A.14), the partial pressure of gaseous H_2SO_4 ($P_{H_2SO_4}$) can be written as,

$$P_{H_2SO_4} = \frac{P_{Net}\ (\ 1 - D\ )}{(\ 1 + D\ )} \qquad \textbf{(A.15)}$$

Thus the partial pressure of gaseous sulfuric acid can be computed from equation (A.15) provided that the net pressure measured and the resulting dissociation factor are known. For

the special case when the dissociation factor is unity, equations (A.10) and (A.12) yield,

$$P_{Net} = 2\ P_{SO_3} = 2\ P_{H_2O} \qquad \textbf{(A.16)}$$

Another important quantity that is used in the literature (Gmitro and Vermeulen, 1964) is K_p which is known as the equilibrium constant and it is defined as,

$$K_p = \frac{P_{SO_3}\ P_{H_2O}}{P_{H_2SO_4}} \qquad \textbf{(A.17)}$$

In order to use our results to calculate the equilibrium constant of gaseous sulfuric acid, we need to express K_p as a function of the dissociation factor and the partial pressure of gaseous sulfuric acid. A direct manipulation of equations (A.11) and (A.17) yields,

$$K_p = \frac{D^2\ P_{H_2SO_4}}{(\ 1 - D\ )^2} \qquad , \quad D \neq 1 \qquad \textbf{(A.18)}$$

Using equation (A.18) one can calculate the equilibrium constant from our inferred dissociation factor and our inferred partial pressure of gaseous H_2SO_4. This calculation serves as a comparison between our results and the ones reported by Gmitro and Vermeulen (1964) and it can used in correcting the partial pressure of H_2SO_4 at temperatures below 480 K which were reported by Ayers et al.(1980).

A.3 Measurement Results

Measurements were carried out on two liquid H_2SO_4 samples, each having a different concentration. Measurements were conducted at six distinct temperatures ranging from 480 to 603 K. The lower temperature point is dictated by the sensitivity of the gauge P2 and its ability to accurately measure pressures below 1 torr while the upper bound on the temperature range is dictated by the maximum allowable temperature of the oven and the ability of some parts in the system to withstand these high temperatures.

The partial pressure of gaseous H_2SO_4 (99%, by weight) is shown in Figure A.3. In this figure, the illustrated points are results from the laboratory measurements (including error bars) while the solid line is a best fit model of the data according to the Clausius-Clapeyron model. From the best-fit model, the vapor pressure of gaseous sulfuric acid for temperatures between 480 and 603 K can be written as,

$$\ln p = 6.65 - \frac{6100}{T} \qquad \textbf{(A.19)}$$

where p is the sulfuric acid vapor pressure (atm) and T is the temperature in K. A similar result is obtained for 95.9% concentration and is shown in Figure A.4. A best fit expression for the latter concentration is given by,

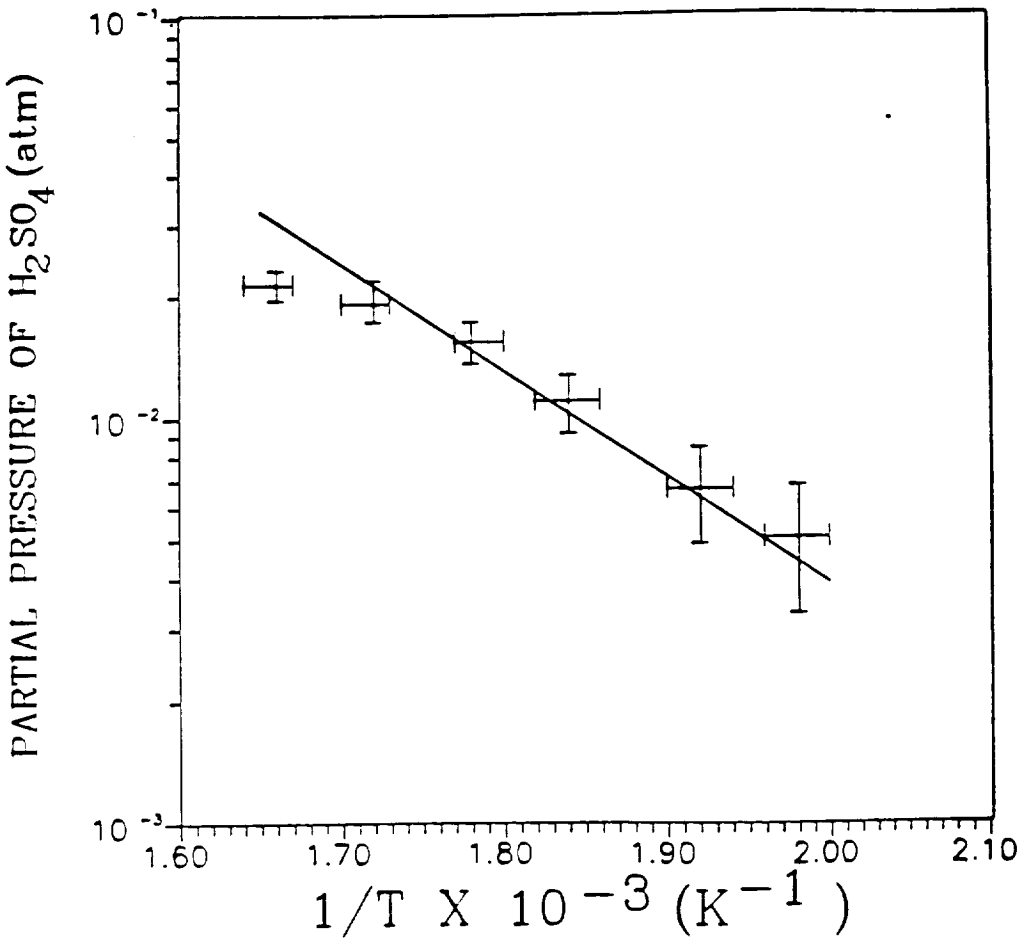

Figure A.3 Vapor pressure of gaseous sulfuric acid (99%) as a function of temperature. The illustrated points are from laboratory measurements while the solid line represents a best-fit model.

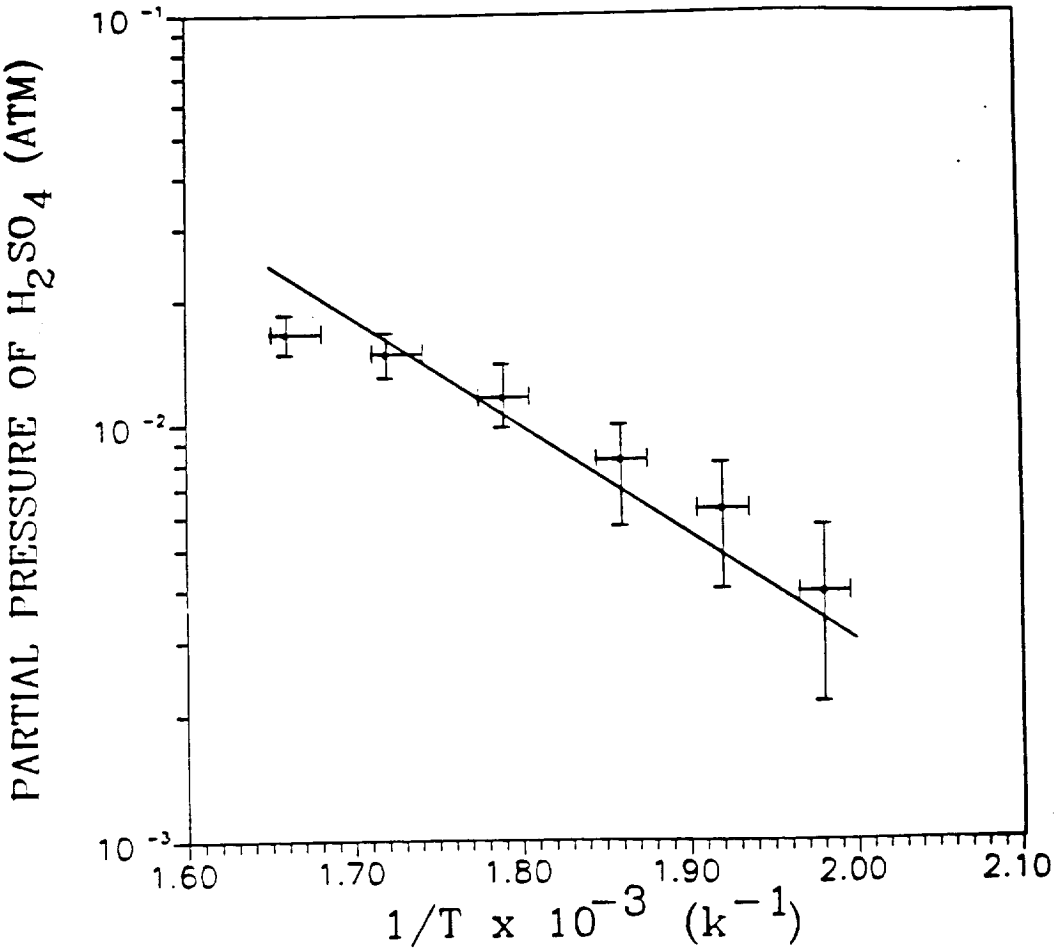

Figure A.4 Vapor pressure of gaseous sulfuric acid (95.9%) as a function of temperature. The illustrated points are from laboratory measurements while the solid line represents a best-fit model.

$$\ln p = 5.25 - \frac{5430}{T} \qquad \textbf{(A.20)}$$

A careful examination of the two figures reveals that the best-fit expression agrees with the measured data except for temperatures above 590 Kelvins where a deviation from the best fit model is observed. The laboratory measurements seem to indicate that a saturation effect is occurring at these high temperatures while our best fit model indicates a further increase in the partial pressure of gaseous sulfuric acid with temperature. This observed phenomenon is not yet fully understood but one can speculate that the Clausius-Clapeyron model may not be valid for these temperatures and an alternate model may be required (additional discussion regarding this effect is presented later in this Appendix).

A comparison between our expressions and the ones reported by Steffes(1985), Ayers et al., (1980) and Gmitro and Vermeulen (1964) is shown in Figure A.5. An examination of this figure reveals that Steffes overestimated the partial pressure for high temperatures while he underestimated the partial pressure for temperatures below 510 K. This deviation may be attributed to the fact that Steffes did not measure the dissociation factor but he assumed a 47% dissociation factor over the measured temperature range. The comparison between our results and the extrapolation of the results reported by Ayers et al. shows that their expression overestimates the

Table A.1 Dissociation factor of Sulfuric Acid H_2SO_4.

DISSOCIATION FACTOR OF GASEOUS H_2SO_4							
99% CONCENTRATION (ϱ=1.816 g/ml)				95.9% CONCENTRATION (ϱ=1.762 g/ml)			
T (K)	P_{water} (atm) $x10^{-8}$	P_{h2o} (atm) $x10^{-3}$	D	T (K)	P_{water} (atm) $x10^{-3}$	P_{h2o} (atm) $x10^{-3}$	D
505	6.49 6.35 6.22	3.88 5.42 6.96	.364 .519 .680	505	2.67 2.61 2.56	7.21 8.73 10.2	.445 .610 .782
521	11.2 11.0 10.9	9.94 11.5 13.0	.542 .634 .728	521	5.39 5.34 5.28	17.8 19.3 20.9	.610 .783 .768
543	15.3 15.1 15.0	12.3 13.9 15.4	.491 .559 .627	538	8.18 8.13 8.07	28.4 29.9 31.5	.644 .710 .756
561	23.4 23.3 23.1	21.2 22.8 24.3	.550 .595 .640	559	11.5 11.4 11.3	41.9 43.5 45.0	.694 .734 .774
583	30.9 30.7 30.6	29.8 31.4 33.0	.587 .621 .656	580	14.7 14.6 14.6	54.1 55.7 57.2	.699 .730 .762
603	36.3 36.1 36.0	36.4 38.0 39.6	.610 .640 .670	603	19.7 19.7 19.6	76.9 78.4 80.0	.756 .779 .803

partial pressure of gaseous sulfuric acid in this temperature range. This discrepancy may be due to the fact that the results reported by Ayers et al. were for temperatures ranging between 338 to 445 K. In addition, an examination of the best fit models for the two concentrations indicates that their

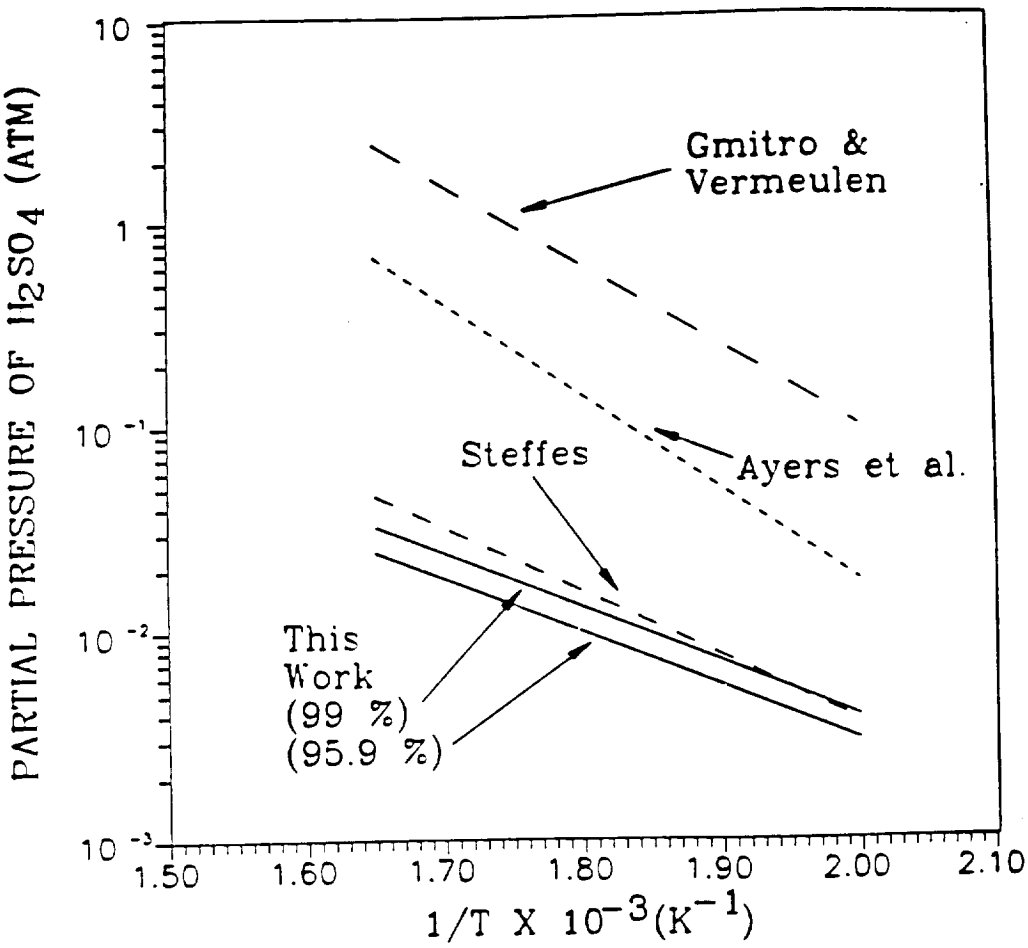

Figure A.5 Best-fit expression of the H_2SO_4 partial pressure (solid line) of our data in comparison with the results of Steffes (1985), Ayers et al. (1980), and Gmitro and Vermeulen (1964).

slope did not change with acid concentration which suggests that the partial pressure is directly related to the concentration of liquid sulfuric acid. Thus as the concentration of the acid decreases so does its vapor pressure.

The resulting values of the dissociation factor for both liquid concentrations calculated from our measurement are listed in Table A.I. These values are obtained from the measured pressure and the volume of liquid that evaporated during the measurement by using equation (A.13). In addition, Table A.I lists the calculated values of P_{h2o} and P_{water} as determined from our measurements. The upper and lower values of the dissociation factor and calculated pressures presented in this table include uncertainties due to the pressure reading in addition to uncertainties in the evaporated liquid volume.

To use the above results in the determination of the saturation abundance and mixing ratio of gaseous sulfuric acid in the atmosphere of Venus, we must evaluate the partial pressure of H_2SO_4 at lower temperatures (330 to 480 K). A Direct extrapolation of our results to lower temperatures may not be valid since the actual partial pressures often deviate from the Clausius-Clapeyron model. Since the laboratory measurements by Ayers et al. were conducted in a more appropriate temperature range (338-445 K), we instead apply

our results for the equilibrium constant K_p to the Ayers et al. data in order to recalculate a new partial pressure. (This is because these authors had previously used a theoretically derived value for the equilibrium constant for deriving the partial pressure). This process requires the calculation of a best-fit expression for the equilibrium constant according to our measurements which can be written as,

$$\log k_p = - \frac{3925}{T} + 8.33 \qquad \textbf{(A.21)}$$

where K_p is in Torr and T is the temperature in K. A plot of the above result compared with the result reported by Gmitro and Vermeulen (1964) is shown in Figure A.6. In this figure, the dashed line represents a best fit model for K_p as reported by Gmitro and Vermeulen, the illustrated data points are the calculated values for K_p from our laboratory measurements, and the solid line is a best-fit model to our data as given in equation (A.21) (In the calculation of our best-fit expression, the effect of the equilibrium constant at 521 K on the model was not included. The exclusion of this data point is mainly due to the high value of the dissociation factor observed at that temperature point as seen in Table A.I). In order to compute the partial pressure at temperatures between 330 and 480 K, we need to extrapolate the best fit model to cover that temperature range. The results of this extrapolation are shown in Figure A.7 where the dashed line

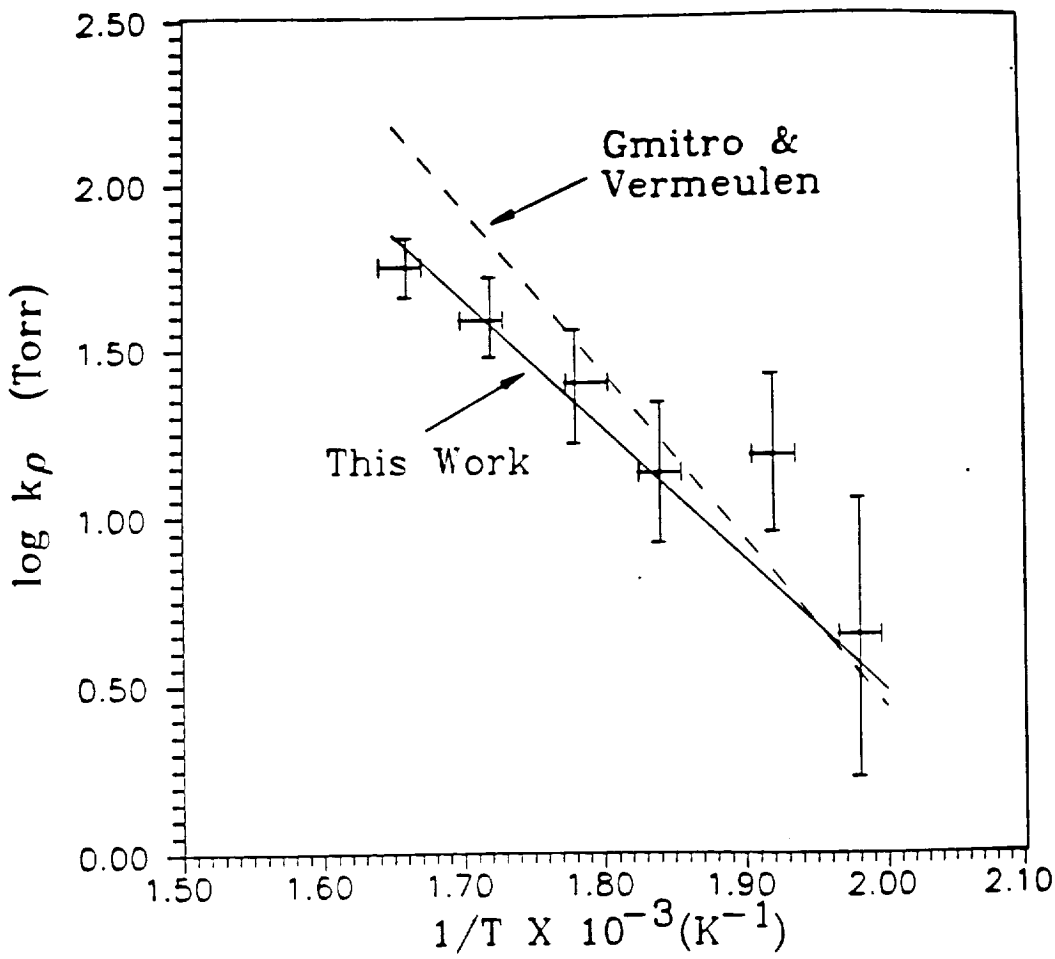

Figure A.6 Comparison between our best-fit expression for the equilibrium constant and the data reported by Gmitro and Vermeulen (1964). Error bars due to temperature and pressure are shown.

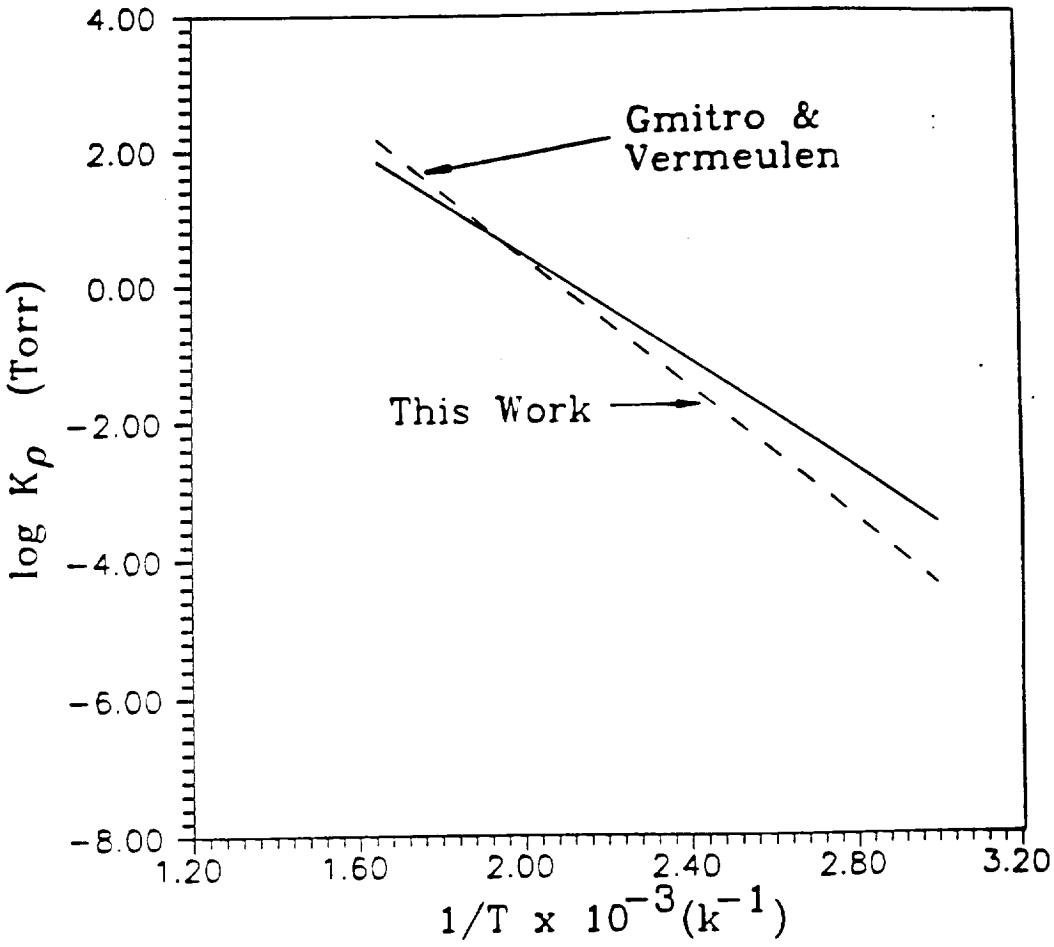

Figure A.7 Comparison between our best-fit expression for the equilibrium constant and the data reported by Gmitro and Vermeulen (1964) between 330 and 603 K.

represents the extrapolation of the data reported by Gmitro and Vermeulen and the solid line represents the extrapolation of our best-fit model. A comparison of the two best-fit lines reveals that a noticeable difference between the two respective values of the equilibrium constant is observed.

As stated, the computation of the partial pressure of H_2SO_4 for temperatures between 330 and 480 K requires the correction of the data reported by Ayers et al. (1980) using the new values of K_p. This process requires the calculation of the total vapor pressure indicated by Ayers et al. (which was not presented in their paper) and the recalculation of the new partial pressure of gaseous sulfuric acid using the new K_p values. The values of the water vapor pressure used in this calculation were from the data reported by Gmitro and Vermeulen since they did not greatly differ from the one measured in our experiment (480 to 603 K) and were also used by Ayers et al. . The resulting best-fit expression for the partial pressure of gaseous H_2SO_4 (in the 330 to 480 K range) using our values for K_p can be expressed as ,

$$\ln p = - \frac{10331}{T} + 16.4 \qquad \textbf{(A.22)}$$

where p is the pressure in atmospheres and T is the temperature in Kelvins.

A complete plot of the partial pressure of gaseous sulfuric acid as a function of the temperature is shown in

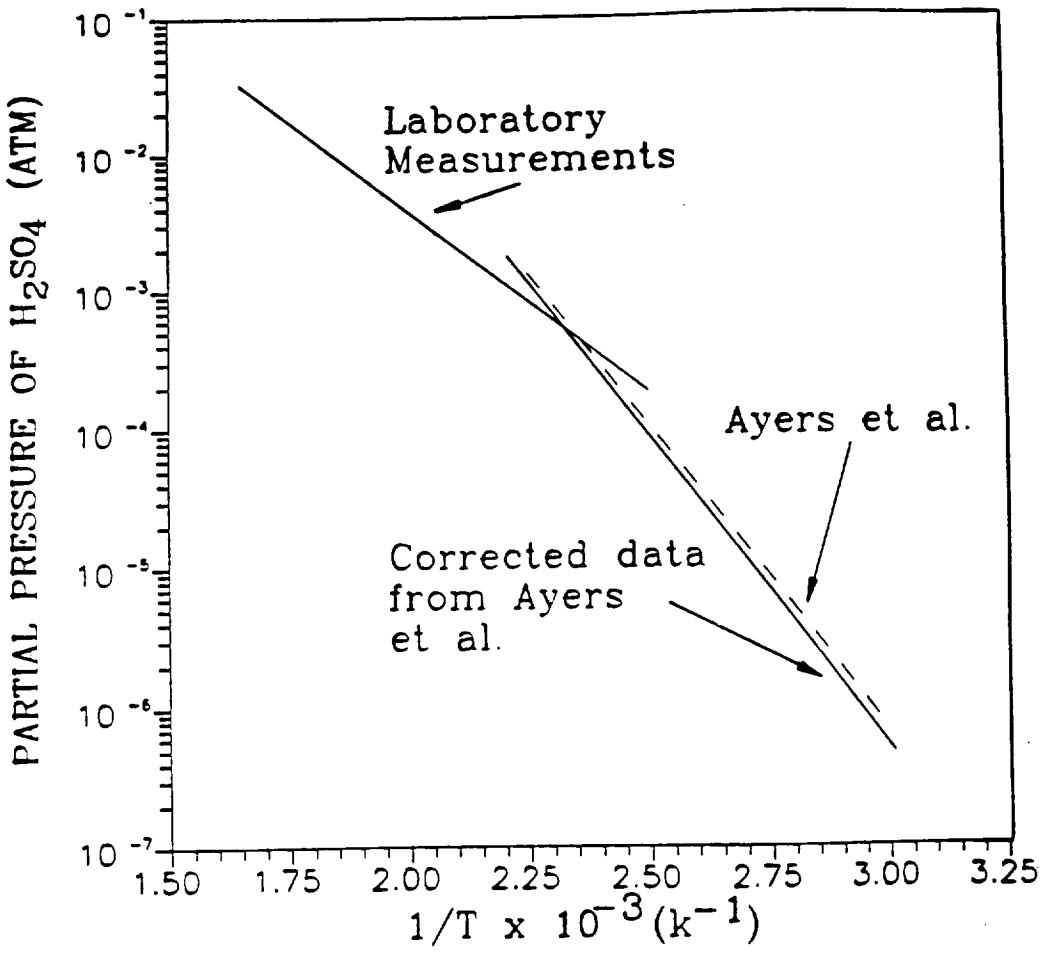

Figure A.8 Best-fit plot of the measured partial pressure of gaseous sulfuric acid (99 %) over a wide range of temperatures.

Figure A.8. An examination of this figure shows that there exists different pressure-temperature dependencies in the two ranges shown. For temperatures below 480 K, equation (A.22) can be used to infer the partial pressure while equation (A.19) can be used to infer the partial pressure for temperatures higher than 480 K. In addition, the comparison between our results and the results reported by Ayers et al.(1980) do show a slight difference in the partial pressure values for temperatures between 330 and 480 K. However, a significant change in the partial pressure of gaseous sulfuric acid is observed for temperatures above 480 K. Thus for the lower temperature range, our results seem to agree with the results reported by Ayers et al. while for temperatures above 480 K a significant change between the two results is observed.

A further examination of Figure A.8 indicates a change in the slope of the partial pressure line as a function of the temperature is also observed. This effect is not uncommon in the vapor-pressure behavior of many chemical solutions. For instance, various chemicals have been reported to have a similar vapor pressure-temperature dependence as gaseous H_2SO_4 (e.g., KCl, KBr, and Benzyl Alcohol, (CRC handbook)). Thus the slope of the partial pressure of the chemicals listed above greatly depends on the temperature at which the measurement is being conducted.

Another possible factor which may cause a difference in the slopes in Figure A.8 may be attributed to the formation of sulfuric acid clusters (clusters have been reported to form in the vapor phase, Kay 1984). This mechanism can greatly affect our results by reducing the actual vapor pressure and causing inaccurate measurements of the vapor pressure in the system. In addition, this phenomena can lead to inaccurate values of the boiling point temperatures of the sulfuric acid solutions used in our measurements. Although we have no evidence that clusters were formed, we believe that this effect may have caused the roll-off in the pressure measurement at higher temperatures (T> 580 K, where we note a saturation in the sulfuric acid vapor pressure curve as temperature is increased (see Figure A.8). Nevertheless , we have computed the boiling point temperature of the acid used in our measurement based on the extrapolation of the partial pressure of sulfuric acid and the equilibrium constant k_p in order to obtain a total pressure of 1 atmosphere. The computed values are : 377 C for 99.0% and 363 C for the 95.9% acid concentration. These projected values are higher than previously reported boiling point temperatures (Gmitro and Vermeulen, 1964) which indicates that clusters may have formed thus causing lower vapor pressure readings and hence higher boiling point temperatures.

BIBLIOGRAPHY

Ayers, R.P., R.W. Gillet and J.L. Gras. On the vapor pressure of sulfuric acid. Geophys. Res. Lett. 7, 433-436, 1980.

Barrett, A. H., Microwave absorption and emission in the atmosphere of Venus, J. Astrophys., 133, 281-293, 1961.

Battan, L.J., Radar observation of the atmosphere. University of Chicago Press, Chicago, 1973.

Brand, J.C.D., J.C. James and A. Rutherford, Dielectric dispersion in sulfuric acid, J. Chem. Soc., 2447-2456, 1953.

Bullington, K, Radio Propagation Fundamentals, Bell System Technical Journal, 36, 593-626, 1957.

Chedin, A., N. Husson, N.A. Scott, I. Colten Hellacat, A. Berroir 1982. GEISA data bank (No. 3).

Cimino, J. B., The composition and vertical structure of the lower cloud deck on Venus, Icarus, 51, 334-357, 1982.

Cole, K.S. and R.H. Cole, J. Chem. Phys., 9, 341, 1949.

Dryagin, Yu A., A.G. Kislyakov, L.M. Kukin, A.I. Naumov, and L.I. Fedoseev. Sov. Radiophys., 9, pp. 1078, 1966.

de Pater, I., F. P. Schloerb, and A. Rudolph, Venus images with the hat creek interferometer in the j=1-0 CO line, Icarus, 90, 282-298, 1991.

Esposito, L. W., R. G. Knollenberg, M. Y. Marov, O. B. Toon, and R. P. Turco. The clouds and hazes of Venus. In Venus (Hunten et al., Eds.),pp. 484-564, Univ. of Arizona Press, Tuscon, 1983.

Fahd, A. K., and P. G. Steffes, Laboratory measurements of the opacity of gaseous sulfur dioxide under Venus-like conditions, Icarus, submitted for publication, 1991.

Fahd, A. K., and P. G. Steffes, Laboratory measurements of the millimeter-wave properties of liquid sulfuric acid (H_2SO_4), J. Geophysical Research : Planets, 96, E2, 17471-17476, 1991.

Gasiewski, A. J., Microwave radiative transfer in Hydrometers. In atmospheric Remote sensing by Microwave radiometry (M.A. Janssen, Ed.). To be published by John Wiley and sons, 1990.

Gmitro, J. I and T. Vermeulen, Vapor-liquid equilibria for aqueous sulfuric acid. A.I.Ch.E. Journal. 5, 740-746, 1964.

Goodman, G. C., Models of Jupiter's atmosphere, Ph.D. Thesis, University of Illinois, Urbana , 1969.

Ho, W., I. A. Kaufman, and P. Thaddeus, Laboratory measurements of microwave absorption in models of the atmosphere of Venus, J. Geophys. Res., 71, 5091-5108, 1966.

Janssen, M. A., and R. L. Poynter. The microwave absorption of SO_2 in the Venus atmosphere. Icarus , 46, 51-57, 1981.

Jenkins J. M and P. G. Steffes. Results for 13-cm absorptivity and H_2SO_4 abundance profiles from the season 10 (1986) Pioneer-Venus orbiter radio occultation experiment. Icarus. 1991.

Joiner, J., P.G. Steffes, and J.M. Jenkins, Laboratory measurements of the 7.5-9.38 mm absorption of gaseous Ammonia (NH_3) under simulated Jovian conditions. Icarus, 81, 386-395, 1989.

Kay, B.D. ,Ph.D. dissertation, University of Colorado, 1969.

King, R.W.P. and G. Smith, Antenna in Matter, MIT press, 1981.

Knollenberg, R. G., and D. M. Hunten, The microphysics of the clouds of Venus: Results of the Pioneer Venus particle size spectrometer experiment, J. Geophys. Res., 85, 8039-8058, 1980.

Kolbe, W. F., B. Leskovar and H. Buscher, Absorption coefficients of sulfur dioxide microwave rotational lines, J. Mol. Spectroscopy, 59, 86-95, 1976.

Lewis, S. J. and D. H. Grinspoon, Vertical distribution of water in the atmosphere of Venus: a simple thermochemical explanation, Science, Vol. 249, 1273-1275, September 1990.

Liou, K. L., An introduction to atmospheric radiation, Academic Press, 1980.

Matthaei, G. L., L. Yound, and E. M. T. Jones, Microwave filters, impedance-matching networks, and coupling structures. Artech House book, McGraw-Hill, 1980.

Moore, R., A. MacDonald, and H. Ross Moroz, Permittivity of fiber-polymer composite: A study to determine effects of environment, Microwave Journal, Vol. 34, no.2, 1991.

Ogushi, T., Electromagnetic wave propagation and scattering in rain and other hydrometers, Proceedings of the IEEE, 71, 1029-1032, 1983.

Oyama, V. I., Carle, G. C., Woeller, F. and Pollack, J. B., Venus lower atmospheric composition: Analysis by gas chromatography. Science 203, 802-805, 1979.

Paltridge, G. W. and C.M.R. Platt, Radiative Process in Meteorology and Climatology, American Elsevier Publishing Co., Inc., New York, 1976.

Seiff, A., B.D. Kink, R.E. Young, R.C. Blanchard, J.T. Findlay, G.M. Kelly and S.C. Sommer. Measurements of thermal structure and thermal contrasts in the atmosphere of Venus and related dynamical observation: Results from the four Pioneer Venus probes. J. Geophy. Res. 85, 7903-7933, 1980.

Spilker, T. R., Laboratory Measurements of Microwave Absorptivity and Refractivity Spectra of Gas Mixtures Applicable to Giant Planet Atmospheres, Ph.D. dissertation, Stanford University, 1990.

Steffes, P. G., and V. Eshleman, Laboratory measurements of the microwave opacity of sulfur dioxide and other cloud-related gases under simulated conditions for the middle atmosphere of Venus, Icarus, 48, 180-187, 1981.

Steffes, P.G., Abundances of cloud-related gases in the Venus atmosphere as inferred from observed Radio opacity, Ph.D. thesis, Stanford University, 1982.

Steffes, P. G., M. J. Klein, and J. M. Jenkins, Observation of the microwave emission of Venus from 1.3 to 3.6 cm, Icarus, 84, 83-92, 1990.

Steffes, P. G. , Laboratory measurements of the microwave opacity and vapor pressure of sulfuric acid vapor under simulated conditions for the middle atmosphere of Venus, Icarus, 64, 576-585, 1985.

Steffes, P. G., and V. R. Eshleman, Sulfuric acid vapor and other cloud-related gases in the Venus atmosphere: Abundances inferred from observed radio opacity, Icarus, 51, 322-333, 1982.

Steffes, P. G. Evaluation of the microwave spectrum of Venus in the 1.2 to 22 centimeter wavelength range based on laboratory measurements of constituent gas opacities. Astrophysical Journal 310, 482-489, November 1, 1986.

Townes, C. H., and A. L. Schawlow, Microwave Spectroscopy. McGraw-Hill, New York, 1955.

Ulaby, T. F., R. K. Moore, and A. K. Fung, Microwave Remote Sensing; Active and Passive, Volume 1, Addison-Wesley publishing company, Massachusetts, 1981.

Waters, J. W., Methods of Experimental Physics, M.I. Meeks, Ed., 12 Part B, Academic Press, 1976.

Weast, R. C., Ed., Handbook of Chemistry and Physics 60th edition, CRC Press, 1979.

VITA

Antoine K. Fahd was born on [redacted] He graduated from Bradley University with a bachelor's degree (Summa Cum Laude) in Electrical Engineering in 1985. He obtained a Master's degree in Electrical Engineering from Georgia Institute of Technology in 1986.

As a Ph.D. student, Antoine Fahd conducted research in the area of Planetary Atmospheres. His dissertation involved the study and interpretation of the millimeter-wave spectrum of Venus.